Irradiation Behavior of Bonded Structures

M.H. Hassan

August 1993

UWFDM-919

Ph.D. thesis.

FUSION TECHNOLOGY INSTITUTE

UNIVERSITY OF WISCONSIN

MADISON WISCONSIN

Irradiation Behavior of Bonded Structures

M.H. Hassan

Fusion Technology Institute
University of Wisconsin
1500 Engineering Drive
Madison, WI 53706

http://fti.neep.wisc.edu

August 1993

UWFDM-919

Ph.D. thesis.

IRRADIATION BEHAVIOR OF BONDED STRUCTURES

by

Muhammad Hassan Hassan

A thesis submitted in partial fulfillment of the
requirements for the degree of

Doctor of Philosophy
(Nuclear Engineering and Engineering Physics)

at the
University of Wisconsin - Madison
1993

IRRADIATION BEHAVIOR OF BONDED STRUCTURES

Muhammad Hassan Hassan

Under the supervision of Professor Gerald L. Kulcinski

Analysis of the irradiation behavior of bonded structures, as they are applied in the fusion field, has been conducted by integrating both analytical calculations and experimental measurements. The Monte Carlo method was used for the simulation of atomic redistribution along interfaces of bonded structures due to neutron irradiation. Radiation Induced Mixing (RIM) along interfaces of bonded structures proved to be a significant phenomena for fusion reactor environments. Mixing layer of hundreds of angstroms thick were formed between a beryllium and iron joint structure. The phenomena was found to be significant especially at high fluences and for thick coatings. RIM caused a mixing layer of 0.1 micron along the interface of a 10 micron beryllium coating on iron substrate irradiated in ITER environment. This results in an alteration of the thermophysical and mechanical properties at the interface.

The boundary integral method formulated for time dependent plastic deformation was used for the stress analysis of a first wall structure in a typical DEMO fusion reactor by taking into consideration the impact of stress-enhanced swelling. Stress-enhanced swelling proved to be especially important early in the component life and in the temperature range where thermal creep is negligible resulting in high level of stresses. Also, the phenomena proved to be the key factor that determines the redistribution of stress with time.

When the interrelationship between (stress-enhanced) swelling and creep was taken into consideration, the stress-enhanced swelling was reduced by as much as 40% on the plasma side of the structure. Because of the way stress is redistributed in the substrate of the DEMO design, the increase in swelling was more pronounced at the coolant side of the

substrate, eventually reaching a value of 20% over the stress free value. It was concluded that the impact of stress-enhanced swelling is of a special importance for bonded structures. It was also shown that the fractional reduction in elastic moduli along the stressed interfaces of bonded structures could be twice the reduction predicted when stress is neglected.

Characterization of unirradiated bonded structures was conducted to evaluate properties that are expected to be altered due to irradiation. The Nanoindenter, an ultralow load microindentation machine, was used to investigate of the change in hardness and Young's modulus near the interface of cross-sectioned bonded structures. Based on these measurements, it was shown that inhomogeneities in the interfacial zone can complicate the interpretation of the H/E^2 (hardness over Young's modulus squared) values along the interface of hot isostatic pressed joined structure compared to the more homogeneous and well behaved brazed structure.

Approved:

Aug. 2, 1993

Date

Professor Gerald L. Kulcinski

Department of Nuclear Engineering and Engineering Physics)

Acknowledgement

A scientific research conducted for more than five years can not be attributed to a single person. Above all, I am indebted to Allah for guiding me to the right path and always directing me to what is beneficial.

My advisor Prof. G. L. Kulcinski extended his help to me both professionally and financially. His comments, vision, as well as his directions helped me a lot to build an independent scientific character.

I am also indebted to Prof. J. P. Blanchard for fruitful discussions and suggestions. Two of my Radiation Damage Group helped me a lot. Dr. D. Plantz spent hours transferring his experience on the Nanoindenter, and Dr. S. Han explained, in depth, the dynamic features of the Monte Carlo simulation.

Many people helped in a way or the other. I am indebted to them all. To Dr. M. Sawan and Dr. L. El-Guebally, for their kind, tender care and helpful suggestions. Dr. H. Attaya for fruitful discussions early in the research. Prof. C. Maynard for explaining some of the concepts of the Monte Carlo method as well as the ENDF system. Dr. E. Mogahed for his technical comments and objective directions. Prof. R. Dodd for fruitful discussions. D. Pertzborn and Dr. G. Beshish for helping in the experimental part. I also would like to extend my gratitude to Prof. M. Lagally who explained many aspects of surfaces and interfaces during the course work. Also, many people helped either in supplying the needed data or by fruitful comments. I am indebted to them all.

I am also indebted to my friends in the radiation damage group: , Dr. J. Liang, and Dr. R. Griffin. My colleagues, Dr. M. Hussein, Dr. H. Khater, Dr. M. Elaffifi, Dr. H. Abu-Gabal and Dr. Youssef Farawella extended their help to me whenever I needed it. Without the help of E. DuCharm and D. Bruggink, the final form of this thesis, as well as its related publications, would not have been on their present forms.

My professors in the Dept. of Nuclear Eng. in Egypt established a sufficient background for me to qualify for a graduate research. My friends in Madison helped me in spending very good times during my stay in the United States. I am especially indebted to Dr. M. Azab for his moral support and guidance.

The dedication, continuous support; and above all; prayers of my parents in Egypt made my success a reality. Also, the prayers of my sister and my In-laws, as well as all my family in Egypt were always there to support me.

My small family, my wife and two daughters, endured and sacrificed a lot for the sake of finishing this work. I pray to Allah to accept from them.

This work was partially supported by the United States Department of Energy.

Contents

List of Figures

List of Tables

List of publications resulting from this work

1. M. H. Hassan, J. P. Blanchard and G. L. Kulcinski, Irradiation Behavior of bonded structures: Impact of swelling-creep-stress relationship, **Fusion Technology**, Vol. 21, No. 3, Part 2B, 1927 (1992).

2. M. H. Hassan, J. P. Blanchard and G. L. Kulcinski, Stress-enhanced swelling: Mechanisms and implications for fusion reactors, **UWFDM-901**, University of Wisconsin-Madison (1992).

3. M. H. Hassan, J. P. Blanchard and G. L. Kulcinski, Irradiation Behavior of bonded structures: Impact of stress-enhanced swelling on irradiation creep and elastic properties, Fusion Reactor Materials Semiannual Progress Report, **DOE/ER-0313/12**, 61 (1992).

4. M. H. Hassan and G. L. Kulcinski, Mechanical properties along interfaces of bonded structures in fusion reactors, To Be Published in Fusion Reactor Materials Semiannual Progress Report, **DOE/ER-0313/13** (1993).

5. M.H. Hassan and G. L. Kulcinski, Irradiation behavior of bonded strcutures: Radiation Induced Mixing along interfaces, To be published (1993).

Chapter 1.

Introduction

Current proposals for Plasma Facing Components (PFC) in fusion reactors include duplex thin walled structures. The advantage of such a structure is that the plasma side material can be chosen to minimize sputtering and the coolant side material can be chosen to maximize heat transfer and minimize corrosion. The entire structure may be subjected to high temperatures, high temperature gradients, thermal and irradiation creep, swelling, and thermal expansion [1]. Due to the severe conditions that must be met by bonded structures in the fusion field, coatings in the present fusion devices have suffered many problems: several TiC-coated molybdenum tiles in JT-60 have melted which is attributed to disruption heat fluxes, tiles of the TiC-coated graphite limiter in Doublet III suffered cracking and fracture under the incident heat fluxes, and graphite tiles in TFTR have been damaged and failed [2].

The interface between coating and substrate is of unique significance to bonded structures. Strength of bond, to a greater or lesser extent, is generally the underlying requirement for good adhesion. No completely satisfactory solution has yet been found to adequately assess the adhesion bonding. It is to be noted that investigation of adherence should be conducted under actual and/or closely simulated service conditions to the extent feasible.

Viable technologies for bonded structure fabrication in the near and long term fusion machines are brazing, plasma spray, welding, and diffusion bonding. There are trade-offs to these choices and each will have applications in a different context. In any case, thorough

testing should be combined with analysis to ensure the viability of various material and fabrication choices [2].

Although many of the existing joints in nuclear (both fission and fusion) reactor plants are not subject to a high neutron flux, there are a significant number of them that must be located in high irradiation fields. Very little information is available pertaining to their behavior in such applications. For example, to date, the basis for design welds and brazes in such systems has been based primarily on experience using liberal margins of safety [3]. It is thus apparent that the radiation stability of such joints must be understood to a greater degree.

The requirements for future Tokamak reactors will differ significantly from those for present and near term reactors. In the present reactors, there is essentially no radiation damage or elemental transmutations, the hydrogen ion flux is relatively low and components, generally, are not actively cooled. The principal threat to present components is from disruption heating and the principal impurity injection mechanisms are from thermal effects and sputtering [4].

However, as one moves to intermediate and long term reactors, the neutron irradiation problem will become more urgent.The neutron testing requirements for one of the intermediate term devices; the International Thermonuclear Experimental Reactor (ITER) are [5]: (1) swelling, differential swelling, (2) property degradation, (3) carbon composite response, (4) lifetime, and (5) thermal fatigue. The effect of neutron damage will limit the selection of future Plasma Facing Components (PFC). It is not clear which, if any, of the present candidates are capable of withstanding high fluence levels, and a major development program is needed. Also, the time to start irradiation experiment is now because of the long lead times required to accumulate high fluence data [5]. It is worth mentioning that materials

research should precede machine construction by at least 10 years and typically one irradiation research cycle takes more than 5 years [5].

For PFC's, seven critical neutron damage related issues were identified by Whitley [6]. These issues are:

1. Structural integrity.
2. Thermal shock resistance.
3. Thermal conductivity and other physical property changes.
4. Dimensional changes.
5. Erosion.
6. PMI (Plasma Material Interaction) response.
7. Bonded multimaterial structures.

Concerning the last point, the response to neutron irradiation may be quite different than that of the individual materials due to the presence of the interface and the stresses generated by differential swelling. Also, the bonding method (e.g., brazing) will have a significant influence on the residual stresses within the structures. During operation, the performance of the bond is, of course, crucial to the performance of the structure as a whole.

Currently, there is very little information available on bond properties or on the irradiation behavior. What complicates the problem is that the mechanisms of irradiation damage in bonded structures are not well understood. The damage mechanisms that operate in metallic materials should also apply to coatings (e.g., swelling or creep). Some mechanisms for the radiation damage in bonded structure [7] that have been identified are listed below but it should be emphasized that all of them require more detailed study.

1. Point defect or transmutation induced stress at coating substrate interface, or within the coating.

2. Irradiation induced changes in mechanical and thermo-physical properties of both coating and substrate (this is particularly important if the duplex system must withstand deformation).

3. Impurity and transmutation product migration to the interface region.

4. Gas migration when interface is under stress or maintains a thermal gradient.

5. Intra-coating stresses as a function of coating thickness.

6. Differential swelling and thermal expansion.

In order to adequately assess the radiation damage in bonded structures, a thorough analysis of the microscopic structure along the interface should be done. The first step would be to properly account for the atomic mixing and the generation of point defects along the interface. No data seems to exist for collisional mixing along interfaces due to neutron irradiation [8].

The production of hydrogen and helium atoms per unit of displacement damage (dpa) is one to two orders of magnitude more in fusion reactors than in fission reactors for most of the plasma facing components, and it is well known that gas atoms play a major role in changes of mechanical properties and dimensional stability [9]. The proper assessment of the spatial distribution of these gas atoms is the first step in determining their role on the performance of bonded structures.

The difficulty of using analytic methods for the solution of the particle transport problem in solids increases as the basic assumptions to solve the transport equation are removed in multilayered targets. The Monte Carlo method has proved to be a powerful tool to investigate the collisional mixing along the interface of bilayers [10]. From the analysis of the various mechanisms involved in ion beam mixing [10], it should be expected that the

same effects will also play a vital role in case of neutron irradiation of bonded structures. The Monte Carlo method will be used in this thesis for the simulation of intermixing, transmutation production, and atomic redistribution along interfaces of bonded structures due to neutron irradiation. The essence of the approach lies in the dynamic simulation. This consists of sectioning the target into different layers. After the termination of a neutron history (with its related knock-on atoms), the net change in the composition of each layer is calculated. This is different from the "static mode" in which target composition remains constant during irradiation simulation.

Irradiation-induced swelling in the core structural materials of a fast breeder reactor played a critical role in the design and economics of the LMFBR. Theoretical studies have clearly indicated that stress in a reactor core component can affect the swelling [11]. Experimental data clearly show an increase of swelling with increase of stress. The enhancement, however, does not only depend on the stress level, but also on the irradiation temperature and on the swelling already achieved. Knowledge of the effect of stress on swelling is critical to a complete understanding of reactor core component deformation after prolonged exposure to a fast neutron flux. It is anticipated that stress-enhanced swelling may play a larger role in fusion devices than it does in breeder reactors due to the complicated stress histories imposed on the structures. In examining the practical use of alloys as structural components of a fusion reactor, it is necessary that the simultaneous effects of displacement damage, applied stress, thermal aging, etc., are taken into consideration. Since it is well recognized that the swelling problems in bonded structures may be one of the key elements for the failure of these components, incorporating the stress-enhanced swelling phenomena into the stress analysis is vital for the proper understanding of the behavior of bonded structures. This in turn will have an impact on the interrelationship between swelling

and creep. If the swelling is enhanced due to stress, this may enhance creep and further reduce the stress level, ultimately reducing the swelling level.

While extensive stress analyses have been carried out for plasma facing components made of single materials such as 316 stainless steel, stress analysis for bonded structures is only in its early stages of development [12]. The major work in this area is mainly from Mattas [13-15], Glasgow [16], and Blanchard [17-18]. None of these previous studies, as well as the few inelastic stress analyses that included radiation effects [19-27], have incorporated the effect of stress on the swelling. Only Mattas [13] took the interrelationship between creep and swelling into consideration.

The concept of the boundary integral method formulated for time dependent plastic deformation will be used for the stress analysis of a first wall structure in a typical DEMO fusion reactor. Input to the problem will be from the GTSTRESS code [28] which is a one-dimensional inelastic stress analysis code. Four different sources of stresses will be considered: (1) membrane loads from internal coolant pressures, (2) temperature gradients through the wall caused by steady-state heat fluxes, (3) irradiation induced stress-enhanced differential swelling gradients through the wall, and (4) residual stress gradients caused by both thermal and irradiation creep-induced stress relaxation, taking into consideration the impact of stress-enhanced swelling on irradiation creep. Also, the impact of stress-enhanced swelling on the reduction of Young's modulus along the interface will be investigated.

One of the main points in a fusion material characterization program is extracting information from small test volumes [29]. A Miniaturized Specimen Technology had to be developed to account for smaller irradiation volumes and lower post irradiation testing doses to personnel. Only one type of mechanical test was found that could satisfy all the requirements of a mechanical properties microprobe on coated materials [30]. Properly

instrumented and controlled, a (depth sensing) microindentation test can accomplish many of the goals needed from any material characterization program. During an indentation test, both elastic and plastic strains are generated. For many materials, the strains from both fields are of sufficient magnitude to be measured. The test can be scaled down so that submicron volumes of materials are sampled. Determination of hardness values along the interface of a bonded layers is one of the most widely parameters to get an indication of the adhesion of the bonded structures. Also, it is known that the Young's modulus will change along the thickness of a bonded structure due to fabrication and/or irradiation. The Nanoindenter; an ultralow load microindentation machine, with its high resolution and capability of detecting minor changes on the submicron levels of the mechanical properties, will be used for the investigation of the change in hardness (H), Young's modulus (E), as well as H/E^2 values along the thickness and interface of bonded structures.

Regardless of the fact that bonded structures are likely to continue to be used in both near-, intermediate-, and long-term fusion reactors, the existing analytical and experimental studies are inconclusive in terms of the expected lifetime of such designs. Additional work is required in both areas. As far as is known, this thesis work is one of the first to analyze the irradiation behavior of bonded structures in the fusion field integrating both the analytical and experimental concepts. Concepts related to bonded structures; such as fabrication techniques, adhesion, and nature of interfaces; are reviewed. Distributed published literature on the effects of irradiation on the behavior of joints in the nuclear field (pertaining to thermal and fast reactors) has been put together and an in depth analysis of the radiation damage mechanisms in bonded structures is presented. First, the Monte Carlo method will be used for the simulation of Radiation Induced Mixing (RIM) of atomic constituents and redistribution of gas production along interfaces due to neutron irradiation. Second, the effect of stress history on the development of swelling in bonded structures, as well as the role

played by stress-enhanced swelling in irradiation creep calculations will be investigated using the concept of the boundary integral method formulated for time dependent plastic deformation. Also, the impact of stress-enhanced swelling on the change of Young's modulus along interfaces of bonded structures will be analyzed. Third, the Nanoindenter will be used to probe related mechanical properties along the interfaces of cross-sectioned bonded structures. This helps in characterizing unirradiated bonded structures to evaluate properties that are expected to be altered due to irradiation.

References

[1] B. B. Glassgow and W. G. Wolfer, Fusion tech. **8**, 596 (1985).

[2] J. P. Blanchard and R. D. Watson, Nucl. Eng. and design/fusion **4**, 61 (1986).

[3] W. R. Martin and G. M. Slaughter, in: Source book on brazing and brazing technology, eds., M. M. Schwartz, American Society for metals (Metals Park, 1987) p. 406.

[4] D. M. Mattox and M. J. Davis, J. Nucl. Mat. **111/112**, 819 (1982).

[5] S. Ishino, in: Proc. of the Japan-U.S. workshop p-119 on 14 MeV neutron source for material R&D based on plasma devices, eds., A. Miyahara and F. coensgen, IPPJ-T-37, 21 (1988).

[6] J. B. Whitley, in: Proc. of U.S.-Japan workshop Q86 on plasma-materials interaction/high heat flux data needs for the next step and steady state devices, eds., J. B. Whitley and A. Miyahara, SAND88-1072, 94 (1988).

[7] R. W. Conn, et al., UCLA PPG-815, (1984).

[8] H. J. Wollenberger, in: Proc. Fourth International Conference on Fusion Reactor Materials (ICFRM-4), Kyoto, Japan, 1989, J. Nucl. Mat. **179-181**, 1209 (1991).

[9] D. M. Goebel, et al., PPG-1125 UCLA-ENG-88-02 (1988).

[10] S. Han, University of Wisconsin report UWFDM 789 (1988).

[11] see the detailed literature survey in chapter 6.

[12] N. M. Ghoneim and J. B. Whitley, J. Fusion Energy **8**, 157 (1989).

[13] R. F. Mattas, Fusion Tech. **19**, 1487 (1991).

[14] R. F. Mattas, Fusion Tech. ,637 (1990).

[15] R. F. Mattas, ANL/FPP/TM-160 (1982).

[16] B. B. Glasgow and W. G. Wolfer, Fusion Tech. **8**, 596 (1985).

[17] J. P. Blanchard and N. M. Ghoniem, J. Nucl. Mat. **172**, 54 (1990).

[18] J. P. Blanchard, Analysis of singular stress fields in fusion components, Ph.D. thesis, UCLA (1988).

[19] J. P. Blanchard and N. M. Ghoneim, Nucl. Eng. Desi./Fusion **2**, 19 (1985).

[20] W. Daenner and J. Raeder, in: Proc. 3rd Top. Meeting on the Technology of Contr. Nucl. Fus., Santa Fe', New Mex., USA, 347 (1976).

[21] B. M. Ma, Nucl. Eng. Des. **28**, 1 (1974).

[22] W. Daenner and J. Raeder, J. Nucl. Mat. **85/86**, 147 (1979).

[23] W. Daenner, J. Nucl. Mat. **103/104**, 121 (1981).

[24] R. D. Watson, R. R. Peterson, and W. G. Wolfer, UWFDM-433 (1981).

[25] R. D. Watson, R. R. Peterson, and W. G. Wolfer, J. Pressure Vessel Tech. **105**, 144 (1983).

[26] S. D. Harkness and B. Cramer, J. Nucl. Mat. **85/86**, 135 (1979).

[27] H. Oomura, et al., Fusion Tech., 8 (1985).

[28] R. R. Peterson, University of Wisconsin report, UWFDM 382 (1980).

[29] G. E. Lucas and G. R. Odette, Nucl. eng. and design / fusion **2**, 145 (1985).

[30] W. C. Oliver, MRS Bulletin **11**, 15 (1986).

Chapter 2.

Plasma Interactive Components

2.1 Introduction

The term "Plasma Interactive Components" (PIC's) [1] refers to any component inside the vacuum vessel that is in direct contact with the plasma. This includes the first wall, impurity control systems, direct convertors, RF antennas and other structures [1]. Plasma interactive components are subjected to mainly four forms of radiation from a DT plasma (see Figure 2.1): (1) electromagnetic radiation, (2) neutral particles such as unburned fuel particles and impurity atoms, (3) charged particles, mainly helium, deuterium, and tritium ions, and (4) energetic neutrons with energies up to 14 MeV. It is also to be noted that burn length, availability, neutron wall loading, and neutron fluence will increase as one progresses from near term to long term devices [2].

The design requirements for PIC's vary due to the different components, different confinement concepts, and varying stages of development. These components are not only subject to high heat flux but also to physical and chemical sputtering, arcing, blistering, hydrogen/helium retention and release, neutron activation, radiation damage and metal fatigue. Thus, the various disciplines involved include: plasma physics, surface physics, solid state physics, metallurgy, ceramics, thermal hydraulics, chemistry and electromagnetics. Plasma Interactive Components have an impact on plasma performance, tritium systems, magnet systems, vacuum systems, blanket systems, and remote maintenance. The lifetime of the PIC's depends on two key parameters [3]; erosion (requires thick structures), and mechanical failure (thermal stresses increase with plate thickness and therefore thin structures

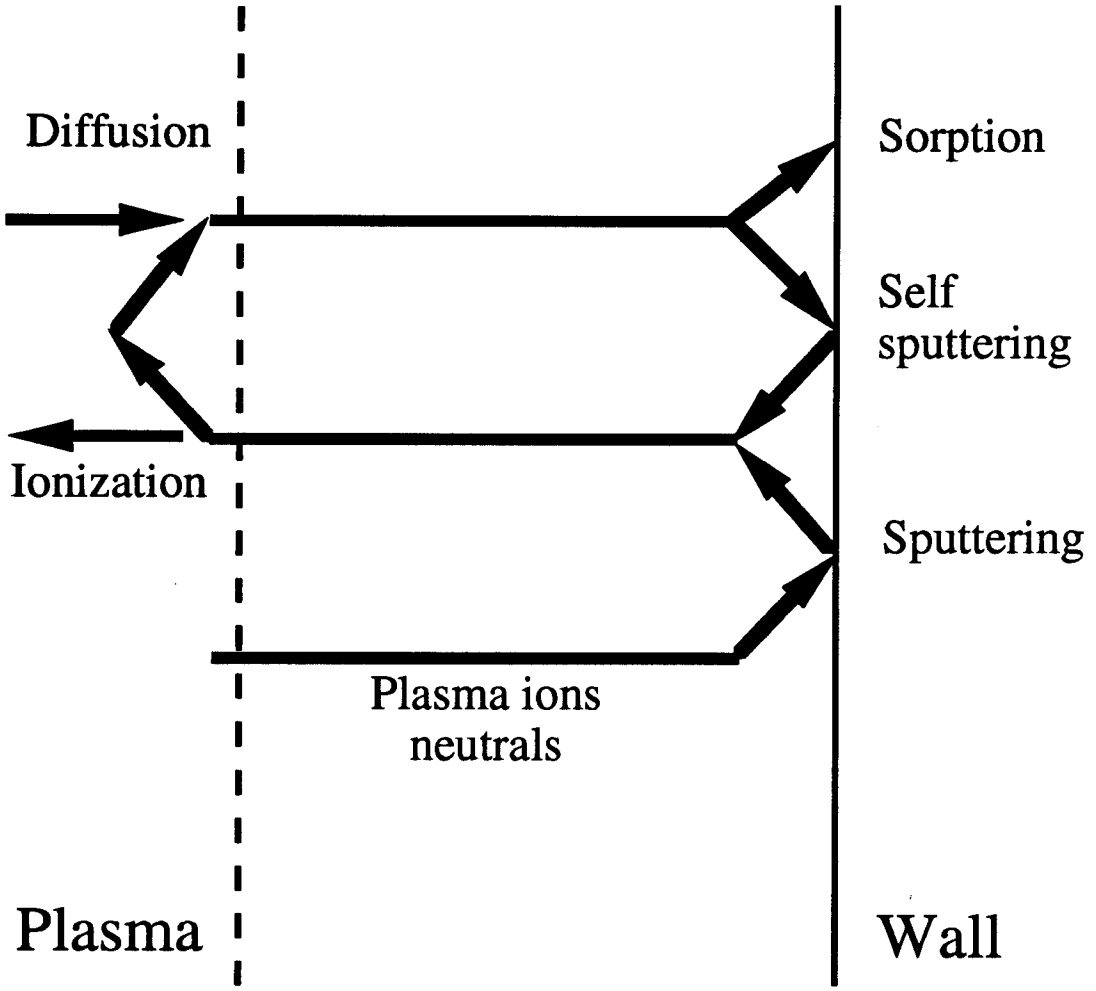

Figure 2.1: Simple modelling of plasma-wall interactions [4]

are preferred). Reliability of bonded structures is dependent upon a number of factors that are related to design, fabrication and material properties.

As indicated in the following two sections, different requirements are demanded from the plasma facing materials and the bulk materials. To meet the different contradicting requirements of the Plasma Facing Components, several new coating/cladding technologies were used to allow the separation of surface properties from structural requirements as will be shown in section 2.4.

2.2 Plasma facing materials

Requirements for plasma facing materials are [2]: (1) high thermal conductivity, (2) high specific load, (3) a low coefficient of thermal expansion, (4) low sputtering coefficient, (5) a low elastic modulus to minimize thermal gradients and stresses, (6) mechanical properties that guarantee structural integrity for the desired operating life time of the component (important properties are tensile, creep, fatigue and crack growth), (7) resistance to changes caused by radiation induced swelling and creep, and (8) ability to be fabricated to the required geometry, and successfully joined together.

Candidate plasma-facing materials are [3]: (1) tungsten, molybdenum, or tantalum, if the plasma edge temperature is low, (2) beryllium, silicon-carbide, or titanium-carbide, for moderate edge temperature (to avoid self-sputtering of high-Z materials), and (3) graphite, if the tile temperature can be controlled to prevent chemical sputtering. The following types of graphite have been considered: (1) highly anisotropic (like pyrolitic graphite) in which the hexagonal crystals are all aligned resulting in anisotropic thermal coefficients and swelling

rates, (2) near isotropic, fine grains and high strength, and (3) highly isotropic, low swelling and high strength.

2.3 Heat sink materials

Requirements for heat sink materials are [2]: (1) good high temperature strength and ductility, (2) high thermal conductivity, (3) low thermal creep rates, (4) good high temperature fracture toughness, (5) the ability to form strong bonds with the chosen surface material, (6) low neutron activation, (7) good fabricability, (8) reasonable cost, and (9) good radiation damage resistance.

Candidate heat sink materials are [3]:

1. Copper alloys, which have good thermal properties but are incompatible with liquid metal coolants. Some of the copper alloys considered for fusion machines are: (1) pure copper, (2) oxygen-free high-conductivity copper (OFHC), (3) MZC, precipitation hardened alloy, (4) AMZIRC, precipitation hardened alloy, and (5) Glidcop Al-20, dispersion hardened alloy.
2. Stainless and ferritic steels, which have adequate strength but unsatifactory thermal properties.
3. Vanadium and tantalum which may be incompatible with helium coolants due to the susceptibility to embrittlement by oxygen impurities in the helium coolant. They are also subject to radiation damage.
4. Refractory metals (Mo, W) have good high-temperature strength, low interstitial atom pickup, and good thermal conductivities. However, Mo is susceptible to a high ductile to brittle transition temperature (DBTT) after irradiation which may exceed room temperature. As for W, in its pure form, it has a large DBTT shift with

irradiation (100 - 400 °C) making it brittle at room temperature. Thus, residual stresses by the fabrication process or during shutdown are present. Tungsten, on the other hand, has a decay heat problem.

5. Inconel, a nickel-based alloy which also has good high-temperature strength.

2.4 Bonded structures in fusion machines

2.4.1 Early conceptual designs of power plants [3]

The first design to apply a "duplex" structure for the PFC's was UWMAK-I (see Figure 2.2). The plasma side in the limiter was a flowing lithium film. The heat sink material was a stainless steel structure. As for the UWMAK-III (see Figure 2.3), the collector plate was a very thin (0.1 mm) TZM (a molybdenum-based alloy) sheet separated from a more substantial TZM backing plate by a falling lithium film. Also, a carbon curtain protects the outer first wall and 25 cm of graphite protects the inner first wall. In the early fusion commercial design reactor STARFIRE, both the limiter and the first wall were coated with beryllium. The structural material was to be chosen from four alloys: copper-, vanadium-, tantalum-, and niobium-based.

2.4.2 Existing fusion devices [3]

In Doublet III, a Tokamak physics testing device at GA technologies in San Diego, a TiC coated graphite limiter was installed in 1980; however, the graphite failed when neutral beam power was increased. Thicker tiles had to be used. The graphite tiles were mechanically bolted to the first wall to provide neutral beam dumps. Graphite tiles on the limiter and first wall were then coated with SiC and pyrolytic carbon by a Chemical Vapor Deposition (CVD) process. In ASDEX upgrade (a Tokamak in Garching, Germany), graphite, brazed to molybdenum tubes, was used as a surface material in the limiter. In

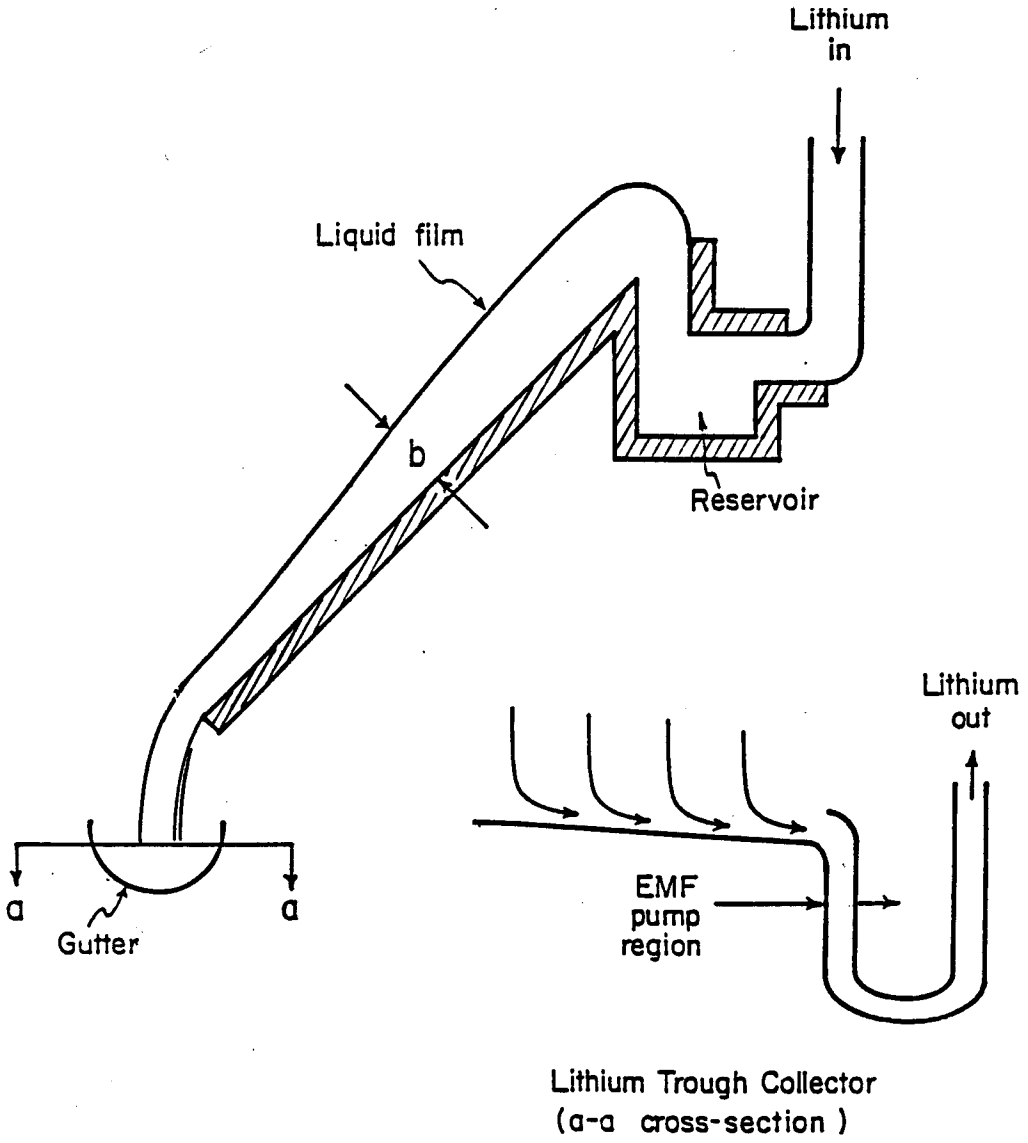

Figure 2.2: Schematic of one divertor liquid lithium collector plate for the UWMAK-1 [5]

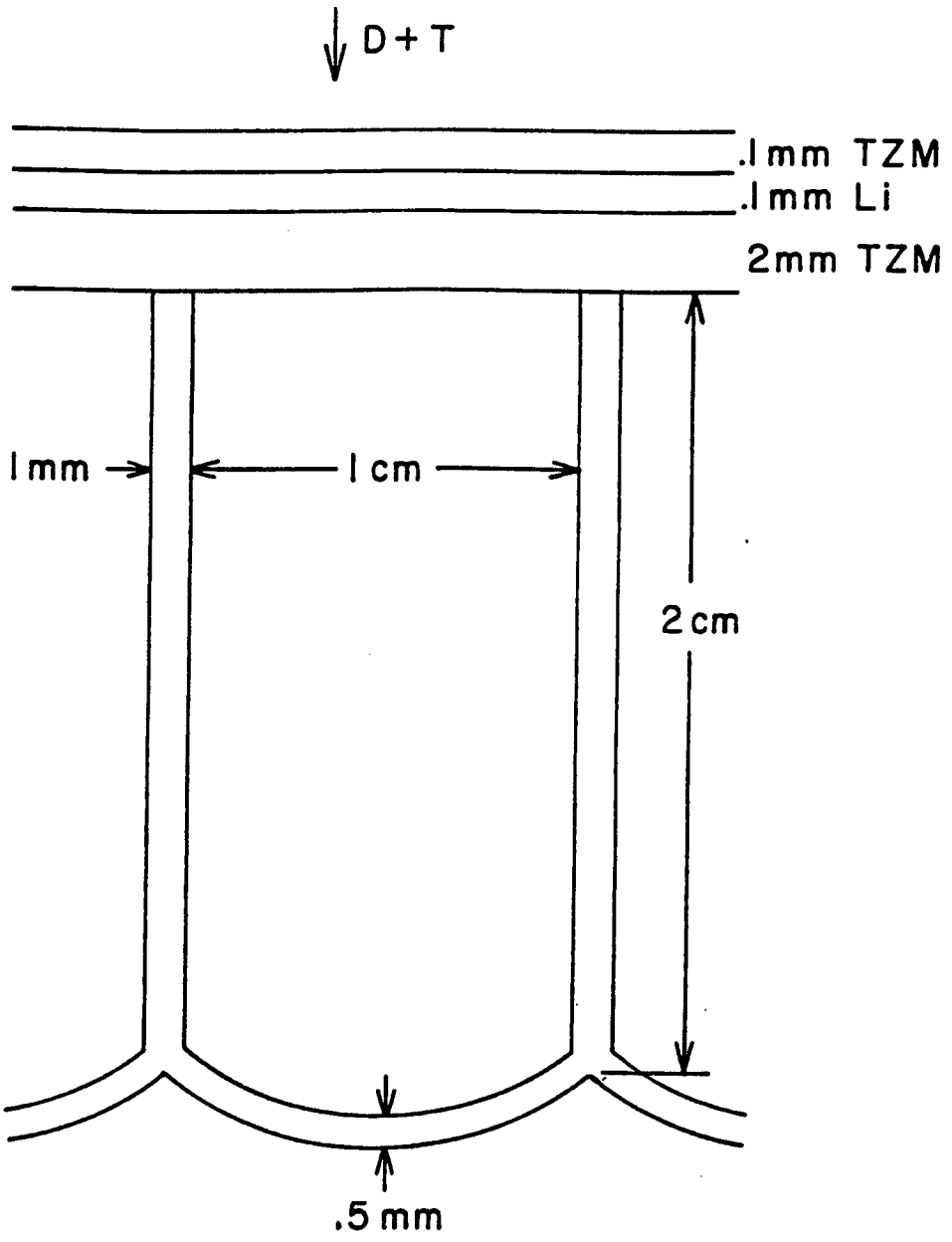

Figure 2.3: Cross section view of the collector plate of the UWMAK III [6]

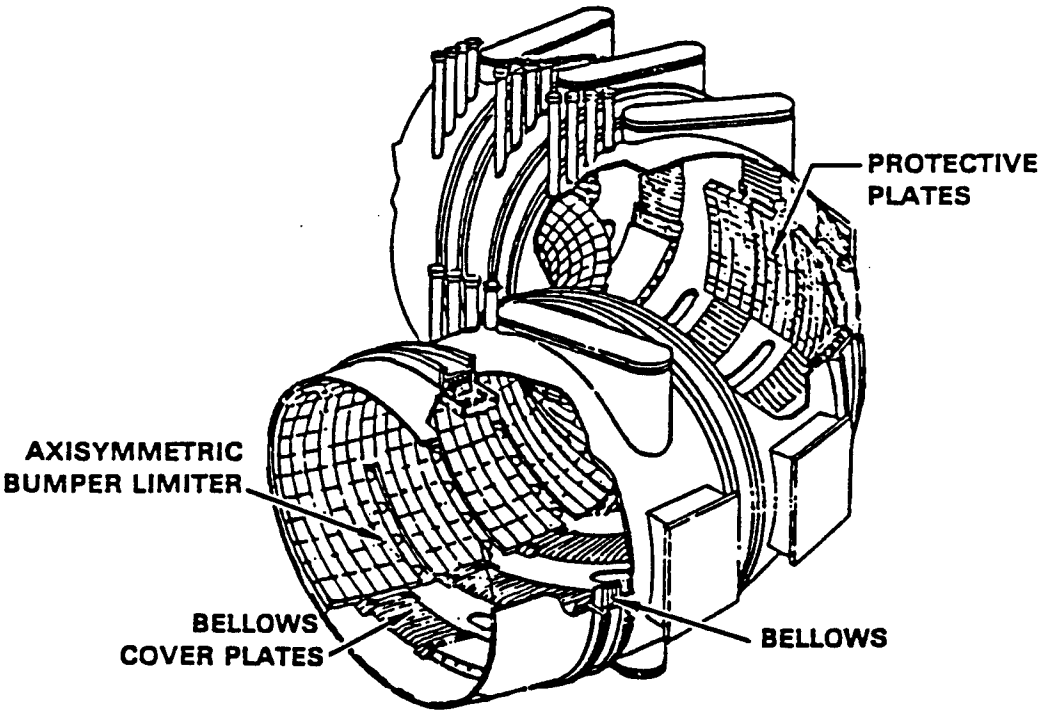

Figure 2.4: TFTR protective armor location [3]

TFTR (see Figure 2.4) at Princeton Plasma Physics Laboratory in New Jersey, a movable poloidal bumper limiter was used. It consists of three inconel blades covered with TiC-coated tiles mechanically attached to the inconel plate. As for the JT-60 at JAERI in Japan, molybdenum and inconel liner plates were bolted to the inconel vacuum vessel. Also, TiC coatings were applied on all plasma-facing surfaces.

In the JET machine at Culham laboratories in England, an inconel vacuum vessel was initially covered with additional inconel heat shields. Also, Inertially cooled graphite (recently replaced by Beryllium) tiles were attached to the first wall in 1984. In the TEXTOR German experimental device (originally known as the ALT-II), the limiter was designed as a triplex structure with a stainless steel baking plate, a copper cover plate and a SiC-Al composite surface material. The final design, however, incorporated graphite tiles mechanically attached to an inconel baking plate. Finally, the first wall of the TORE SUPRA Tokamak in Cadarache France is protected by brazed graphite tiles [7].

2.4.3 Intermediate-term devices under design

The CIT (The Compact Ignition Tokamak), later named BPX (Burning Plasma Experiment), was to be sited in the US before its cancellation in the early 1990's. The vacuum vessel was supposed to be inconel with mechanically attached graphite tiles on the first wall [3]. As for the FER (Fusion Experimental Reactor) in Japan, the first wall will be stainless steel with no coating or tiles. The divertor will be a tungsten armor brazed to a copper heat sink [3]. The first wall in the NET (Next European Torus) is a carbon-reinforced tile on solution-annealed austenitic steel as shown in Figure 2.5 [8]. Also, tiles of a tungsten rhenium alloy are brazed to a copper divertor substrate. Finally, for the first wall and the divertor in the International Thermonuclear Experimental Reactor ITER (Figure 2.6), the materials in the Conceptual Design Activities (CDA) were 316 SS and copper respectively

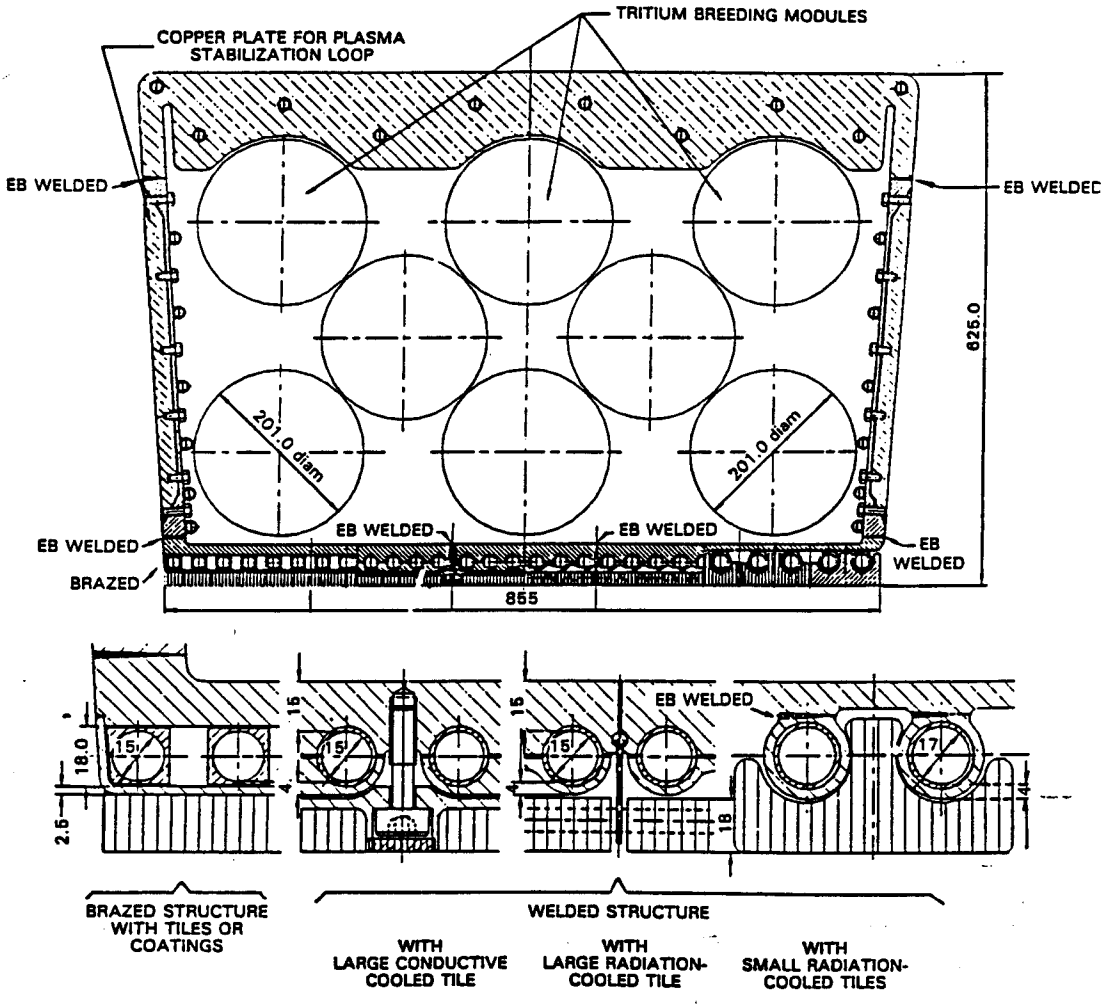

Figure 2.5: Midplane cross section of NET outboard FW and blanket segments with alternative FW panel concepts for poloidal-contained water cooling, and plasma-side protection. Dimensions are in millimeters [8]

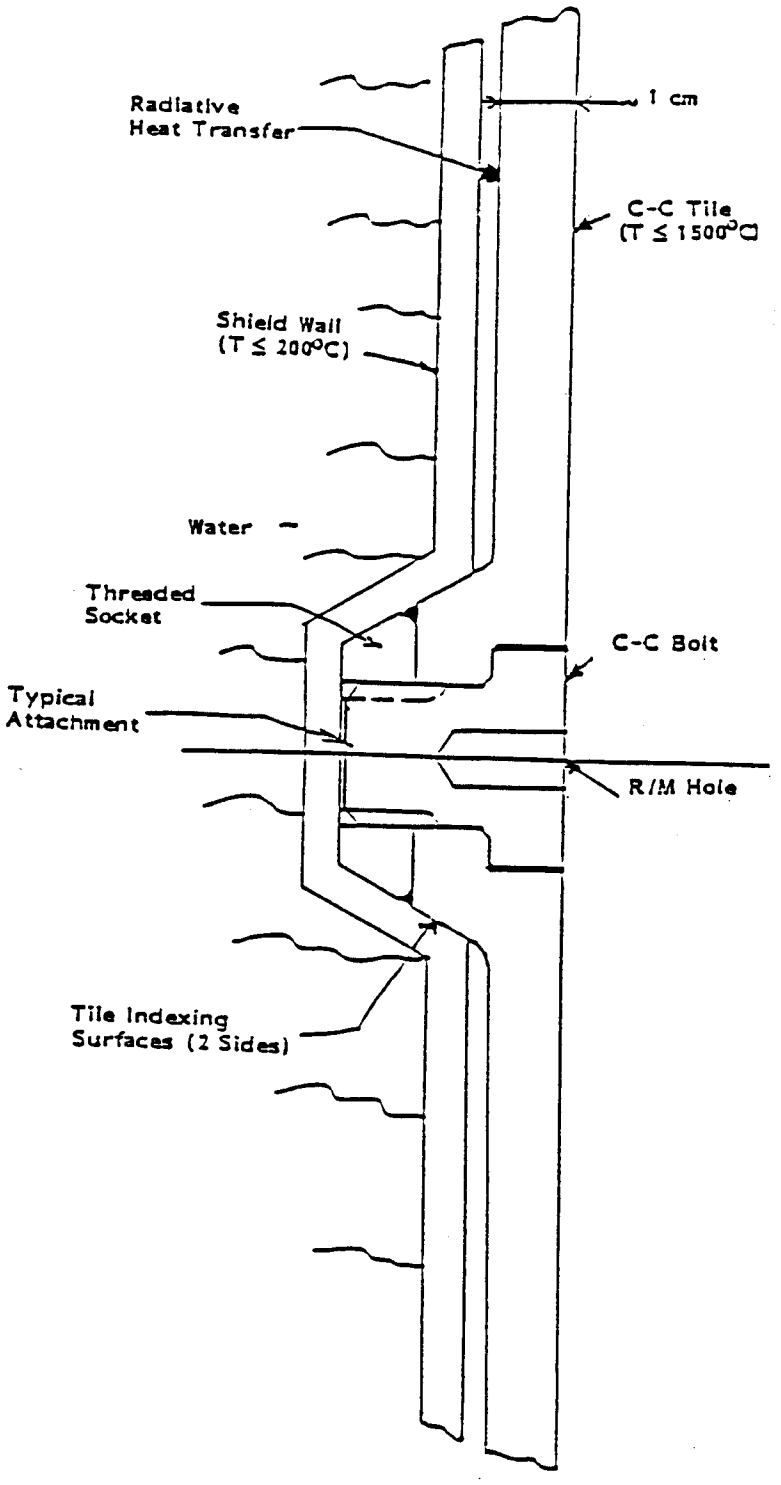

Figure 2.6: First wall tile concept for ITER [9]

[9]. Candidate armor materials for first wall are Be, graphite and SiC. For the divertor, candidate materials are Be, graphite and tungsten.

2.5 References

[1] R. F. Mattas, J. Nucl. Mat. **141/143**, (1986).

[2] R. W. Conn, et al., UCLA PPG-815, (1984).

[3] J. P. Blanchard, Analysis of singular stress fields in fusion components, Thesis (1988).

[4] A. Miyahara, J. Nucl. Mat. **111/112**, (1982).

[5] B. Badger, et al., UWMAK I, UWFDM 68, a University of Wisconsin report (1974).

[6] B. Badger, et al., UWMAK III, UWFDM 150, a university of Wisconsin report (1975).

[7] Laboratoire de recherche de l' Association EURAROM-CEA, rapport 1987-1988 (1989).

[8] Max Chazalon, et al., Fusion Tech. **14**, (1988).

[9] The TIBER/ITER design review meeting, Fusion Engineering Design Center (1987).

Chapter 3

Design, Fabrication, and Characterization of Bonded Structures

3.1 Introduction

Current proposals for Plasma Facing Components (PFC's) in fusion reactors include duplex thin walled structures. The advantage of such a structure is that the plasma side material can be chosen to minimize sputtering and the coolant side material can be chosen to maximize heat transfer. The structure will be subjected to high temperatures, high temperature gradients, thermal and irradiation creep, swelling, and thermal expansion [1].

This chapter will deal with the general definitions, aspects, and adhesion of coatings together with the design, fabrication, as well as the interface characterization of bonded structures in the fusion field. A 'Coating' [2] is a near-surface region having properties differing from the bulk of the material and is prepared by adding a material to the surface. A 'Film' is a thin coating (< 1 μm). In some instances the film properties are influenced by the substrate properties. A "Cladding" is the bonding of a sheet of overlay material to the substrate by thermal (brazing, soldering, diffusion bonding) or mechanical deformation (explosive bonding, roll bonding, cold welding etc.).

Generally speaking, coatings may be desirable or even necessary for a variety of reasons including improved performance (e.g., wear and erosion resistance), improved processing (e.g., electrical contact), lowered costs, and enhanced appearance [3]. Thus, regardless of the fact that coatings, in general, allow the separation of surface properties from

structural requirements; they still suffer from major drawbacks: (1) presence of interface and the need for adhesion, (2) a sharp discontinuity in material properties and response to applied stresses, (3) need for novel fabrication methods, some of which are expensive, and (4) need for process control so as to have a reproducible product.

Coating properties are different from bulk materials due to certain intrinsic factors, e.g., microstructure, intrinsic/extrinsic stress, composition/stochiometry, and graded structure and properties [3]. Thus, the microstructure and compositional forms of coatings have the following characteristics: (1) a wide variety of microstructures, from amorphous to single crystals, (2) unique phases and phase distributions, (3) unique microstructures-columnar microstructure, and (4) high intrinsic stresses and defect concentrations.

3.2 Bonded structures in the fusion field

Bonded structures in fusion machines are required to have the following characteristics: (1) the thermal conductivity and contact conductance of the materials should be high enough to handle the high heat flux of the reactor environment, (2) the variation of thermal expansion of the tile, interface, and heat sink should be minimal for all heat loads, (3) the thermal stresses should be evenly distributed over the heat sink by the interface material and fabrication technique, (4) the interface attachment should be strong enough to protect the tile or coating from the induced electromagnetic force or torque caused by plasma disruptions, (5) the reduction in contact thermal conductance caused by neutron irradiation should not make the component lifetime shorter than that of other reactor components, (6) the contact thermal conductance should not be affected by thermal shocks, high cyclic heat loads, or galvanic erosion during the component lifetime, (7) the design, interface materials, and fabrication methods should minimize debonding of the bonded structure, which may be

caused by interface embrittlement, brittle fracture, fatigue failure, or fabrication damage, (8) thermal stresses induced during cooldown from the fabrication temperature must also be taken into consideration, and (9) the normal peak stresses of the components should be within safety limits that will prevent plastic or creep deformation, ductile failures, and creep rupture.

3.2.1 Design features

Two distinctive designs can be used;

1. Mechanically attached tiles, shown in Figure 3.1, can be replaced in-situ by remote maintenance equipment. Usually, the tiles are thick armors (several millimeters or more) that can be properly used for flat or nearly flat surfaces (divertor or collector plate). However, it has the disadvantage of having large mismatch in thermal expansion between cladding and substrate.

2. Bonded tiles (claddings) / coatings, should be used as the heat loads become even higher in future devices. These can be used for surfacing of complex shapes (curved limiter blades). Thus, coating of large areas (first wall repair) and in situ repair of damaged or eroded surfaces can easily be accommodated. Bonding technology and replacement procedures for maintenance have not yet been developed. However, the thermo-mechanical performance required, especially of the thick coatings, is reported to be poor.

3.2.2. Fabrication

The two mechanisms that are currently used for coating/substrate formation are:

1. Bolting: The interface thermal conductance between the tile and the heat sink will be relatively low, the tile temperature relatively high, and the fatigue life of the heat sink relatively high.

2. Chemical vapor deposition CVD: Presently, this is the primary technology for coating of thin layers (< 20 μm). It is suitable for a large variety of materials,

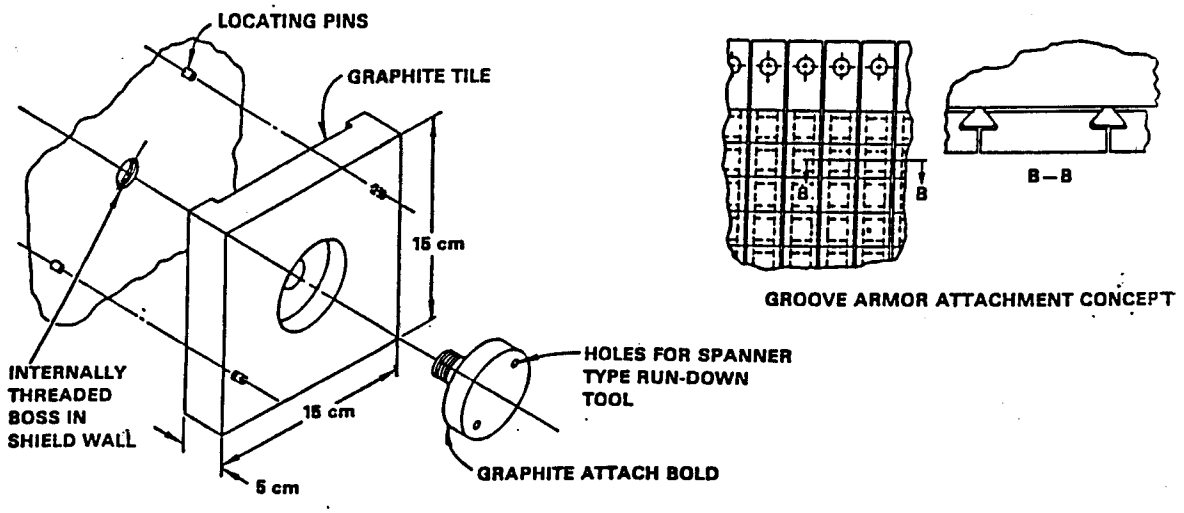

Figure 3.1: Bolted and grooved tiles [5]

including metals, semiconductors, nitrides, borides, and beryllides. However, this process has the following disadvantages: (1) low deposition rate (typically only microns per hour), (2) production of corrosive by-products, (3) high process temperatures are required which can adversely affect metal substrates, and (4) the difficulty in accommodating a large thermal expansion mismatch.

Viable technologies for bonded structure fabrication in the near and long term fusion machines are brazing, plasma spray, welding, and diffusion bonding (see Figure 3.2). There are trade-offs to these choices and each will have applications in a different contexts. In any case, thorough testing should be combined with analysis to ensure the viability of various material and fabrication choices [4].

It should also be noted that thermal stresses induced by different thermal expansion coefficients between the coating and the substrate can be relieved by using a composite coating; reducing the width of the tile or coating with maximum allowable thickness; or by introducing a compliance layer in the bonding or brazing interface zone [5]. The last concept utilizes a metal fiber compliant layer that is brazed between the surface material and the substrate. The compliant layer is composed of randomly arrayed metal fibres which are sintered together to produce a fiber network of high porosity. The properties of the layer are controlled by the density, which is chosen to achieve a balance between compliance, thermal contact conductance, and strength. Finally, it should be noted that the key issue for such compliant layer is the effect of radiation damage on the integrity of the fibres [5].

3.2.2.1 Brazing

Brazing [6] is the joining of metals through the use of heat and a filler metal (whose melting temperature is above $\approx$ 450 °C but below the melting point of the metals being

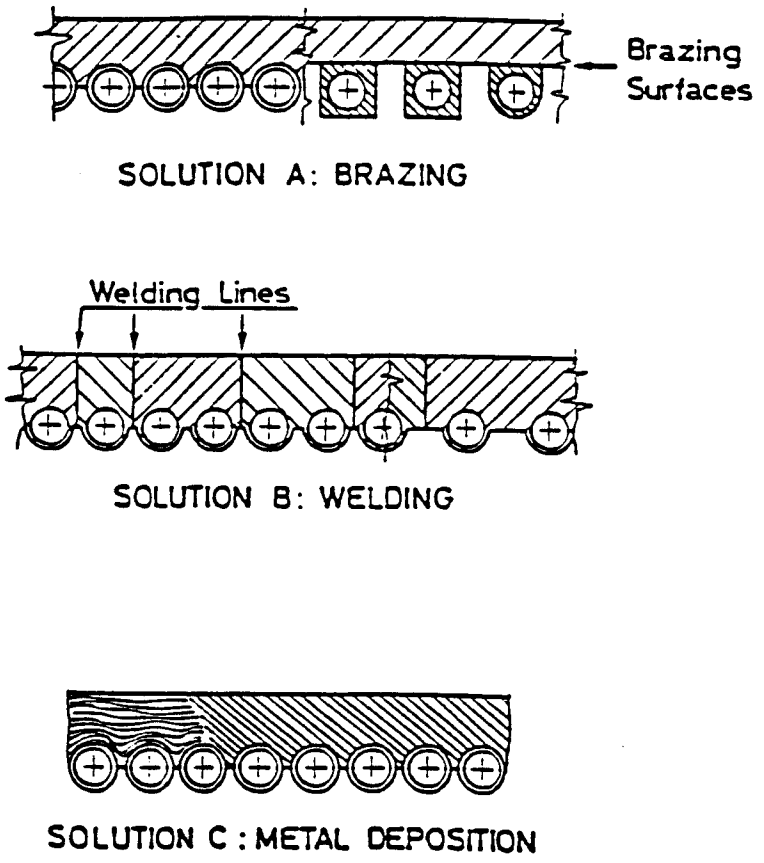

Figure 3.2: Different technological options for the first wall panel [7]

joined). The process has the following advantages: Brazed joints are (1) strong, (2) ductile, (3) easy and rapid to make, (4) suitable for dissimilar metals, (5) one-operation processes, (6) performed at relatively low temperature, (7) economical, (8) adaptable to automated methods, and (10) since no melting occurs, base metals retain all their physical properties basically unchanged.

Brazing in the fusion field has the following advantages: (1) it eliminates welds close to the plasma, (2) good contact between the armor tiles and the substrate helps keep the surface temperature low, (3) it offers a great deal of flexibility in the choice of different materials combinations. However, brazing suffers from the following drawbacks: (1) it requires a major R&D effort involving critical issues such as joint gap control, irradiation effects and repair, (2) it is not a preferred method for materials combinations where one of the materials is much thinner than the other, as in a thin coating, (3) It is difficult when complex contours are required, and (4) scale-up to an industrial process may also be a problem.

3.2.2.2 Plasma spray

A plasma [8] is a gas of sufficient energy content such that a significant fraction of the species present are ionized and hence are conductors of electricity. Figure 3.3 shows the plasma density used in the spray process compared with the other types of plasmas. There are basically two types of plasma for this application: (1) high pressure, thermal or equilibrium plasma (e.g., encountered in welding arcs, plasma torches), and (2) low pressure, non-equilibrium plasmas (includes glow discharge).

Thermal spray [2], is a generic term for a group of commonly used processes for depositing metallic and nonmetallic coatings. Thermal spray coatings are formed (Figure 3.3) by melting the particles, accelerating them to high velocities in a gas stream and "impacting"

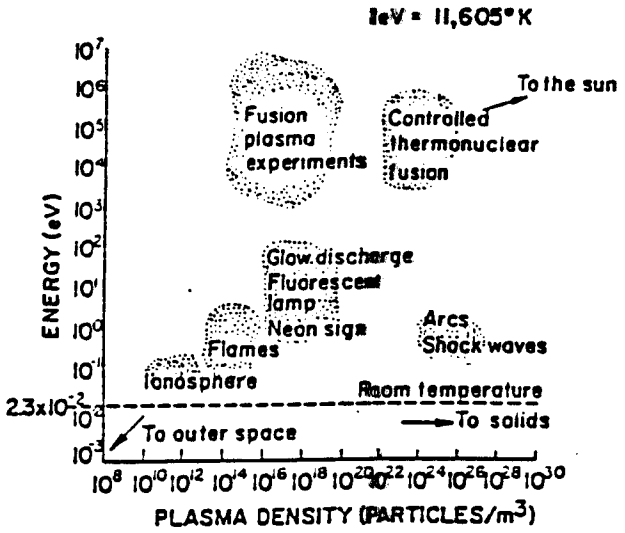

Figure 3.3: Energy-density diagram of the plasma state [8]

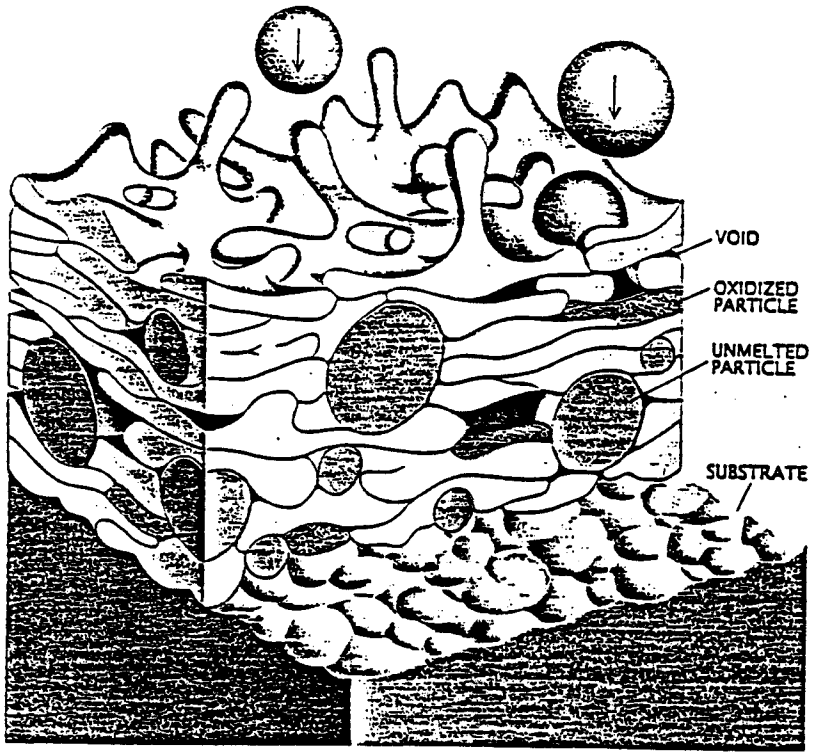

Figure 3.4: plasma-sprayed coating structure [9]

them against the substrate where they rapidly cool. The result is a coating comprised of overlapping lenticular cooled particles which are fused to each other. Thermal spray coatings exhibit two common features; a "sandpaperlike" surface finish and inherent porosity.

The characteristics of plasma-sprayed coatings are [2]: Low density deposits may be 50 - 60% dense with many open (connected) voids. Higher density material may have 80-90% density with closed voids while high density materials > 95% will have some closed porosity. Lamellar microstructure is formed with possible internal microcracking. It should be noted that plasma-sprayed coatings are affected by the spray environment. Coatings sprayed in a vacuum (actually a low-pressure atmosphere of an inert gas) are much denser and more homogeneous than the coatings sprayed in air, which contains voids and oxidized patches. In a vacuum the droplets travel faster and spread out more thoroughly when they strike the surface; in addition there is no air to be trapped in the coating or to react with it [9].

Plasma sprayed coatings offer many advantages [2]: (1) almost any material with liquidus range can be sprayed, (2) materials may be mixed or graded, (3) the process has the ability to coat large areas and to form thick layers, (4) substrates can be heated or maintained at low temperatures, (5) relatively high density (> 90%) coatings can be applied, and (6) there is much less of a risk in degrading the coating and substrate than in many other high-temperature processes, because the gas in the plasma flame is chemically inert and the target can be kept fairly cool. On the other hand, the plasma spray processes still have some disadvantages [2]: (1) materials with narrow (or no) liquidus range can not be sprayed, (2) materials that decompose can not be deposited, (3) materials with a high vapor pressure are difficult to spray, (4) line-of-sight deposition process limits the useable geometries, (5) some materials are very process sensitive (particle size, stand-off distance, feed rate, power input), (6) there is a possibility of incorporating and reacting with the environment, (7) surface

preparation is required for adhesion (rough surfaces), (8) deposits are not fully dense and may have poor mechanical properties, and (9) deposits may require densification (hot isostatic pressing) or void filling.

3.2.2.3 Welded structure

Since all candidate alloys for heat sink materials have high thermal conductivity, welding is difficult because of the heat sink effect of the surrounding material [10]. Electron beam (EB) or laser welding are preferred due to the following: (1) it reduces the extent and distortion of the heat-affected zones, (2) there is an extensive data base available on the welding process.

3.2.2.4 Diffusion bonding

Diffusion bonding is divided into two categories [5]: liquid phase and solid state. Liquid phase diffusion bonding is a variation of brazing in which a dissimilar metal combination within the joint region reacts to form a transient, relatively low-melting liquid phase. As time progresses, interdiffusion of elements between this transient phase and the base metal gradually raises the solidus temperature of material in the joint region to a point above the bonding temperature.

In the solid state bonding process pressure is applied at an elevated temperature to produce the bond. The bond forms in three major stages. In the first stage, initial contact is made and there is an immediate yielding of surface irregularities. This localized deformation breaks up surface films and creates limited areas of intimate metallurgical contact. In the second stage, a time dependent creep deformation greatly increases the contact area. Finally, the original interface is eliminated by one or more diffusion-controlled mechanisms such as

grain growth across the interface, the solution or dispersion of interfacial contaminations, or by simple diffusion of atoms along or across the interface.

Diffusion bonding has the following advantages: (1) it produces very high quality joints, (2) like brazing, it has been used for both metal-metal and ceramic-metal joining, even though the data base for the second type is limited, (3) in some instances; the process temperature is lower than brazing. This may be suitable for materials such as copper. Major disadvantages of this process are: (1) it is more expensive than brazing and there are practical limitations on the size and geometry of the surfaces to be joined, also, (2) there is a major problem for bonding ceramics to metals where there is a large mismatch in the thermal expansion, and (3) problems such as the formation of brittle intermetallic compounds, insufficient atomic mobility, or extremely stable surface oxides often occur [5]. In systems which form brittle intermetallic compounds, an intermediate layer can be used to restrict interdiffusion of the offending elements.

Finally, it should be noted that erosion is the primary issue that drives coating fabrication requirements in the fusion field. Since the accuracy of erosion predictions cannot be adequately evaluated on the basis of existing experimental data, the only prudent course of action is to continue to develop technology to apply thicker coatings of plasma side materials. This approach aggravates the thermal stresses in coated materials.

3.3 Interfaces

The topic of interfaces in materials is a very broad one: indeed, if one excludes single crystal research, one could claim that the balance of the field of metallurgy relates to interfacial properties [11]. Generally, the interface is a mathematical plane and can be realized only in

the case of a nonsoluble/noncompound combination. On the other hand, an interfacial region possesses a certain thickness, and its mechanical properties are different from those of the continuous phases [12]. Interfacial regions may be classed as [13] mechanical, monolayer-to-monolayer (abrupt), compound, diffusion, or pseudo-diffusion and combinations of these types. Other features include:

(1) The mechanical interface is characterized by mechanical interlocking of the film material with a rough surface. The strength of this interface will depend on the mechanical properties of the materials.

(2) The monolayer-to-monolayer (abrupt) interface is characterized by an abrupt change from the film material to the substrate material in a distance on the order of the separation between atoms. It may be formed when there is no diffusion and little chemical reaction between the film atoms and the substrate surface. Thus, defects and stresses will be confined to a narrow region.

(3) The compound interface is characterized by a constant composition layer, many lattice parameters thick, created by the chemical interaction of the film and substrate material. Often during compound formation there are segregations of impurities at the phase boundaries and stresses are generated due to lattice mismatching. Porosity may develop in the interfacial region.

(4) In the diffusion type there is a gradual change in composition, intrinsic stress, and lattice parameters across the graded interface.

(5) Under more energetic situations such as ion bombardment, a pseudo-diffusion type interface may be formed by materials which are normally insoluble.

It is convenient to categorize the interfaces on the basis of the nature of the phases that they separate [14]. What is of interest for the bonded structures in the fusion field is the phase boundary between two different solids. It is usually characterized by 5 orientation

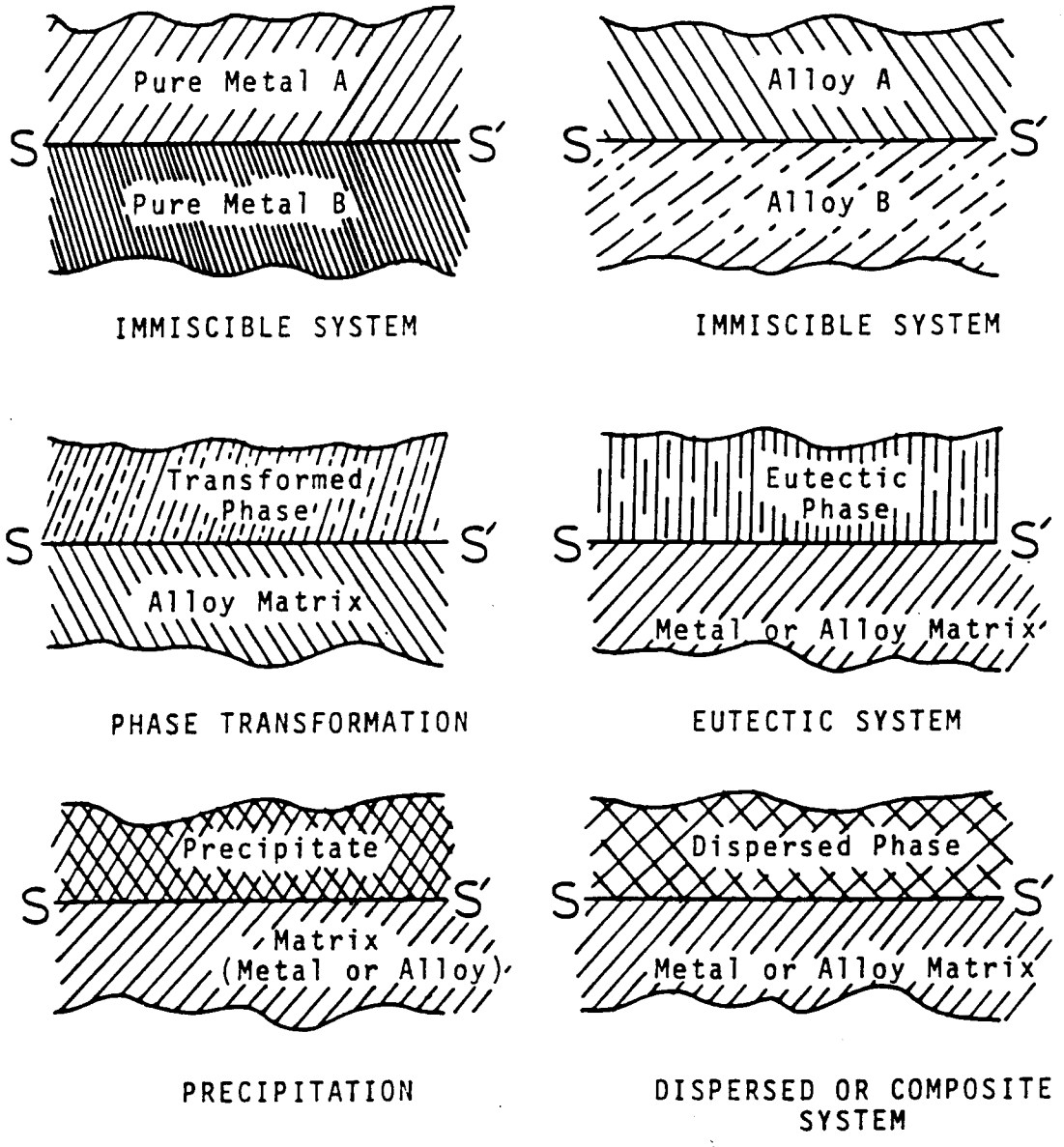

Figure 3.5: Idealized cases giving rise to interphase interfaces. In all cases the phases may have the same or different crystal structure and different lattice parameters if both are solids [16].

parameters and two chemistry/structure parameters [see reference 15 for more details]. Various general examples of heterogeneous systems in a simple two-phase situation are illustrated in Figure 3.5 [16].

3.3.1 Structure of interfaces

The inherent structure of boundaries and their dependence on the crystallographic relationship of adjoining phases is a topic of active concern [17]. Microstructural features at the interfaces such as cracks, debonded areas and intermediate reaction layers can strongly influence the mechanical properties. The mechanical behavior of many materials, including single-phase polycrystals and multiphase composite materials, is influenced by the ability of the grain- or phase-boundaries to either withstand the stresses generated across them or to accommodate the differences in strain of adjoining grains, thus preventing the build-up of localized stresses [17]. When considering the adhesion of a bonded structure, we must consider the mechanism of the failure at the interface, and since this failure is controlled by the structure and composition at the interface, the understanding of the interface structure should be the goal in any bonded structure evaluation program.

The study of the interface structure includes the description of the crystallinity of solute atoms and of the local atomic arrangements and directionality of bonding of segregated or adsorbed species at the interface. The interface structure is even more complex when one considers the interface kinks and steps which also play an important role along the interface [18]. In the perfectly general case between two phases, there is generally no systematic crystallographic habit or orientation characterizing the interface. Phase boundaries are distinct from grain boundaries, however, because they separate regions of different crystal structure or composition, or both. Despite these differences, phase boundaries possess structural characteristics that are conceptually identical to grain boundary structure. These include

dislocations, ledges, and coincidence units or predominant interfacial portions which lie along particular sets of {*hkl*} planes defined in the matrix or a reference phase [16].

Information on the structure of metal-ceramic interfaces (and interfaces in general) is still quite limited, especially compared to the structure of grain boundaries. One of the difficulties with these studies is that more factors which might control their structures have to be considered than are relevant for grain boundaries, e.g., (1) differences in lattice parameters, thermal expansion coefficients, elastic constants between the the two materials at the interface, (2) chemical reactions at the interface, (3) processing factors, such as temperature, pressure, and (4) surface conditions before interface formation. [19].

Interphases may be classified (according to the structure along the interface) as: (a) coherent, (b) semicoherent, or (c) incoherent [20]. At a coherent interface, rows and planes of atoms continue across the interface but change direction locally. The solids on either side of the interface must have similar lattice parameters. The small amount of mismatch is accommodated by elastic distortion. The conditions which lead to a coherent interface, between a thin film on a thick substrate or between a small precipitate and the surrounding matrix, favour formation of a semi-coherent interface for thicker films and larger precipitates. It becomes energetically favorable to accommodate a larger fraction of the mismatch by a dislocation array. An incoherent interface is a narrow, highly-disordered region, which can not be described simply as an array of dislocations because the mismatch is too large [20].

An important property of some types of interfaces is that they can act indefinitely as defect sources or sinks [20]. A coherent interface cannot be regarded as a defect source or sink since it contains no sites where defects can be created or annihilated. Semi-coherent

interfaces are not ideal sources or sinks for defects when there are infinitesimal departures from equilibrium defect concentration. Incoherent interfaces are ideal defect sources or sinks.

3.3.2 Chemistry of interfaces

The composition of grain boundaries (as well as interfaces) in a material are often quite different from the composition of the matrix (or the neighboring materials in case of interfaces). This difference occurs as various solute elements diffuse to the boundary and become trapped there. This trapping occurs because it is energetically favorable for the solute to remain in the grain boundary rather than diffuse back into the matrix. In particular, impurity elements often become very enriched at the grain boundary. The process by which this enrichment takes place is known as grain-boundary segregation [18].

Segregation may simply be the Gibbsian type adsorption, where the reduction in interface energy is the driving force. The quantity of solute associated with such segregation is usually small. In several instances, the extent of segregation normal to the interface has been found to be very small, usually no more than the width of the lattice imperfection near the boundary width as shown in Figure 3.6 [18]. Nonequilibrium segregation can occur in many materials due to solute-vacancy interactions and insufficient time allowed for achieving equilibrium as in irradiated materials [18].

The consequences of the segregated species on the performance of the material depend very much on whether or not the segregant amplifies or relaxes the local stresses associated with the disturbance in ideal crystal ordering at the interface. Thus, grain boundary embrittlement may be caused by the adsorption of relatively large atoms; the chemical potential of the solute in the disordered interface is less than in the close-packed lattice but it is thought to cause a dilation of the boundary and thereby reduces its cohesive strength. The

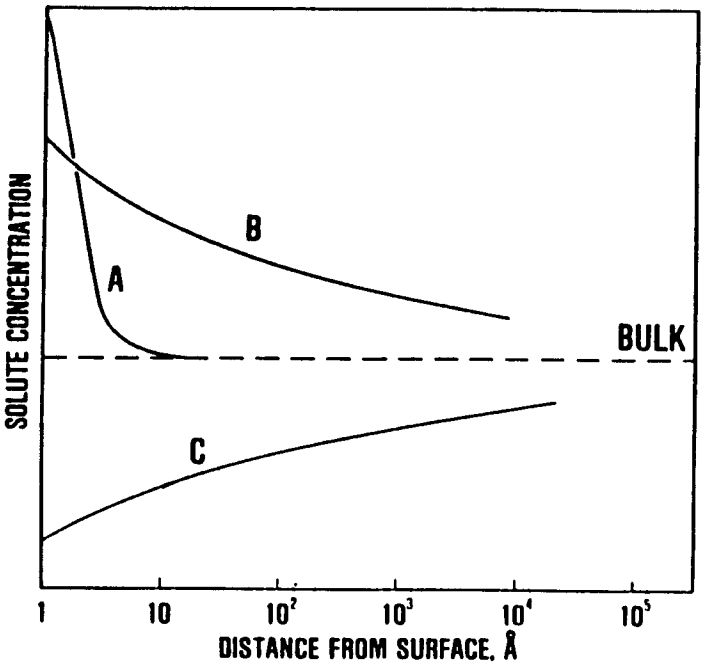

Figure 3.6 Schematic showing some common solute distributions near an interface.

A: Gibsian type adsorption. B: Nonequilibrium segregation. C: Solute depletion [18]

embrittlement is usually manifested by a loss in fracture toughness accompanied by a change in failure mode from transgranular to intergranular [21]. Small atoms may fill the relatively open interface structure causing some relaxation of the local stresses which strengthens the material [17]. Generally speaking, the role of segregation of impurities to an interface in controlling the adhesive strength of that interface is only very poorly understood [21].

The migration of a grain boundary phenomenologically involves the transfer of atoms of one grain or crystal lattice to another grain or crystal lattice. This can be accomplished ideally by the transfer of groups of atoms by a simultaneous movement of atoms from the boundary region to the ordered lattice, or the movement of dislocations by glide or climb into lattice. Boundary migration can also occur by the transfer of single atoms across the interface from one grain or the other either by a mass transfer process where each atom moves from a site in the boundary, associated with one lattice configuration into a new site in the interface associated with the other lattice. It could also occur by a vacancy-diffusion mechanism [16].

Diffusion-induced grain-boundary migration (DIGM) is one of many phenomena that may occur during the diffusion of a solute in a polycrystalline material. In any diffusion process in which there is substantial solubility of the diffusing species and in which the lattice parameters of the solid solution vary with composition, high stresses can develop wherever diffusion is significant. One possible response to these stresses is dislocation generation and plastic flow, which can even lead to recrystallization. However, when lattice diffusion is orders of magnitude slower than grain-boundary diffusion, the high stressed regions in the material are confined to thin slabs at the grain boundary; in this case grain-boundary migration can occur. When neighboring segments of the same boundary migrate in opposite directions, characteristic "wavy" boundary morphologies are frequently produced [22].

One would generally expect that either segregation or precipitation at grain boundaries along interfaces would restrict the motion of boundaries. In one case, there would be a solute drag effect whereby a boundary would continue to move but it would be necessary for the solute to be pulled along. In the case of a precipitate or void, these defects are usually left behind and create an area of grain boundary equivalent to the area occupied by the void or precipitate [23].

One of the interfacial effects at elevated temperatures is the diffusion along the interface accompanied by the production of nonequilibrium vacancy concentrations [11]. This has several consequences. First, the effective diffusivity will differ from the value usually measured in the case where a near equilibrium of vacancies is maintained. Secondly, the local equilibrium concentration of atomic species at the interface can be modified by the vacancy supersaturation [11]. Also, the concentration of impurity ions at various kinds of interfaces is expected to be higher than the lattice concentration, depending on factors such as size effect, modulus interaction, etc. [20].

3.3.3 Mechanics of interfaces

For a joint formed by several materials, with different characteristics of deformation-resistance and deformation-rate, the stresses caused by externally applied loads are nonuniformly distributed [6]. Besides external stresses generated during their life time, bonded structures will originally be subjected to intrinsic stresses. In addition to thermal stresses (generated during and after fabrication) other sources of intrinsic stresses are: (1) incorporation of atoms, for example, residual gases or chemical reactions, (2) differences of the lattice spacing of the substrate and coating, (3) variation of the interatomic spacing with crystal size, (4) recrystallization processes, (5) microscopic voids and special arrangements of

dislocations, and (6) phase transformations [24]. In the following section, the influence of interfaces (between grain boundaries) on mechanical properties will be discussed.

3.3.3.1 Induced stresses at interfaces

When a surface is modified or a coating is deposited on a surface, it is usually found that the system develops a unique form of stress gradients. The total stress state is due to two factors. The extrinsic stress is that which is developed between two materials having different chemical properties being bonded together. The stress may be due to thermal expansion differences and a temperature change or may be due to lattice parameter changes. This type of bimaterial stress is not dependent on the stress state of the individual materials and will not change with annealing (if there is no plastic deformation). Intrinsic stress; on the other hand; is the stress developed in a material due to atom displacement from equilibrium lattice sites, from a grain boundary, or from defect strains [3].

One of the general features of solid-solid interfaces is the generation of incompatibility stresses because of elastic and plastic anisotropy [11]. Qualitatively, the incompatibility elastic stresses are maximum at the interface and decrease continuously with distance from the interface. There are a number of consequences for these stresses. The shear stresses acting in the plane of the interface, would tend to lead to interface decohesion. A phenomena also involving the concept of compatibility at an interface is that of image stresses acting on dislocations near interfaces [11]. The image effect is easy to rationalize qualitatively. A dislocation near an interface has a strain field extending into both phases along the interface. The strain energy in the harder medium is larger per unit displacement because the elastic constants are larger. Hence a dislocation in the softer medium is repelled from the interface to reduce the energy of the system, while a dislocation in the harder medium is attracted to the interface for the same reason. Thus, the image stresses or elastic

incompatibility stresses can produce strong repulsive forces acting on a single dislocation. Also, these stresses may induce local cross slip or climb and the jogs formed in these processes can pin or impede the glide of the dislocation [11].

3.3.3.2 Interface hardening

The presence of an interface can serve as both a source and a sink for dislocations, and the flow or work hardening of a metal or alloy can be related to the efficiency of dislocation generation or obstruction at the interface [16]. Because of this production and densification of dislocations along interfaces, an effective hardening can be observed. The boundary region (region adjacent to the interface plane) becomes hardened because the internal elastic stresses resisting flow are greater there, and because the local flow stress to penetrate the dislocation forest and tangles adjacent to the interface can be relatively larger in that region than in the bulk [16].

Another contradicting phenomena is the softening along interfaces due to vacancy annihilation [16]. Also, softening could occur as result of a very high ledge (source) density in the grain boundaries which give rise to an initial easy glide condition and acts as a stress relief mechanism at the boundary.

3.3.3.3 Stress relaxation across interfaces

The application of a shearing stress to a structure containing an interface may make the relative glide of the two grains possible on opposite side of the interface. Such movement may be regarded as a consequence of the inability of an interface to maintain a shearing stress across it; the process is known as stress relaxation across an interface and occurs in the following manner: immediately upon application of a shear stress to a material which surrounds an interface, a uniform state of stress is set up within the material. If the interface

is unable to maintain the shear stress across it, a subsequent readjustment occurs by which the stress over most of the interface goes to zero; stress is, therefore, concentrated at the boundary of the interface and an increase in the over-all shear strain is produced. This strain is recoverable; when the applied stress is removed, a residual stress, of opposite sign to the applied stress, will exist across the interface. Such a condition can not be sustained any more than that which existed when the original stress was applied; the interface must, therefore, perform a reverse relaxation which returns it to its original state. The kinetics of the process are closely associated with the actual structure of the interface [25]. Stress relaxation across grain boundaries must be taken into consideration if one wishes to study the elastic properties of polycrytalline substances, particularly at high temperatures [25].

3.3.3.4 Fracture

Fracture is composed of crack initiation and propagation. Initiation will begin at a flaw which allows stress concentration or bond weakening. Propagation of the fracture will occur by repeated bond breaking [13]. Fracture in metals and alloys has been traditionally characterized by two modes: ductile and brittle. Ductile fracture, which normally characterizes metals and alloys, is associated with dislocation motion (slip) and residual necking, and there is no-long range association of microcracks with crytallographic or interfacial phenomena. Cracks that do develop during ductile failure are characterized by plasticity effects which involve the movement and concentration of dislocations at the tip of the advancing crack [16]. Brittle fracture, on the other hand, is associated with elastic stress behavior, that is, a lack of readily recognizable dislocation motion.

Two criteria must be satisfied before fracture takes place. First the energy balance must favor the occurrence for fracture. Secondly, an atomic mechanism must be possible whereby the fracture process can operate [26]. A fracture will preferentially propagate in a

plane of weakness such as might be found in an abrupt interface, an interface with a large number of voids, or a region of high intrinsic stress [13]. Pores in the interfacial region act not only as crack initiators and stress concentrations but allow interfacial cracks to be propagated parallel to the direction of the applied stress [13]. Segregated atoms can lower the fracture strength of a grain boundary by weakening the grain boundary bonding [16]. In addition, the structure itself, like the structure of a free surface, can nucleate cracks which, if they propagate along the interface, are aided by the cohesively weak interface [16].

3.4 Adhesion

The interfacial adhesion between coating and substrate is of unique significance to coatings. The ASTM Definition of Terms Relating to Adhesives [11] defines adhesion as " the state in which two surfaces are held together by interfacial forces which may consist of valence forces or interlocking forces or both". Adhesion is a general term used for a solid substrate to which other materials adhere; and Mittal [11] has suggested the term adherate to represent the material which adheres to an adherend. In this case, the thinner phase is called the adherate. Examples are thick films and coatings. Adhesive is a special kind of adherate in that it adheres to two adherends instead of one. It is very important to differentiate between an adherate-adherend combination-called adhering system- and an adhesive joint (expressed in short term as adhint), because ideally in the former there is only one interface and two bulk phases, whereas in the latter there are two interfaces and three bulk phases. It should be pointed out, however, that in many real situations, there are additional interfaces and interphases present.

Adhesion is a macroscopic property that depends on the chemical and mechanical bonding across the interfacial region, the intrinsic and applied stresses and stress gradients

and the adhesive failure mode [27]. Good adhesion is attained when the interfacial region or nearby materials does not fail under service conditions. It is promoted by: (1) strong bonding across the interfacial region, (2) low stress gradients either for intrinsic or applied stresses, (3) absence of easy fracture modes, and (4) no long term degradation modes [27].

Bonding between unlike atoms and materials may be due to chemical, electrostatic, or polarization bonding. In chemical bonding the interaction is due to the transfer or sharing of electrons. Electrostatic bonding is due charge separation and the resulting electrostatic attraction. Polarization bonding is due to asymmetry in the electric field around atoms or molecules and the resulting attraction [13]. In the case of metal-ceramic interfaces, the bonding can be classified into two categories: "reactive" where compounds are formed, and "non-reactive" where compounds are not formed. The latter case, while being the simplest to consider since it involves only physical interactions between atoms or ions, is still important in practical applications. It must be realized that some systems may fit into either category depending upon the equilibrium state of the species, which is determined by whether an oxidizing or a reducing atmosphere is present [19].

There are essentially two aspects of an adhesion study program: understanding of the factors affecting adhesion and thereby improvement of adhesion strength, and the measurement of adhesion strength. In an adhering system, adhesion can be expressed in terms of forces or work of attachment, or in terms of forces or work of detachment. If expressed in the former manner, then the terms "basic adhesion" or "interfacial adhesion" can be used. Basic adhesion signifies the interfacial bond strength and should depend exclusively on the interfacial properties, without any contribution from any other sources. Unless there is a well-defined interface between the adhering phases, the term basic adhesion does not have any significance. Basic adhesion should be independent of the thickness of adherate,

thickness of adherend, specimen size, specimen geometry, temperature, measurement technique, manner of applying external forces, manner of performing the test, test rate, bulk properties of adhering phases, etc. However, the so-called adhesion measurement techniques measure practical adhesion, which is affected by all these factors [11].

Two kinds of information are obtained in measurements of force or energy of adhesion. One is quantitative- the numerical value of the force or energy. The other is of a very different nature- it is the location of the failure, for example, whether or not separation occurred at the interface between two phases [28].

The residual strength of a bond [29] is that remaining when the inherent strength has been reduced to allow for these internal stress factors. The measured strength of a bond will always be different from this residual strength. In the process of stressing the bond, the various internal stresses will be altered before it breaks. Usually, the internal stresses are increased and the measured strength is less than the residual strength. The relationship of the factors is shown in Figure 3.7.

3.4.1 Adhesion of brazed joints

Coalescence in brazing is an interface phenomena due to adhesion and/or diffusion between the base metal and the filler metal. Under suitable operating conditions, a perfect bond can be obtained by simple adhesion, due to the molecular forces acting at the interface of the two metals. In practical brazing, however, it is the diffusion between the atoms of the base metal and of the filler metal which plays the decisive role, even if the diffusion depth does not exceed a few lattice constants [6].

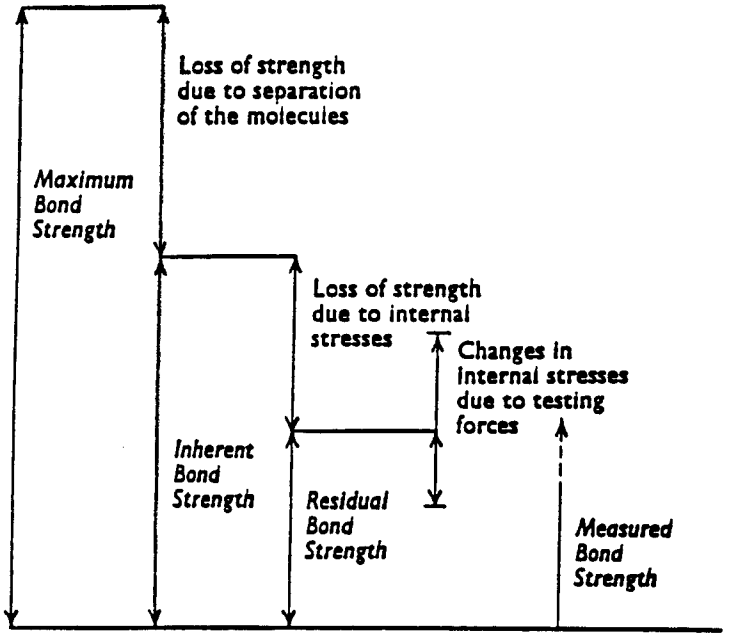

Figure 3.7: Relations between bond strength factors [29]

As atoms from the base metal migrate by diffusion into the filler metal and vice versa, changes in the properties of the boundary layer between the two metals may occur. This can sometimes affect the joint strength by formation of brittle intermediate phases. In other cases, one can obtain, deliberately or not, a high joint quality [6]. In either case, the strength of the joint no longer depends upon the bond strength between the base metal and the filler metal. Instead it depends upon the bond strength between either of these and the newly formed intermediate layer [6]. Another point of interest for the newly formed compounds, is the irregularity that these structures may take. Thus, upon stressing, these structures may produce unpredictable stress conditions which affect the strength of the joint [6].

3.4.2 Adhesion of plasma sprayed joints

As the molten or semi-molten plastic-like particles in a plasma spraying process impinge upon the substrate, one or more of three possible bonding mechanisms (depending on the process, coating material, and substrate composition) cause a coating to build up: [30]

1. Mechanical bonding occurs when the particles splatter on the substrate. The particles interlock with the roughened surface and/or other deposited particles, forming a coating.
2. With some combination of substrates and coating materials, localized diffusion or alloying can occur.
3. Some bonding may occur by means of Van der Wals forces. This is similar to the mutual attraction and cohesion which occurs between any two clean surfaces in contact.

Another point of interest for the performance of plasma-sprayed coatings is that the inherent porous nature of these coatings (especially those which are air sprayed) will toughen

the material by interrupting the propagation of cracks that inevitably form as the material is strained [31].

3.5 Adhesion failure

In general, failure of a system can either be by yield, when the flaws present in the system facilitate the slipping of one layer of the material over another or it can be by fracture in which case the flaws act as stress concentrators so that the flaw can propagate as a crack under a comparatively low load [32]. The failure mode depends on the interfacial structure and the stresses to which the interface is subjected [27]. These stresses can arise during the change of state at interfaces: (1) because of changes of temperature causing different expansions of the two materials, (2) through changes of composition, and (3) from the slower changes which occur during 'ageing' [33]. If the coating is under a residual tensile stress, there are at least four possible mechanisms by which failure can occur as shown in Figure 3.8. For example, a brittle coating may fracture by the development of cracks through the thickness of the film. Tougher coatings may fail by delamination along the interface or even by the propagation of a crack within the substrate. The failure mechanism associated with a compressive stress in the coating involves simultaneous buckling and delamination. Conditions may be such that more than one mode of failure is energetically favorable. Under these conditions, kinetics effects become important and failure will be dominated by the mechanism that has the faster kinetics of crack growth.

Evans and coworkers [34] pointed out that in the absence of buckling, and for planar interfaces, there is no driving force for growth of a delamination which exists at the coating-substrate interface; this initial delamination may arise because of interfacial contamination or by void formation and coalescence. Consequently, for such interfaces buckling becomes a

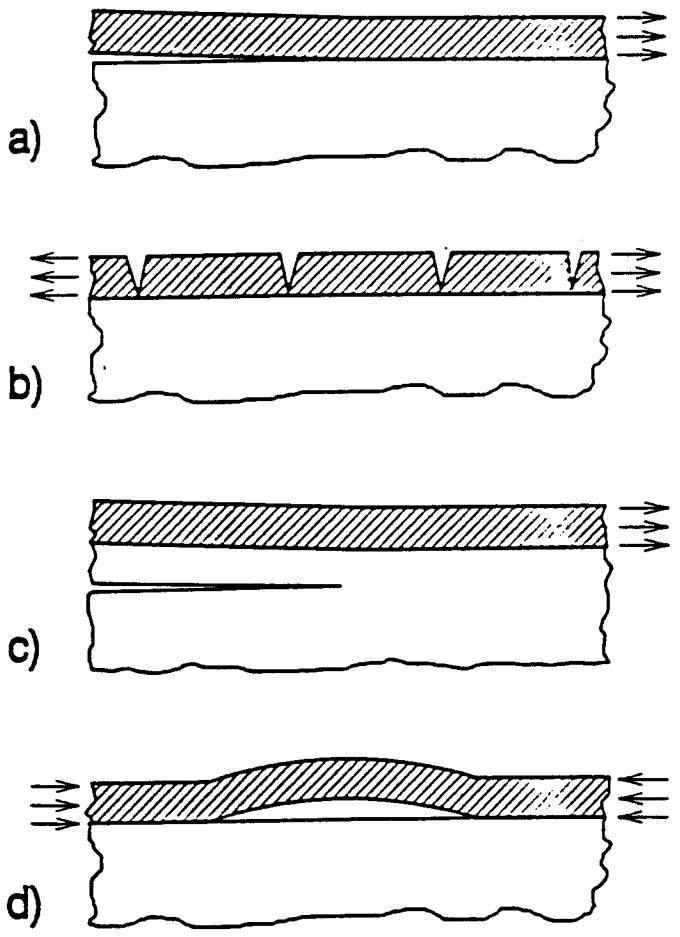

Figure 3.8: Four general types of failure that may occur in coated systems: (a) delamination of the interface; (b) multiple cracking of the film; (c) substrate cracking; and (d) film buckling and associated delamination [36]

prerequisite for fracture propagation and eventual spalling. A complicated case may arise when the deformation modes are different between the coating and the substrate. This is manifested for a metal-ceramic interface where the metal deforms by plastic deformation and the ceramic by elastic deformation [35].

If separation takes place in the bulk (usually in the weaker phase); this is termed cohesive failure [12]. An actual locus of failure may be in any of five different regions (see Fig. 3.9). This figure is drawn for a film on a solid, a system in which each phase is assumed to be uniform as to composition and molecular orientation. In regions 2 and 4, local mechanical behavior is influenced appreciably by the presence of the interface and of the other phase. For example, if phase B has a much higher Young's modulus than phase A, then in region 2 there is a serious constraint on the Poisson's contraction of the matter under tensile loading. This influence, of course, increases as the interface is approached [28]. In any case, visual inspection is inadequate to ascertain the locus of failure in a separated system, and the techniques like electron spectroscopy for chemical analysis, Auger electron spectroscopy, or secondary ion mass spectrometry should be employed for this purpose [11].

3.6 Screening tests for bonded structures

One of the major challenges for the study of interfaces is the development of experimental tools to characterize the in situ properties, keeping in mind that they can differ substantially from bulk properties. A complete picture of an interface can only be obtained by combining different types of analysis [17]. That is why the collaboration of many laboratories is required to characterize bonded structures in the fusion field [37]. Screening tests for bonded structures can be divided into two broad categories [33]: (1) physical and metallurgical examinations (see Table 3.1), and (2) functional tests. The requirements

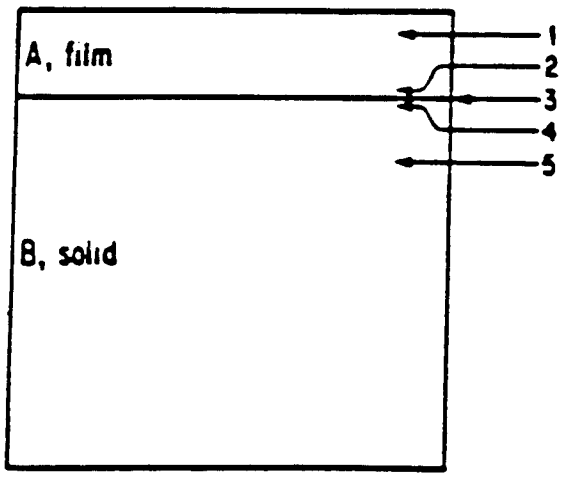

Figure 3.9: The five possible regions for the locus of failure [11]

Table 3.1: Physical and metallurgical examinations [33]

Coating thickens and its uniformity (gauge or cross-section)
Coating porosity
Surface roughness (stylus or optical methods)
Surface hardness (Brinell, Rockwell, Vickers, Knoop)
Ductility or toughness (pull test)
Coating-to-substrate adhesion
Grain structure (acid etching and microscope examination)
Elemental analysis (energy dispersive analysis of X-rays or EDAX, Auger)
Compound analysis (electron spectroscopy for chemical analysis)
Crystal structure (X-ray or electron diffraction, or transmission electron microscope)

demanded of a bonded interface vary with the application and this fact has naturally modified the inspection approach. Strength of bond is, to a greater or lesser extent, generally the underlying requirement. No completely satisfactory solution has yet been found to test this property. One is consequently obliged to approach the problem indirectly by trying to find a property which is directly related to strength. The most obvious secondary characteristic to work on is the extent of the bond. It is reasonable to assume that if parts of the interface are not physically joined together the strength will be proportionally reduced [38].

3.6.1 Adhesion tests

Investigation of adherence should be conducted under actual and/or closely simulated service conditions to the extent feasible. An ideal test for measuring practical adhesion should be [2]: (1) reproducible, (2) quantitative, (3) nondestructive, (4) easily adaptable to routine testing, (5) applicable to all combinations of adherates and adherends, (6) valid over a wide range of specimen sizes, (7) applicable to products and processes, (8) able to measure wide range of practical adhesion strengths, (9) free from interpretational complexities, and (10) amenable to standardization. Furthermore, machining requirements for specimen preparation should be minimum, and no specialized equipment should be necessary. However, such idealization is not realized in practice, as there is no technique which fulfills even half of the foregoing attributes.

Adhesion tests based on fracture mechanics principles are the most likely source of quantitative procedures. Fracture mechanics methods exhibit several attractions. Firstly, an adhesion parameter, such as the interface fracture resistance (or toughness) K_c^{inter} can be defined. Secondly, the potential exists for developing sound, theoretically based, measurements of interface toughness. Finally, fracture mechanics provides a mathematical framework for using the fracture toughness as a design parameter. However, currently

available tests, are of restricted application and are too complex for most purposes [39]. Thus, mechanical methods are commonly used to measure adhesion of the coatings. Practically they measure the force required to remove a coating from the substrate; and can be categorized as follows: peel, tension, lap shear, scratch, and bend tests [33]. See Figures 3.10, 3.11, and 3.12 [40]. Despite the difficulty of predicting the serviceability of a coating from its hardness value, it is probably the mechanical property most often measured [41]. This will be explained later in chapter 7.

In some cases [12], microhardness measurements can be made on a cross-section of the sample. In one technique, a mechanically stable crack is introduced into the coating-substrate interface by the use of conventional indentation procedures; both Vicker's and Brale indenters have been used. The resistance to propagation of the crack along the interface is then used as a measure of adhesion and, by analogy with the fracture resistance parameter and a strength parameter. The fracture resistance parameter relates uniquely to the bonding across the interface, and is more fundamental measure of adhesion, whereas the strength is determined by the combined influences of the fracture resistance, the strength controlling defects and the residual stresses within the coating. The test is based on the rationale that an interface (in the vicinity of the plastic zone created during indentation), with a lower toughness than that of either the film or the substrate material, will be a preferred site for lateral crack formation. When fracture cannot be induced at the interface (but occurs in the film or substrate) it can be concluded that the interface toughness is at least as large as that of the weaker component [34]. A possible advantage of the indentation adhesion test is that the values of the indentation adhesion parameters (load and interface fracture toughness) are insensitive to substrate hardness (at least, compared with the corresponding parameters for a scratch adhesion test) [34].

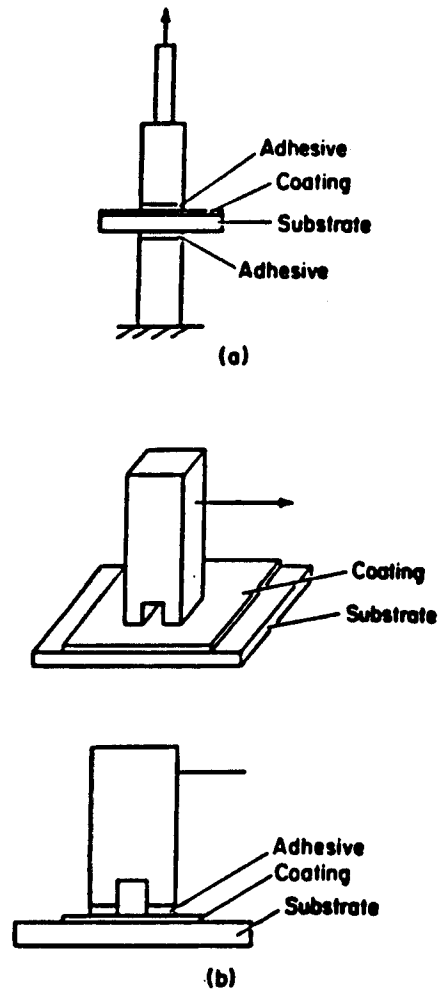

Figure 3.10: (a) Schematic illustration of direct pull-off method. (b) Schematic illustration of moment or tropple method [33]

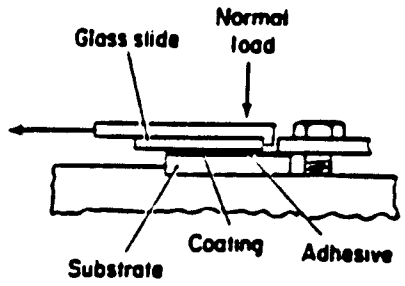

Figure 3.11: Schematic illustration of the lap-shear method [33]

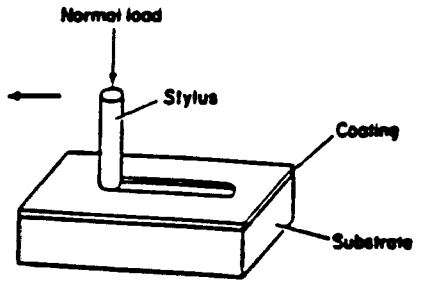

Figure 3.12: Schematic illustration of the scratch method [33]

3.6.2 Structure and composition of interfaces

The complete structural analysis of interfaces requires at least some attention paid to the determination of interface morphologies [42]. The problem of probing through the surface layers to study the interface provides challenging problems [42]. In general, visual inspection is inadequate to ascertain the locus of failure in a separated system [12]. The chemistry of interfaces has been successfully analyzed in many instances [43] with electron microprobe (EMP), scanning transmission electron microscopy coupled with energy dispersive x-ray analysis (STEM-EDX), electron energy loss spectroscopy (EELS), or Auger electron spectroscopy (AES) with sputter depth profiling, and high resolution electron microscopy (HREM). In the following, some features of these techniques will be presented.

3.6.2.1 Transmission Electron Microscopy

The structure along the interface can be probed by high spatial resolution methods of direct imaging using the techniques of electron microscopy. The TEM has persistently maintained its advantage in the study of interfacial structure. Normally, coherent phases will be associated with strain, and these can be studied in detail by contrast analysis [44]. The semicoherent interfaces consist of interfacial dislocations which accommodate the misfit and relieve the strain. The nature of dislocations and their distribution and arrangements provide insight into the properties of the multiphase materials and thus are of both theoretical and practical interest [44].

A few studies incorporating transmission electron microscopy of the interfaces have recently been conducted [45]. A major problem in this type of analysis is the preparation of an electron-transparent TEM specimen that consisted of not only the coating but also the substrate material. This problem was solved in later studies by the development of a method incorporating low-angle ion-beam-milling plus partial shielding [45]. when cross-sectioned

samples are used, the electron beam is made to pass along a direction within the interface, and the image directly shows atomic positions across the bonding region [42].

3.6.2.2 The electron microprobe

One useful technique to study the composition changes along interfaces is the electron microprobe [46]. Although in principle it is a surface analysis tool, it is especially useful in situations where lateral variations in composition are important. Cross sectioning a certain coating/substrate structure would provide such arrangement. Thus, the transfer of particles from one surface to another can be detected and some idea of the location of adhesive transfer can be obtained. Also, the technique does have a rather unique feature in that it can analyze various spots on the surface and do a point by point analysis. [46].

3.6.2.3 Other techniques for compositional determination

The wide range of X-ray wavelengths available with synchrotron radiation plus the low beam divergence and high intensity allows a novel technique for imaging defects or other microstructure in overlayers and interfaces [42]. For impurity detection, the X-ray florescence techniques has a sensitivity of about 1 part per million. The variation with angle can determine whether impurities are uniformly distributed or are segregated at the interface [42].

The use of positrons for studies at interfaces is unique because of two features of positrons: the depth of penetration can be controlled by the positron energy, and; positrons become bound at open volume defects. In a normal experiment, the energy of the positron beam is made high enough so that the positrons are implanted beyond the interface. The trapping of positrons by interfacial defects becomes evident as a decreased number of positrons returning to the surface [42].

Semiquantitative information on long range grain boundary segregation can be obtained using microhardness measurements [18]. However, the method suffers from selectivity of solutes. The measurement can also lead to erroneous conclusions in instances where the surface flow during metallographic preparation interferes with segregation induced hardening [18].

3.7 References

[1] B. B. Glasgow and W. G. Wolfer, Fusion tech. **8**, 596 (1985).

[2] Donald M. Mattox, Short course on films and coatings for science and technology, American Vacuum Society (1986).

[3] S. D. Brown and M. K. Ferber, J. Vac. Sci. Tech. **A3 6**, Nov/Dec (1985).

[4] J. P. Blanchard and R. D. Watson, Nucl. Eng. and design/fusion **4**, 61 (1986).

[5] USA FED-INTOR/82-1 (1982).

[6] Melvin M. Schwartz (Ed.), Source book on brazing and brazing technology, American Society for metals, Metals Park (1987).

[7] G. Casini and F. Farfaletti-Casalli, Nucl. Eng. Design/Fusion **3** (1986).

[8] Julian S. Zekely, An overview of plasma processing, Mat. Res. Soc. **30** (1984).

[9] Herbert Herman, Plasma-sprayed coatings, Scientific American, Sept. 112 (1988).

[10] R. W. Conn, et al., UCLA PPG-815 (1984).

[11] J. P. Hirth, Met. Trans. **3**, 3047 (1972).

[12] K. L. Mittal, in: ASTM 640, Adhesion measurement of thin films, thick films, and bulk coatings (K. L. Mittal, ed.), p. 5 (1976).

[13] D. M. Mattox, in: ASTM 640, Adhesion measurement of thin films, thick films, and bulk coatings (K. L. Mittal, ed.), p. 55 (1976).

[14] M. Mclean in : Proc. on Interfaces in Materials, p. 8, Brussels (1988).

[15] J. Van Landuty, Proc. on Interfaces in Materials, p. 32, Brussels (1988).

[16] L. E. Murr, Interfacial Phenomena in Metals and Alloys, Addison-Wesley publishing company, Massachusetts (1975).

[17] A. Deruyttere and L. Froyen (eds) in: Proc. on Interfaces in Materials, p. 3, Brussels (1988).

[18] A. Joshi, in: A seminar on Interfacial segregation, Materials Science Division of the American Society of Metals (W. C. Johnson and J. M. Blakely, eds.), p. 39 (1977)

[19] F. S. Shieu and S. L. Sass, Acta metall. Mater. **38**, 1653 (1990).

[20] G. B. Gibbs and J. E. Harris, in: Conf. on Interfaces, The Australian Institute of Metals, p. 53, Melbourne (1969) .

[21] D. P. Pope and M. A. Smith, in: Proc. of an International Workshop: Metal-ceramic interfaces, p. 326, Santa Barbara, California, USA (1989) .

[22] M. D. Vaudin, et al. in: Structure and Property Relationships for Interfaces (J. L. Walter ,et al., eds.), p. 329, The Materials Information Society (1991).

[23] D F. Stein and L. A. Heldt, in: A seminar on Interfacial segregation, Materials Science Division of the American Society of Metals (W. C. Johnson and J. M. Blakely, eds.), p. 239 (1977) .

[24] R. W. Hoffman, Mechanical properties of non-metallic thin films, in: Mechanical properties of thin films, Education Committee, American Vacuum Society (1978).

[25] A. S. Nowick, in: A seminar on Metal Interfaces held during the thirty-third national metal congress and exposition, p. 248, Detroit, American Society of Metals (1951).

[26] G. W. Greenwood, in: Conf. on Interfaces, The Australian Institute of Metals, p. 223, Melbourne (1969).

[27] M. Lagally, Metallurgical coatings, course notes, Wendt Eng. Lib., UW-Madison (1981).

[28] R. J. Good,in ASTM 640, Adhesion measurements of thin films, thick films, and bulk coatings (K. L. Mittal, ed.), 18 (1976).

[29] K. W. Allen, in Aspects of Adhesion, in: Proc. of the conference held at Northampton College of Advanced Technology, ECI on 21 and 22 March (D. J. Allen, ed.) **1**, 11 (1963).

[30] James A. Clare and Daryl E. Crawner, Thermal spray coatings, Metals Handbook, 9th ed., American Society for Metals, Vol. 9 (1982).

[31] H. Herman, Scientific American, September (1988).

[32] B. W. Cherry, et al., in Aspects of Adhesion in: Proc. of the conference held at Northampton College of Advanced Technology, ECI on 21 and 22 March (D. J. Allen, ed.) **6**, 80 (1963).

[33] B. Bhushan, in ASTM 947, Testing of metallic and inorganic coatings (W. B. Harding and G. A. Di Bari, eds.), 310 (1986).

[34] D. S. Rickerby, Surf. Coat. Tech. **36**, 541 (1988).

[35] D. C. Agrawal and R. Raj, Acta Metall. **37**, 1265 (1989).

[36] M. D. Thouless, J. Vac. Sci. Technol. **A9 4**, 2510 (1991) .

[37] M. Kaminsky, Thin Solid Films **73**, 117 (1980).

[38] R. S. Sharpe, in Aspects of Adhesion in: Proc. of the conference held at Northampton College of Advanced Technology, ECI on 21 and 22 March (D. J. Allen, eds.), **5**, 25 (1963).

[39] S. S. Chiang, et al., in: Materials Science Research, Surfaces and interfaces in ceramic and ceramic-metal systems (J. Pask and A. Evans, eds.) **14**, 603 (1980).

[40] J. W. Dini, et al., in ASTM 947, Testing of metallic and inorganic coatings (W. B. Harding and G. A. Di Bari, eds.), p. 321 (1986).

[41] G. A. Di Bari, in: ASTM 947, Testing of metallic and inorganic coatings (W. B. Harding and G. A. Di Bari, eds.) 4 (1986).

[42] Coatings and surface modifications, Panel report, Council on Materials Sciences (1984).

[43] F. S. Ohuchi, in: Proc. of an International Workshop: Metal-ceramic interfaces, p. 93, Santa Barbara, California, USA (1989).

[44] C. Thomas, et al., Mat. Sci. Res. **14**, 35 (1981).

[45] A. Erdemir and C. C. Cheng, Ultramicroscopy **29**, 266 (1989).

[46] D. H. Buckley, Surface effect in: Adhesion, friction, wear, and lubrication, Elsevier Scientific Publishing company (1981).

Chapter 4.

Radiation Damage in Bonded Structures

The use of welds and brazes (and bonded structures in general) in the construction of components for nuclear systems has received considerable attention in the past years [1]. The major emphasis, of course, has been concerned with the development of methods for obtaining extremely sound joints, with their long-time integrity being of paramount importance.

Although many of these joints in reactor plants are not subject to a high neutron flux, there are a significant number of them that must be located in high irradiation fields. Very little information is available pertaining to their behavior in such applications. For example, to date, the basis for design welds and brazes in such systems has been based primarily on experience using liberal margins of safety [1]. It is thus apparent that the radiation stability of such joints must be understood to a greater degree.

The requirements for future Tokamak reactors will differ significantly from those for present experiments. In the present devices, there is essentially no radiation damage, few elemental transmutations, the hydrogen ion flux is relatively low and components, generally, are not actively cooled. The principal threat to present components is from disruption heating and the principal impurity injection mechanisms are from thermal effects and sputtering [2].

However, as we move to intermediate and long term reactors, the neutron irradiation problem will become more urgent. The neutron testing requirements for one of the near-

term devices; the International Thermonuclear Experimental Reactor (ITER) are [5]: (1) swelling, differential swelling, (2) property degradation, (3) carbon composite response, (4) lifetime, and (5) thermal fatigue. The effect of neutron damage will limit the selection of future Plasma Facing Components (PFC). It is not clear which, if any, of the present candidates are capable of withstanding high fluence levels, and a major development program is needed. Also, the time to start irradiation experiment is now due to the long lead times required to accumulate high fluence data [5]. It is worth mentioning that materials research should precede machine construction by at least 10 years and typically one irradiation research cycle takes more than 5 years [5].

For PFC's, seven critical neutron damage related issues were identified by Whitley [3]. These issues are (1) structural integrity, (2) thermal shock resistance, (3) thermal conductivity and other physical property changes, (4) dimensional changes, (5) erosion, (6) PMI (Plasma Material Interaction) response, and (7) bonded multimaterial structures. Concerning the last point, the response to neutron irradiation may be quite different than that of the individual materials due to the presence of the interface and the stresses generated by differential swelling. Also, the bonding method (e.g. brazing) will have a significant influence on the residual stresses within the structures. During operation, the performance of the bond is, of course, crucial to the performance of the structure as a whole. At this point, there is very little information available on bond properties or on the irradiation behavior [6]. Fig. 4.1 delineates the fluence-related effects in plasma-facing material.

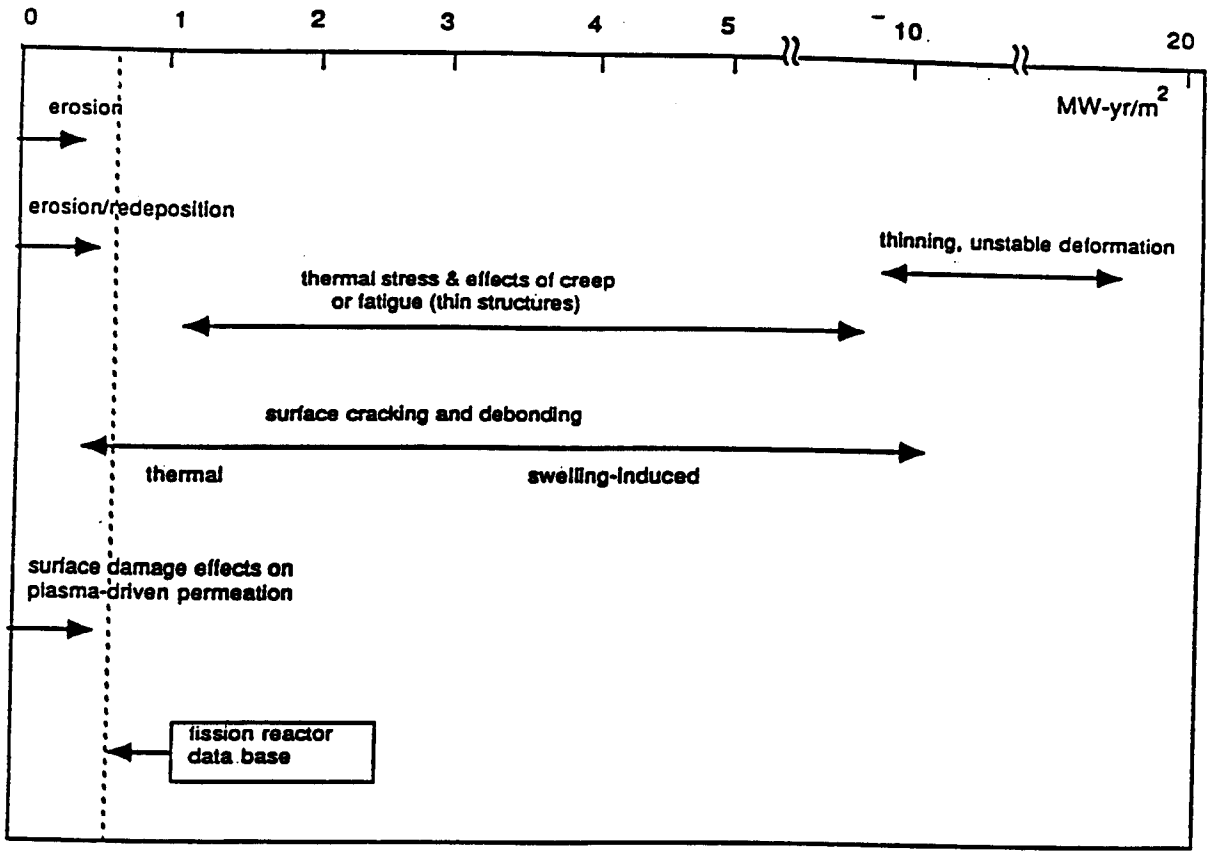

Figure 4.1: Fluence-related effects in plasma-facing components [3]

4.1 Damage mechanisms in bonded structures

The mechanisms of irradiation damage in bonded structures are not well understood. The damage mechanisms that are operative in metallic materials should also produce damage in coatings (e.g., swelling or differential swelling). Since 1975 [7], it was realized that:

> *"additional work is needed on the effects of radiation damage at material interfaces, particularly bonding interfaces. In the vicinity of these interfaces radiation damage will not produce defect clusters, but will also lead to transport of the dissimilar atomic species across the common boundaries, both through enhanced diffusion and through recoil of atoms from collisions with the primary radiations. Further understanding of the role of these effects might have on the degradation of the interface properties is needed to allow meaningful design choices of materials to be used in such applications"*

Mechanisms for the radiation damage mechanisms in a bonded structure that were identified by Mattas et al. [8] are listed below. It should be emphasized that all of them will require more detailed study before a comprehensive model can be proposed.

1. Point defect or transmutation induced stress at coating substrate interface, or within the coating.
2. Irradiation induced changes in mechanical and thermo-physical properties of both coating and substrate. This is particularly important if the duplex system must withstand deformation.
3. Impurity and transmutation product migration to the interface region.
4. Gas migration when interface is under stress or maintains a thermal gradient.
5. Intra-coating stresses as a function of coating thickness.
6. Differential swelling and thermal expansion.

Other possible mechanisms of radiation damage that are of concern here include:

1. Intermixing of atomic constituents and redistribution of gas atoms along interfaces.
2. Evolution of dislocation networks at interfaces due to irradiation.

It is important to note that stress plays a major role in each of these points. Also, various synergistic effects must be taken into consideration. Helium, for example, has an impact on Radiation Induced Segregation (RIS) and swelling. Each of these points should be studied separately to assess its impact, then the overall behavior of the structure taking all these elements into consideration should be done. In the following sections, some probable mechanisms of radiation damage in bonded structures will be discussed. The issue of differential swelling and the impact of stress-enhanced swelling on the irradiation behavior of bonded structures will be discussed in chapter 6.

4.2 Microstructural evolutions due to irradiation

Radiation damage is manifested in a variety of ways, none of which are conducive to long-term structural integrity. Neutron flux influences the mechanical and physical properties of surrounding materials through two processes that occur in the bulk. The first process is associated with atomic displacements, created when a neutron strikes a lattice atom and displaces it from its equilibrium position, forming a vacancy and interstitial. The damage is further multiplied when the struck atom in turn displaces many other atoms. The damage production process depends on neutron energy and is independent of temperature. However, the rearrangement of the damaged zone after the damage production event is strongly dependent on temperature, stress, and other variables [9].

Charged particles [such as heavy ions, electrons and the Primary Knock-on Atoms (PKO's) produced by fast neutron collisions] transfer energy in different ways than neutrons. Fast neutrons have no charge so that they transfer energy to the material only by elastic collisions and have a relatively small collision cross-section. Therefore, they will travel a relatively longer distance in the material and cause a more homogeneous distribution of point defects. Charged particles, on the other hand, transfer energy both by electronic and nuclear processes and the energy transfer rate is a function of the energy of the charged particles. For high energy, the transfer rate is smaller and vice versa. [10]

The defect clusters that form in metals take several forms. The simplest is the small group of vacancies probably formed together at the core of a single collision cascade, which form a small void. As this grows larger it apparently becomes unstable and collapses first into a pancake shaped disc then the center of the disc collapses leaving a toroidal ring of a lattice defect. On a larger scale such rings are known as dislocation loops and certain types of dislocation loops are responsible for plasticity of crystals. Clusters of interstitials have a very similar configuration, they often form a pancake of extra atoms that lie between the planes of the crystal, forcing them apart [11].

Besides radiation damage caused by displacement of atoms, a second process of damage is due to the introduction of foreign atoms. Transmutations are due to nuclear reactions which result from neutron capture and then the decay of the excited nucleus. The transmutation reactions that yield helium, mainly (n, α) reactions, are of greatest importance. These nuclear reactions are dependent on neutron energy only and are unaffected by other components of the reactor environment such as temperature and stress state [9]. A very important class of impurity damage is caused by introduction of the inert gases because they are highly insoluble and precipitate out of solid solution or along grain boundaries to

form small bubbles. In doing this they combine with large numbers of vacancies, and often cause a macroscopic swelling of the crystal [11].

As far as the fusion reactor designs are concerned, the most important parameters with respect to material property changes are generally considered to be displacements per atom (dpa), helium production and, to a lesser extent, hydrogen production. Formation of new transmutation elements can also be important to the metallurgy of an alloy. The damage parameters associated with transmutation generally depend on the location of the relevant material relative to the plasma position, the neutron wall load and operating history [12].

4.3 Impurity and transmutation product migration to the interface region.

The microchemical structure after irradiation will be altered due to several processes. One of them is the radiation enhanced diffusion. As mentioned before, during irradiation many lattice atoms are displaced creating vacancies and interstitials , the concentrations of which often exceed the thermal equilibrium values by several orders of magnitude. This increased concentration of point defects drastically enhances the diffusional processes in the target, which is called radiation enhanced diffusion [13].

The segregation of solute elements to point defect sinks has been observed in numerous alloys after irradiation. As reported in the literature, solute segregation has been found near external surfaces, at grain boundaries, around voids, and around dislocation loops. The experimental evidence, as well as the general physical basis for radiation-induced segregation (RIS), strongly suggests that this phenomena is general and likely to occur in any alloy and even in metals with minor impurities [14].

RIS may occur for two reasons [14]. First, the presence of high supersaturation of vacancies (and interstitials) enhances the mobility of impurities and solute elements. Equilibrium segregation may be too sluggish to occur without irradiation may therefore be speeded up. The second reason for segregation is connected with the continual flux of point defects to sinks. The associated atomic jump processes may preferentially transport certain solute elements leading to their enrichment or depletion at the sinks. The resulting compositional gradients are truly non-equilibrium gradients and require continuous point defect fluxes to the sinks. But even for a continuous and constant irradiation, a truly stationary state may never be achieved since the sink structure changes both in space and with irradiation time besides the segregation itself will lead to a modification of the sink bias factors and therefore directly influence the microstructure evolution.

RIS is an important phenomena for candidate fusion structures because the segregation of certain elements to surfaces, grain boundaries and interfaces do influence physical as well as mechanical properties. The effects could be especially large when continual films of a phase, which may not even be present in the alloy under equilibrium conditions, would start to be formed at interfaces [15]. RIS could have deleterious effects on the creep-rupture, fatigue crack growth rate or ductile to brittle transition temperature of the involved materials [16].

RIS also affects other irradiation mechanisms. Because of the sensitivity of void nucleation to segregation-induced bias modifications, one must inevitably conclude that void formation and swelling is to a large degree dependent on, if not entirely determined by, the radiation-induced segregation and precipitation. This conclusion lends much support to the empirically derived hypothesis by Garner [14] that microchemical evolution is one of the

major factors which controls the onset of swelling in austenitic stainless steels, and perhaps other alloys.

It should be emphasized that regardless of the fact that the general features of RIS, such as temperature and displacement rate dependence, are qualitatively understood, quantitative applications of the RIS models is hampered by the lack of knowledge of many physical quantities required for the models, such as solute-defect binding energies and complex migration energies [15].

There are still other chemical changes due to irradiation. Precipitates may form in locally enriched regions even though the precipitate phase is unstable at the average composition. Alternatively, precipitates which are stable may dissolve in depleted regions. In addition, a local alteration in surface composition may give significant changes in the rates of void nucleation and growth [13].

4.4 Irradiation induced changes in mechanical and thermo-physical properties

Changes in the microstructure of a metal are usually accompanied by changes in the mechanical properties. In the case of neutron irradiation, the microstructural changes are the formation of cavities, dislocation loops and dislocation networks. In most materials, this produces a stronger matrix and results in reduced ductility. Complications to this simple guideline abound. Among the most important complications for fusion reactors is the ductility reductions by helium due to promoting intergranular failures. Other complications to the lattice hardening-ductility reduction guidelines include softening of cold-worked structures through irradiation-enhanced recovery, and radiation effects on the precipitate structure and

stability. It is quite clear that many considerations are related to the post-irradiation evaluation of mechanical properties of fusion materials [13]. In the following sections, the impact of irradiation on certain experimentally measured mechanical properties will be reviewed. Measurements of mechanical properties of some unirradiated materials are presented in Chapter 7. Also, the effect of irradiation on the thermal conductivity will be discussed because it is directly related to the stress analysis of bonded structures.

4.4.1 Hardness

Indentation hardness measurements have been used extensively in following property changes in irradiated metals and alloys [17]. The hardness itself is a difficult property to interpret in basic terms. Nevertheless, by the right choice of load coupled with appropriately shaped indentors, hardness measurements furnish a sensitive method for detecting slight property changes in irradiated metals and alloys, e.g. the course of precipitation may be followed continually by hardness measurements. Numerous correlations have been worked out between hardness and tensile strength for many metals and alloys, so that in the absence of the large samples required for stress-strain curves this measurement can be used to advantage [17]. Also, the microhardnes technique proved to be a good mechanical test that complements TEM observations since the measured hardness is the net result of all irradiation induced defects, including those which are not resolved by TEM [18].

Based on a large number of hardness measurements of a wide variety of metals and alloys after irradiation, the following conclusions may be drawn [17]:

1. If the temperature of irradiation is low enough, then all metals and alloys show increased hardness after irradiation.

2. The lower the hardness prior to irradiation, the greater the increase in hardness after irradiation. Well-annealed crystals always gives a larger hardness increase than cold-

worked samples, though the final hardness value in the cold-worked sample may still be higher. There is some indication that fully hardened metals may be softened slightly by irradiation.

3. The hardness achievable by irradiation does not exceed the hardness obtainable by conventional means.

4. The work-hardening coefficient of metals does not appear to change upon irradiation as indicated by hardness measurement.

5. Hardness changes have been observed after bombardment with electrons, deutrons, alpha particles, and neutrons.

6. The character of one or more solute atoms added to a metal prior to irradiation does not appear to influence the hardness change other than by the way in which the pre-irradiation hardness is changed.

7. No distinction between single and polycrystalline metals could be made.

Diamond Pyramid Microhardness (DPH) data is generally acknowledged to be a measure of the flow strength of a metal at a strain of about 8% [18]. In order to equate DPH values with the tensile flow strength, σ, at 8% strain, the following approximation [18] is commonly used for metals:

$$\sigma \approx \frac{DPH}{3} \tag{4.1}$$

The volume of the metal which is plastically deformed during a DPH test is localized. The deformation of this volume, therefore, is constrained by the balance of the specimen which suffers only elastic deformation during the test. The constant 1/3 in equation 4.1 accounts for this constraint. The relationship between DPH/3 and the 0.2% offset yield strength is illustrated schematically in Figure 4.2.

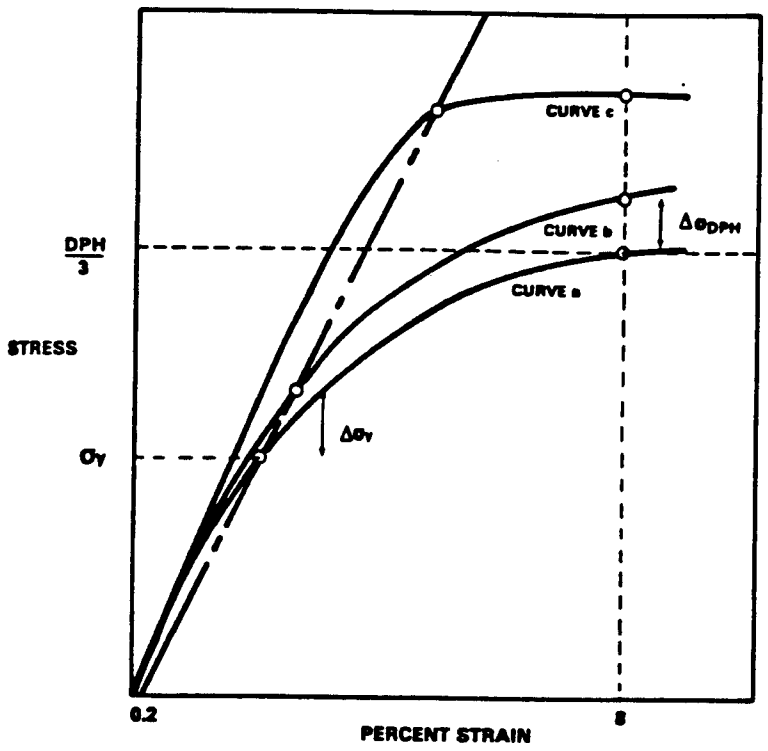

Figure 4.2: Schematic stress-strain curves: curve a, the unirradiated response; curve b, the slightly irradiated response; curve c, the highly irradiated response [18]

4.4.2 Elastic properties

Changes in microstructure, as well as microchemical changes, are also known to affect elastic moduli. Thus, elastic properties are affected by irradiation since the presence of interstitials and/or vacancies produces a change in lattice spacing and interatomic binding [17]. A theoretical estimate of the effects of irradiation-produced vacancies and interstitials upon the elastic constants of both face-centered and body-centered metallic structures has been made by Dienes [17]. He concluded that the effect of vacancies would be to reduce the elastic constants, while interstitials would cause an increase. Furthermore, the effect of the interstitials would far outweigh the vacancy effect due to the sharp increase in the repulsive interaction of the interstitial with its neighbors. Thus an irradiation where both vacancies and interstitials are produced should show an increase in Young's modulus, for example. Billington indicated that the increase expected from the interstitial contribution must be observed at low temperatures [17].

The presence of dislocations can also affect the elastic region of the stress-strain curve, for even the smallest stress will cause some glissile segments of the dislocation network to bow. Provided the stress does not tear the dislocation away from its anchoring points, or cause sources to operate, the segment will return to its original position under its own tension and the strain will disappear when the stress is removed. The effect of dislocations on the shear modulus can be represented by the equation [11]

$$\mu_{eff} = \frac{\mu}{1 + D} \tag{4.2}$$

where; μ is the shear modulus of the perfect crystal, μ_{eff} is the effective modulus, and D is a parameter related to the dislocation network.

Voids are expected to affect the elastic moduli because they alter the lattice spacings. Hashin [19] has formulated an approach to calculate the elastic moduli of a two-phase, non

homogeneous material, using elasticity theory and a concentric-spheres model. Using Hashin's approach, Christensen [20] has derived expressions for the bulk as well as lower and upper bounds for the shear moduli. Marlowe and Appleby [21] measured the reduction in Young's modulus due to swelling for 316 as well as 347 stainless steels using a dynamic resonance technique. For 316 stainless steel the following relation was reached:

$$(E / E_0)_{316} = [\ 1.086 - 4.435\ S\ ] \tag{4.3}$$

at the 95% confidence level for the coefficients, where the E_0 is the modulus of the fully dense materials, and S is the volume fraction swelling. Straalsund and Kay [22] also used an ultrasonic technique to measure the effect of swelling on the elastic constants of 403 stainless steel. Afzali and Nemat-Nasser [23] calculated, for 316 stainless steel irradiated in EBR-II, the reduction in both the shear and the bulk moduli. They found that the maximum reduction occurs at about 500 °C which corresponds to the peak value for swelling. At lower temperatures, the reduction is low. For metals irradiated in fusion reactor environment, gas bubble production becomes a more dominant factor in the reduction of the elastic moduli.

4.4.3 Thermo-physical properties (Thermal conductivity)

The thermal conductivity is of significance for thermal stress calculations. It is well known that the thermal conductivity is reduced due to swelling which generates pores in the material reducing its ability to conduct heat [24]. Under these conditions, the thermal conductivity, λ, for the expanded material (considered as a mixture of material and pores) is given by [24]:

$$\lambda_{mix} = \lambda_{cont} * \left(\frac{1 - \phi}{1 + \frac{1}{2}\phi}\right) \tag{4.4}$$

where "mix" stands for mixture and "cont" stands for continuous media, and ϕ is the porosity or volumetric swelling. For low values of swelling, this equation can be written as:

$$\lambda_{mix} \approx \lambda_{cont} \left(1 - \frac{3}{2}\phi \right) \tag{4.5}$$

It has been found that experimental results can sometimes be fitted rather better to the equation:

$$\lambda_{mix} = \lambda_{cont} (1 - \beta \phi) \qquad (4.6)$$

where β is an adjustable parameter. This is effectively a structural factor allowing for non-spherical pores and various values can be found for it theoretically. However, since the shape of pores is frequently unknown, equation 4.5 is the one which is commonly used to evaluate the thermal conductivity of a crystalline solid from measurements on slightly porous samples [24].

4.5 Gas migration to interfaces under stress and/or thermal gradients

When materials are irradiated by high energy neutrons, the displacement damage is accompanied by the production of impurity atoms due to nuclear transmutation reactions. Attention has been focused on helium due to the significant impact that helium is known to have on the microstructure of irradiated materials and the fact that the differences between the neutron spectra obtained in a fast fission reactor and in a deutrium-fusion reactor result in much higher helium production rates in the latter. For example, the ratio of transmutant helium to displacement production (He/dpa ratio) will be on the order of 10 to 20 appm He/dpa for steel in the first wall of a fusion reactor compared with 0.3 to 0.5 appm He/dpa in a typical fast fission test reactor.

It is not the intention here to review the impact of helium on the microstructure and material properties. Very extensive review articles were devoted to this topic [for a recent review see reference 25]. What is of interest for the bonded structure behavior is the induced migration of gas bubbles along temperature and/or stress gradients. This will determine

where the gas bubbles will have a significant effect: at or away from the interface. This should be determined as a function of component life time and in the relevant stress environment.

There are different types of potential gradients which can cause inclusions (e.g., gas bubbles) to migrate in solids. Table 4.1 lists these potentials as well as the different mechanisms by which the transport of atoms of the solid from one part of the surface or interface of the inclusion to another part takes place [26]. Olander [26] indicated that there have been no measurements of migration of inclusions in a stress gradient. On the other hand, there is no shortage of theoretical speculation concerning the magnitude and direction of this phenomenon.

Calculation of gas bubble migration in stress and temperature gradients can be divided into two classes, which can be labelled "global" and "local" [26]. The first one deals with the change in the system (bubble and medium) free energy while the second one deals with the distribution of the potential (temperature or stress) on the bubble surface. Both the global and local methods have been applied to temperature-gradient induced bubble migration [26] and the migration velocities computed by the two techniques are the same. In the case of a stress gradient, only the global method has been examined in the western literature with widely discordant results. In the Russian literature, the local method were used.

4.6 Intra-coating stresses

The total stresses developed within coatings can be regarded as being made up of two possible contributions. These are defined as the differential thermal expansion stresses whose origin is understood, and whose value is generally amenable to calculation, and, the intrinsic

Table 4.1: Potential gradients and the atomic mechanisms for inclusion migration in solids [26]

Potential gradient in the host solid	Atomic mechanism of solid atom transport
(1) Temperature	(A) Vacancy diffusion in the host solid
(2) Stress	(B) Surface diffusion along the interphase boundary
(3) Electric field	(C) Volume diffusion in the interior of the inclusion
(4) Accelerational field (e.g. gravity)	
(5) Vacancy concentration in the solid	

stress which is the manifestation of all other contributions [84]. Many review articles by Hoffman, Campbell, Buckel, and Kinosita [27] assimilated the massive experimental literature on measurements of the stress and attempted to interpret them in a few simple concepts. In addition to the thermal stress, Buckel [84] listed six other processes which may produce stress in the following way:

1. Incorporation of atoms, for example, residual gases or chemical reactions.
2. Differences of the lattice spacings between films and substrates.
3. Variation of the interatomic spacing with crystal size.
4. Recrystallization process.
5. Microscopic voids and special arrangements of dislocations.
6. Phase transformations.

For fusion reactors, fabrication techniques of bonded structures are usually accompanied by the generation of stresses. For a brazed part, for example, fabrication takes place at high temperatures, leading to differential contraction during cooling down if the constituents have different thermal expansion coefficients. As the component is cooled from its brazing temperature, the filler metal will freeze at some points, thus locking the interface and causing thermal stresses as the part cools further [28].

4.6 Literature survey of radiation damage to bonded structures in the nuclear field

CANDU fuel bundles incorporate Zr-5wt%Be brazements for attaching Zircaloy interelement spacer pads and bundle-to-pressure tube bearing pads to Zircaloy sheaths, Figure

4.3. The brazed joints have performed extremely well and no fuel defects have been attributed to the brazements or to the surrounding sheath heat-affected zones [29].

The mechanical strength of unirradiated brazed joints was determined using a single lap joint in 12.7-mm-diameter Zircaloy-2 rod specimens [29]. Although no fuel-bundle brazed joints bear any tensile or shear load, the strength of irradiated spacer-to-sheath joints was assessed with two short fuel elements brazed together with a single spacer. After irradiation the strength of the joint was determined by axially loading the two elements in opposite directions. Unirradiated, the shear load at failure was 320 Kg and this increased to 390 Kg after a fuel burnup of 80 MWh/KgU, i.e., 3.4×10^{20} n / cm^2; E > 1 MeV. In all cases, the joint failed by shearing through the sheath around the periphery of the spacer.

The effects of nuclear radiation on polymer coatings were also investigated [30]. The radiation resistance of polymer coatings is most often determined by finding the limit of irreversible decomposition, i.e., by studying their mechanical properties. The limiting radiation dose is usually considered to be that which reduces the toughness of the coating to about 50% of the original value. In estimating the radiation-resistance of polymer coatings, a very frequent procedure is to compare the initial and final tensile strength values of the coating as well as the relative elongation of films subjected to different radiation doses; Figures 4.4 and 4.5. More accurate results may be obtained by thermomechanical investigation, in which the deformation of the film is measured as a function of the temperature; Figure 4.6.

The largest body of information found in the literature on the irradiation effects to the interface/attachment region between a coating and a substrate material was written by Johnson, et al. [8,31], for the development of low friction coatings for the breeder reactor. From this rather extensive program, valuable insights can be gained from the results of

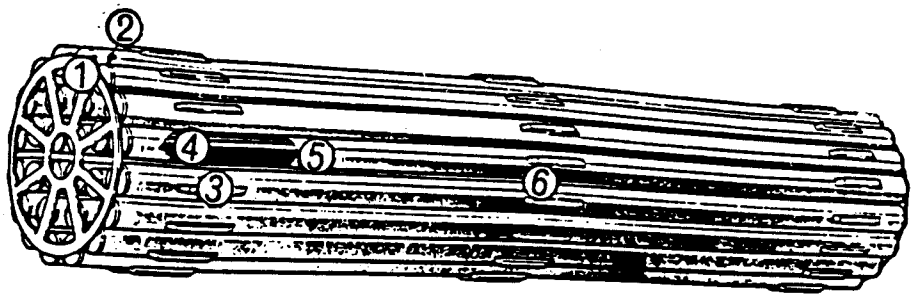

Figure 4.3: Fuel bundle for pickering reactor assembled from six basic components. 1-Zircaloy structural end plate, 2- Zircaloy end cap, 3-Zircaloy bearing pads, 4-Uranium dioxide pellets, 5-Zircalloy fuel sheath, 6-Zircaloy spacers [29]

irradiation tests on over one hundred coating/substrate combinations as well as practical experience regarding the length of time and the amount of effort required to successfully qualify a coating/substrate system for in-reactor application. While many of the design goals for developing materials for breeder reactor applications were unique (e.g., sodium compatible, low friction, close dimension tolerance), others such as mechanical integrity, irradiation resistance and thermal cycling are very similar to those of plasma facing component designers.

The initial coatings selected for evaluation, were $Cr_3 C_2$ -Ni-Cr coatings. Other metallic binders were considered in hopes of improving the friction-behavior. These included Inconel 718, molybdenum, and Tribaloy 700. Inconel 718 is a Ni-base superalloy with the composition 52.5% Ni, 19% Fe, 19% Cr, 5.2% Cb, 3% Mo, 0.8% Ti, and 0.6% Al. Tribaloy contains 50% Ni, 32% Mo, 15% Cr, and 3% Si. Other tested materials were Inconel 718 explosively bonded to 316 SS, diffusion aluminized Inconel 718, and weld-deposited haynes 273 on 304 SS and Inconel 718.

Methods of attaching wear materials to the component surfaces include detonation gun coating, diffusion coating, plasma-spray, explosive bonding, and weld-overlays. Three types of specimens were selected for irradiation; Figure 4.7: 1.56 cm diameter, 0.3 cm thick circular discs for post-irradiation wear and bond tests, 1.88 * 0.94 * 0.18 cm rectangular coupons, all-purpose specimens which occupy very little irradiated space; and 5 cm long, 0.3 cm thick tensile specimens with approximately square gage cross sections for thermal cycling tests under a tensile load. All specimens, except those representing the diffusion "aluminizing" process were coated on one side only, usually to a nominal coating thickness of 0.008 to 0.013 cm. The aluminized specimens were coated on all surfaces to a coating thickness of 0.003 to 0.008 cm. Samples have been irradiated in the EBR-II to total neutron

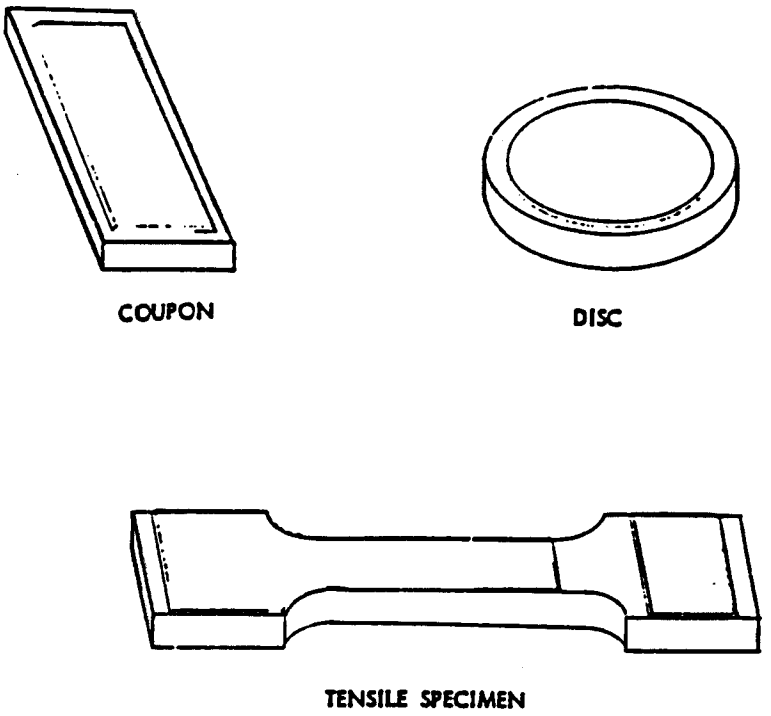

Figure 4.7: Specimens used in evaluation of irradiation effects on low-friction coatings and materials [31]

fluences ranging from $1.0*E^{22}$ to $4.0*E^{22}$ n/cm^2. Irradiation was conducted in sodium filled capsules at temperatures from 451 °C to 627 °C for periods of 1120 hours to 5240 hours.

Post-irradiation examination and testing included visual and low magnification inspection of all specimens and on selected specimens weight and thickness change measurements, optical metallography, scanning microprobe analysis, X-ray examination and bond strength testing (epoxy-lift-off tests).

The following observations have been made regarding the performance of low-friction coatings: (1) irradiation testing of coated materials eliminated more coatings than any other qualification test (e.g., thermal cycling under stress, epoxy lift off, environmental). Irradiation effects, therefore, must be a major consideration in the testing of composite materials, (2) no clear correlations between temperature, fluence and coating damage were apparent, (3) the ability of the mechanically bonded coatings, such as plasma-sprayed and detonation gun coatings, to survive irradiation appeared to be related to coating bond strength, interface stresses, and internal coating stresses. The high strength detonation gun coatings with minimum thermal expansion differences maintained their integrity while most plasma sprayed coatings of the same composition but having different bond strengths, failed by spalling. "Graded" plasma sprayed coatings were more resistant to irradiation-induced failures than other plasma coatings, and offered potential for further development, (4) metallurgical bonded coatings, such as those produced by diffusion coating, electro-spark deposition, explosive bonding, or weld deposition showed no observable deleterious effects of irradiation (cracking, spalling or debonding).

The damaging effect of neutron irradiation on high heat flux materials has been studied with the EBR-II and FFTF fission reactors at the Hanford Engineering Development Laboratory (HEDL) [32]. Specimens of low-Z coatings and claddings on various substrate

materials have been irradiated to damage levels of 1-3 dpa. There have been some failures, presumably caused by differential swelling stresses.

Type 304 stainless steel and Inconel 600 welded and brazed joints were irradiated in the Oak Ridge Research Reactor at 52 °C to a neutron fluence of 2.3 * 10^{22} n/cm^2 (E > 1 MeV) and 6.7 * 10^{22} n/cm^2 (thermal) [1]. Tensile and shear specimens were then tested in short-time tests at several deformation temperatures ranging from 20 to 900 °C. The brazes were made using AWS BNi-7 filler metal (Ni-Cr-P). Irradiation embrittlement was observed in the brazed joints. The toughness of these joints is greatly reduced at temperatures of 270 °C and above for the Inconel and 470 °C and above for the stainless steel; Figures 4.8 and 4.9.

The study of the effect of irradiation on welds has been extensively reported in the literature [33-41]. Recently, a type 316 stainless steel and a modified steel; the Japanese version of the US Primary Candidate Alloy designated JPCA were used to investigate the swelling susceptibility of weld joints formed by electron-beam welding (EB) welding [42]. The electron irradiation was carried out in a High Voltage Electron Microscope (HVEM) and the microstructural evolution during the irradiation of the weld joints was compared with that of the base metal. Energy Dispersive X-ray Spectrometry (EDXS) combined with Scanning Transmission Electron Microscopy (STEM) was also employed for the microanalysis of weld metal. Weld joints were also examined by conventional methods; ultrasonic inspection, radiography, chemical analysis tests and hardness tests.

Ultrasonic inspection and radiography detected no harmful defects in the weld joints. No significant difference in tensile strength was shown between the weld joints and the base metals, although the specimens ruptured at the weld metal and some degradation in elongation and in reduction of area occurred in the weld joints. Hardening in the heat affected zone was

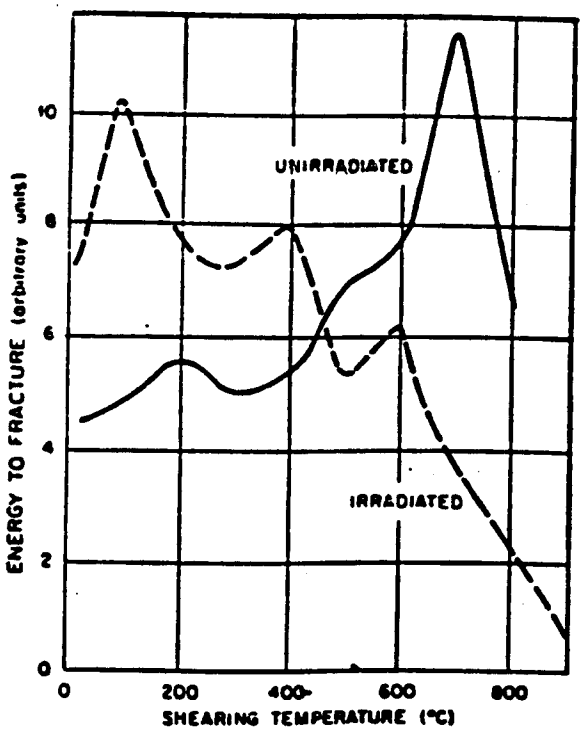

Figure 4.8: Toughness of Type 304 stainless steel (Ni-Cr-P) brazes deformed in shear [1]

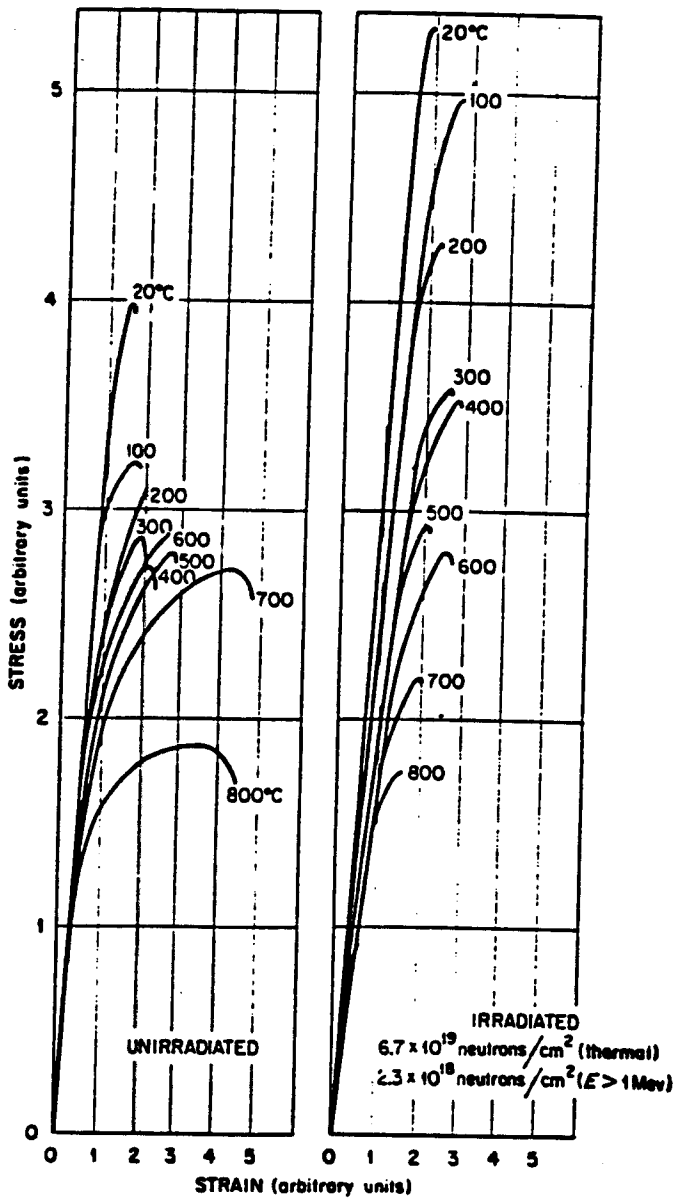

Figure 4.9: Comparison of the stress-strain curves of Type 304 stainless steel (Ni-Cr-P) brazes tested in shear [1]

detected within about 5 mm of the interface of weld metal and heat affected zones. The swelling of the weldment and base metal are summarized in Figure 4.10, showing the marked reduction of swelling resistance in the weld metal of both steels and the differential swelling effect is obvious. This contradict the findings of other irradiation experiment [38] where degradation of the swelling resistance of the weld joints was not detectable either by precision immersion densitometry or by TEM.

Recent works in this area included investigating the microstructural changes in weld joints of 316 SS by dual-ion irradiation [43] (Figure 4.11), the effect of helium on creep properties and the microstructure of 316 L welds [44], the tensile properties of 316 SS welds after neutron irradiation [45], the dependence of the tensile properties of 316 L welds on implanted hydrogen and/or helium [46], and the effect of neutron irradiation on the strength of electron beam welds Japanese ferritic-martensitic steel (JFMS) steel [47].

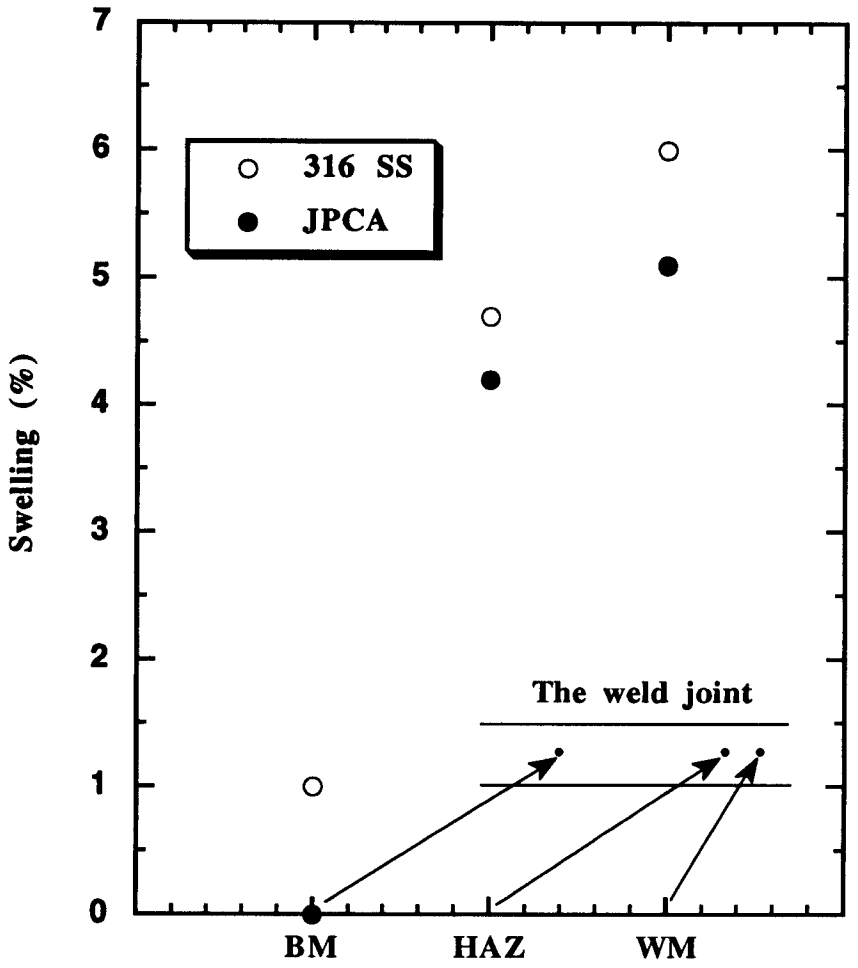

Figure 4.10: Void swelling of weld joint, heat-affected zone, and base metal in 316 SS and JPCA irradiated to 15 dpa at 773 K [42]

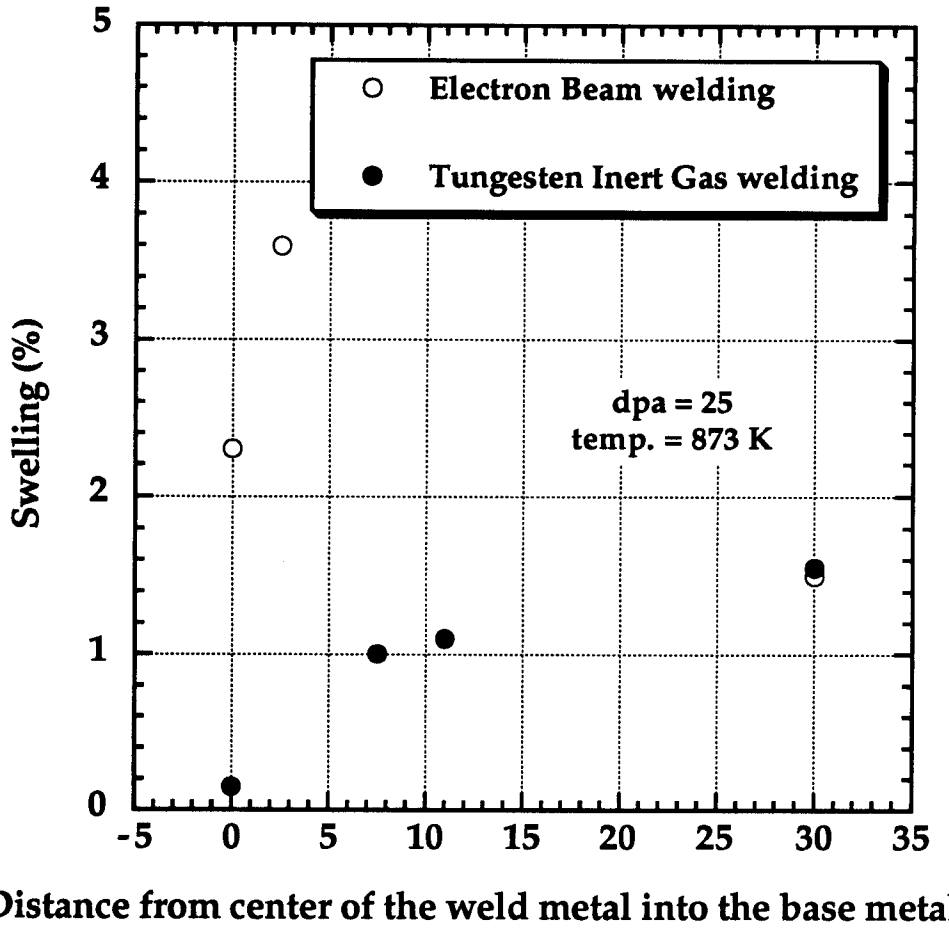

Figure 4.11: Positional characteristics of cavities in EB and TIG welded 316F satinless steel joints dual-ion irradiated [43]

4.7 References

[1] W. R. Martin and G. M. Slaughter, in: Source book on brazing and brazing technology (M. M. Schwartz, ed.) American Society for metals, p. 406, Metals Park (1987).

[2] D. M. Mattox and M. J. Davis, J. Nucl. Mat. **111/112**, 819 (1982).

[3] J. B. Whitley, in: Proceedings of U.S.-Japan workshop Q86 on plasma-materials interaction/high heat flux data needs for the next step and steady state devices (J. B. Whitley and A. Miyahara, eds.), p. 94, SAND88-1072, 94 (1988).

[4] R. F. Mattas, J. Nucl. Mat. **141/143**, 819, (1986).

[5] S. Ishino, in: Proceedings of the Japan-U.S. workshop p-119 on 14 MeV neutron source for material R&D based on plasma devices (A. Miyahara and F. coensgen, eds.) IPPJ-T-37, 21 (1988).

[6] R. F. Mattas **15**, 637 (1989).

[7] F. L. Vook, et al.,in: Report to the American Physical Society by the study group on physics problems relating to energy technologies: Radiation effects on materials, Reviews of Modern Physics 47, suppl 3 (1975).

[8] R. F. Mattas, et al., in: UCLA PPG-815 (1984).

[9] J. T. Adrian Robewrts, Structural materials in nuclear power systems, Plenum press (1981).

[10] J. Kai, University of Wisconsin report UWFDM 688 (1986).

[11] M. W. Thompson, Defects and irradiation damage in metals, Cambridge Univ. press (1969).

[12] R. Conrad, et al., HFR Irradiation Testing of Fusion Materials, Commission of the European Communities (1984).

[13] C. Stein, Critical materials problems in energy production, Academic press (1976).

[14] W. G. Wolfer, J. Nucl. Mat. **114**, 292 (1983).

[15] H. Wiedersich and P. R. Okamoto in: Interfacial Segregation (ASM) (W. C. Johnson and J. M. Blakely, eds.) 405 (1977).

[16] J. L. Brimhall, et. al., J. Nucl. Mat. **103/104**, 456 (1981).

[17] D. S. Billington and J. H. Crawford, Radiation Damage in Solids, Princeton University Press (1961).

[18] N. F. Panayotou, J. Nucl. Mat. **108/109**, 456 (1982).

[19] Z. Hashin, J. Appl. Mech., 143 (1962).

[20] R. M. Christensen, J. Mech. Phys. Solids **17**, 24 (1969).

[21] M. O. Marlowe and W. K. Appleby, Trans. Am. Nucl. Soc. **16**, 95 (1973).

[22] J. L. Straalsund and C. K. Day, Nucl. Tech. **20**, 27 (1973).

[23] M. Afzali and S. Nemat-Nasser, Trans. 5th Int. Conf. on Structural Mechanics in Reactor Technology, Berlin, Germany, N2.5/2 (1979).

[24] J. E. Parrott and A. D. Stuckes, Thermal conductivity of solids, Pion limited (1975).

[25] R. E Stoller, DOE/ER-0313/8, 69 (1990).

[26] D. R. Olander, J. Nucl. Mat. **92**, 163 (1980).

[27] R. W. Hoffman, 273 (1982).

[28] J. P. Blanchard and N. M. Ghoneim, J. Nucl. Mat. **172**, 54 (1990).

[29] D. G. Hardy, and N. A. Graham, Trans. Amec. Nucl. Soc.**19**,122 (1974).

[30] V. B. Tikhomirov, Polymer Coatings in Nuclear technology, Atomzdat, Moskva 1965, translated from Russian , Israel program for scientific translations (1967).

[31] A. L. Ward, et al., HEDL-TME 75-108 (1975).

[32] R. D. Watson, and J. B. Whitley, SAND84-1349 A (1984).

[33] T. Sawai, et al., J. Nucl. Mat. **155/157**, 861 (1988).

[34] E. N. Klausnitzer, et al., ASTM 683, 267 (1978).

[35] W. F. Savage, et al., Welding research, 25-36-S, Feb. (1981).

[36] F. W. Wiffen and P. J. Maziasz, J. Nucl. Mat. **103/104**, 821 (1981).

[37] S. Kaga, et al., J. Nucl. Mat. **179/181**, 588 (1991).

[38] T. Sawai, et al., J. Nucl. Mat. **179/181**, 519 (1991).

[39] J. R. Hawthorne and H. E. Watson, in: Proc. Intern. Confs. on Radiation Effects in Breeder Structural Materials, Scottsdale, AZ, 327 (1977).

[40] M. I. de Vries and B. van der Schaaf, ASTM STP 725, 285 (1981).

[41] J. R. Hawthorne, ASTM STP 956, 191 (1987).

[42] T. sawai, et al., J. Nucl. Mat. **141143**, 444 (1986).

[43] A. Kohyama, et. al., J. Nucl. Mat. **191/194**, 722 (1992).

[44] Y. Dai and H. Schroeder, J. Nucl. Mat. **191/194**, 754 (1992).

[45] S. Jitsukawa, et. al., j. Nucl. Mat. **191-194**, 771 (1992).

[46] H. Schroeder and W. Liu, J. Nucl. Mat. **191-194**, 776 (1992).

[47] K. Fujii, et. al., J. Nucl. Mat. **191-194**, 901 (1992).

Chapter 5.

Computer Simulation of Microchemical Changes at Interfaces of Bonded Structures Due to Neutron Irradiation

5.1 Introduction

In the vicinity of interfaces, radiation damage will not only produce defect clusters but also will lead to transport of the dissimilar atomic species across the common boundaries, both through recoil of atoms from collisions with the primary radiations and through enhanced diffusion. Also, the relocation of atoms produced by irradiation and the cascade of recoils will degrade the sharpness of an interface [3]. These radiation effects have many practical implications. For example, it is well known that energetic heavy ion bombardment induce materials interactions in thin-film composite samples. Also, greatly enhanced adhesion between coating and substrate materials have been reported even in nonreacting, immiscible samples irradiated by ion beam mixing techniques [1]. Also, it is worth mentioning that fabrication techniques for the coatings may result in the formation of certain microphases along interfaces and these phases may react differently to irradiation than either the coating or the substrate. It is thus quite obvious that understanding the role these effects might have on the degradation of the interface properties is needed to allow meaningful design choices of materials to be used in such applications.

In case of ion irradiation, the interest in ion beam mixing has recently increased due to the wide use of ion implantation techniques for surface modifications. Some of the fundamental mechanisms involved in ion mixing can be identified [1]. First, collisional

mixing (ballistic mixing) may be induced by recoil implantation and cascade mixing, as well as displacement spikes. Second, diffusional mixing involves radiation-enhanced diffusion and radiation-induced segregation, which would be caused by mobile defects such as vacancies and interstitials generated by the irradiation.

At high particle fluence ($1*10^{18}$ ions /cm^2 in case of ion irradiation), the target's composition changes significantly from the initial state. The changes in composition arising from the production of recoils or stopping of atoms should be taken into account [4]. Also, the evolution of point defects and their stability during irradiation are among the most important parameters for evaluating radiation damage. The inclusion of spatially distributed vacancies and interstitials; as well as radiation induced segregation; into the analysis of bonded structures, greatly adds to the understanding of the behavior of duplex materials especially along interfaces.

The situation is more complicated in the case of neutron irradiation. Due to the large mean free paths of energetic neutrons (14.1 MeV in case of fusion reactors), they penetrate deep into the structure. As they are transported, energetic target atoms (average energy of 10's of KeV) continually displace other atoms from their sites, producing collisional mixing as well as other processes in places where such atoms may reach by diffusional processes. Figure 5.1 is a schematic of the Radiation Induced Mixing (RIM) along the interface of a Be/Fe joint.

Another point of interest in the case of neutron irradiation is the production of hydrogen and helium atoms. The production per dpa is one to two orders of magnitude more in fusion reactors than in fission reactors for most of the Plasma Interactive Components. Gas production plays a major role in changes of mechanical properties and dimensional

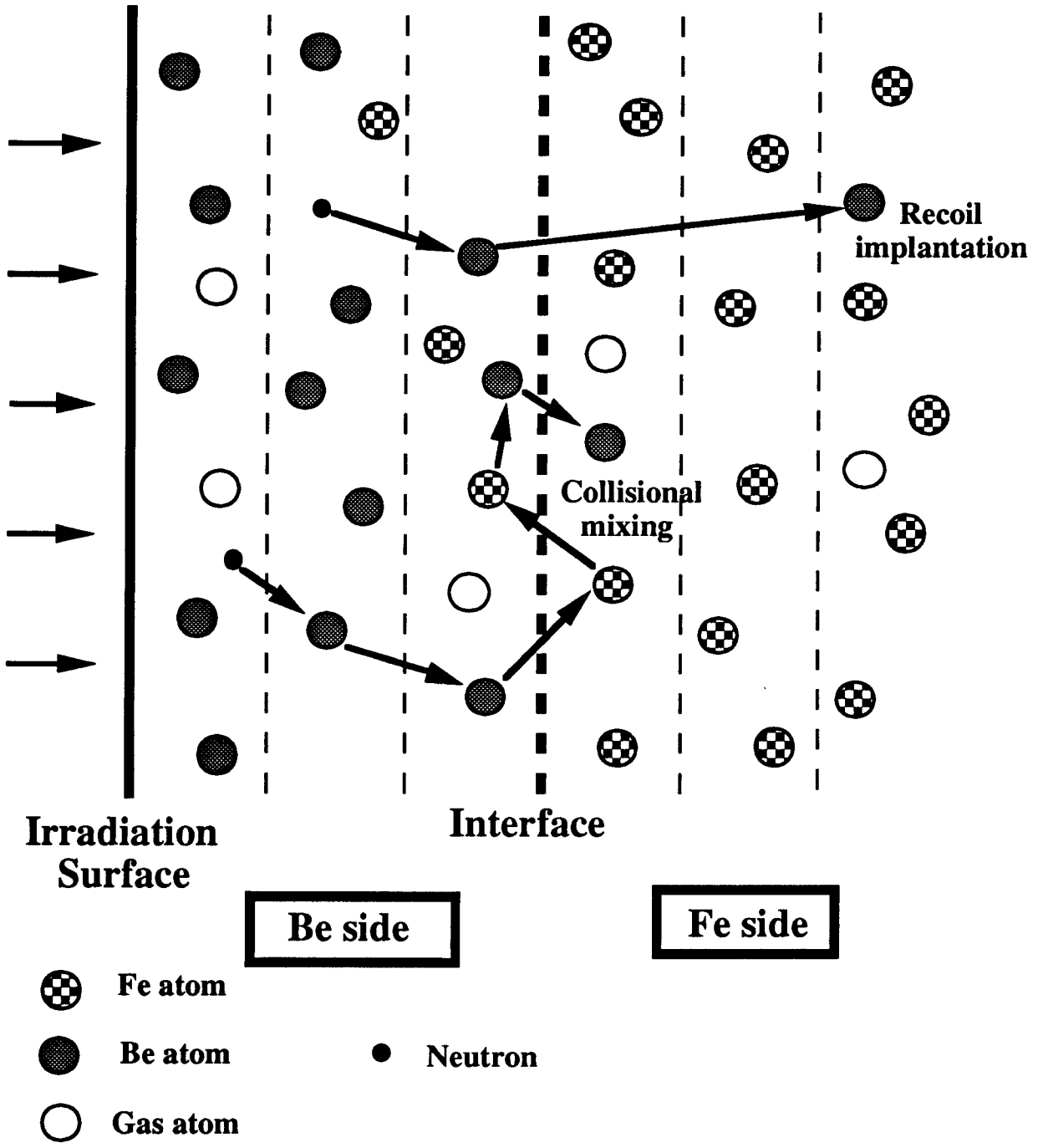

Figure 5.1: Schematic presentation of Radiation Induced Mixing (RIM) processes [1]

stability under some conditions [5]. The proper assessment of the spatial distribution of these gas atoms; especially in the interfacial area; is the first step in determining their role on the performance of bonded structures. Also, the reallocation of these gas atoms can be different from their initial spatial distribution at birth.

5.2 MINIR: A Monte Carlo code to simulate Radiation Induced Mixing (RIM)

The difficulties of analytic methods for the solution of particle transport problem in solids increase as the basic assumptions are removed to solve the transport equation describing more complicated situations such as multilayered targets. The high computational speed and large memory capacity of modern digital computers have enabled scientists to adopt a totally different approach, namely, simulation of the particle transport process directly without referring to the transport equation. These computer simulation methods being used for the study of radiation effects can be categorized in two groups, i.e. molecular dynamics simulation and Monte Carlo method.

The Monte Carlo method proved to be a powerful tool to investigate the collision mixing along the interface of bilayers [1]. In its simplest form, the Monte Carlo technique consists of simulating a finite number of particle histories, say N, through the use of a random number, or, more correctly, pseudo random number generator. In each particle history random numbers are generated and used to sample appropriate probability distributions for scattering angles, track length distances between collisions, and so on [5]. In general, the simulation of the PKA's, the SKA's and so forth will be in principal the same as for neutrons except of course with the nature of interactions that can occur. In case of ions we have to refer to the potentials used for evaluation of the cross sections.

A Monte Carlo code; MINIR (Mixing at Interfaces due to Neutron IRradiation); was developed to deal with the inter-mixing, transmutational production along the interface of bonded structures. Several points are assumed concerning the general simulation process:

1. The target is assumed to be amorphous, that is, the directional characteristics of the real lattice are neglected.

2. A planar target geometry is considered, which imposes one dimensional variations of materials profile, even though the transport procedure is conducted in three dimensional space.

3. The history of moving particle is terminated if it gets out of the target surface or target back end (defined later) or its energy drops to below a cutoff energy.

4. The change in composition of the target does not affect the neutron transport process (see section 5.2.1 below). This becomes necessary when one considers the computer time needed to simulate the change in neutron cross sections in each target layer (thickness in the angstrom range) and the large number of layers considered in the simulation as well as the large mean free path of the neutron (in the centimeter range).

A brief description of the MINIR code will be presented in the following sections. "R" will refer to a random number uniformly distributed between 0 and 1. A "particle" will refer to a knock-on target atom or a transmutation product due to neutron irradiation. Elements of the TAMIX code [1] were used to simulate the particle transport processes.

5.2.1 Dynamic simulation

The so-called "dynamic mode" is the main feature of the MINIR code to account for the change in composition of the target materials especially along the interface. This should be compared with the "static mode" in which target composition remains constant during

irradiation simulation. The dynamic simulation consists of sectioning the target into different layers. After the termination of a neutron history (including the specified number of the simulated secondary knock-ons), the net change in each layer is calculated. Thus, the spatial distribution of intermixing and transmutation production can be adequately tracked. This new composition of the structure will enter into the simulation for the next set of PKA's and so forth.

5.2.2 Mean free path

The distance travelled between collisions (x) is sampled according to the equation;

$$x = \ln (1 - R) / (\sigma_t (E) * N) \qquad (5.1)$$

where; N is the atomic density of the target atoms and σ_t is the total microscopic cross section of the target atom.

5.2.3 Target atom selection

The target atom for collision will be the ith atomic species if the following is satisfied:

$$\frac{\Sigma_t^{i-1}}{\Sigma_t^n} \leq R \leq \frac{\Sigma_t^i}{\Sigma_t^n} \quad , \quad i = 1,....,n \qquad (5.2)$$

where Σ_t is the total macroscopic cross section of the i^{th} specie.

5.2.4 Neutron reactions

Elastic reaction

The energy of the scattered neutron E' in terms of the initial energy E, and the cosine of the scattering angle in the Center of Mass (CM) μ_{cm} (sampled from ENDF files) is given by:

$$E'=0.5\ E\ [(1 - \alpha)\ \mu_{cm} + 1 + \alpha] \qquad (5.3)$$

where,

$$\alpha = \left(\frac{A-1}{A+1}\right)^2 \tag{5.4}$$

and A is the mass number of the target atom.

The energy transferred from a neutron to a an atom in an elastic collision is given by;

$$T = \frac{4Mm}{(M+m)^2} E * \sin^2(\theta/2) \tag{5.5}$$

where, M is the mass of the atom, m is the neutron mass, E is the energy of the incident neutron, and θ is the scattering angle of the neutron in the CM system.

The scattering angles of both the neutron ϕ_1 and the recoil ϕ_2 in the LAB system are given as;

$$\tan\phi_1 = \frac{(M/m)\sin\theta}{1+(M/m)\cos\theta} \tag{5.6}$$

$$\tan\phi_2 = \frac{\sin\theta}{1-\cos\theta} \tag{5.7}$$

Non-elastic reactions

For a reaction of the type (n,x) where x may be another neutron or any charged particle (He, p, etc....), the following equations are used for the energy and angle of the reaction products as explained in Figure 5.2:

$$E_x = a_{1x} E_1 + a_{2y} (E_1 - E_{1\alpha}) + 2 [a_{1x} a_{2y} E_1 (E_1 - E_{1\alpha})]^{1/2} \eta_x \tag{5.8}$$

with x being either of the reaction products and y being the remaining one, i.e., (x,y)=(3,4) or (4,3). The parameters are defined as

$$a_{1x} = \frac{M_1 M_x}{(M_1+M_2)(M_x+M_y)} \tag{5.9}$$

and

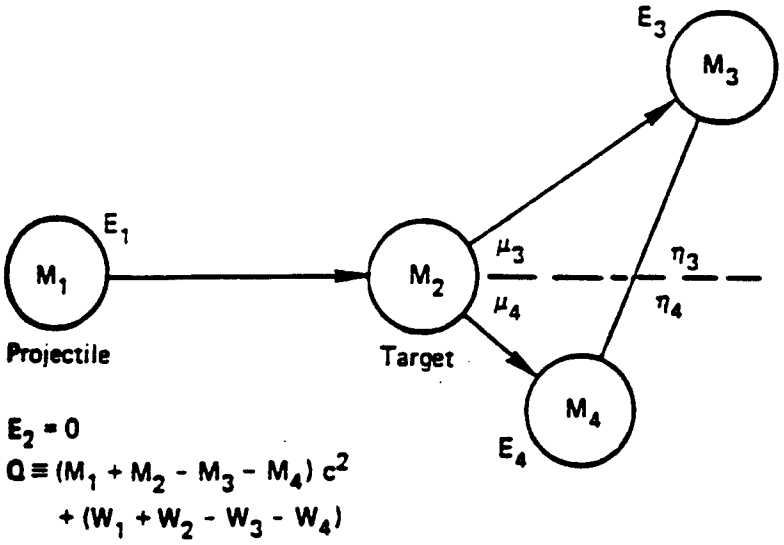

Figure 5.2: Nomenclature for two body reaction

$$a_{2y} = \frac{M_2 M_y}{(M_1+M_2)(M_x+M_y)} \tag{5.10}$$

The value of η is sampled from the related ENDF file. If such distribution is not available, isotropic distribution in the CM system is assumed. The Lab cosine in terms of the particle energies is

$$\mu_x(E_1,E_x) = \frac{[a_{1x} E_1 - a_{2y} (E_1-E_{1\alpha}) + E_x]}{2 (a_{1x} E_1 E_x)^{1/2}} \tag{5.11}$$

(n,2n) reaction

In the energy range relevant to fusion designs, the (n,2n) reaction can not be neglected, especially for materials that are considered neutron multipliers such as Be. The (n,2n) reaction is simulated by treating the first neutron as a normal inelastic neutron. The parameters of the product nucleus is then calculated and it is allowed to decay to another reaction product emitting the second neutron. The angular distribution of the second neutron is considered to be isotropic, and its energy distribution is sampled from the related ENDF file.

5.2.5 Transport procedure for the moving particles

The following assumptions concerning the transport of particles are made:

1. The moving particle loses its energy via nuclear and electronic stopping processes, which are independent on each other.

2. The binary collision approximation is used for the nuclear scattering between a moving particle and a target atom. The simultaneous collision with more than one target atom is neglected.

3. Between nuclear collisions, a moving particle loses its energy continuously through electronic stopping process, which however does not alter the direction of the moving atom.

5.2.6 Particle scattering cross section calculations

Since at high energy most of the collisions give small deflections of the moving atom and consequently, small energy transfer to the target atoms, which do not significantly change the simulation results; an adjusted maximum impact parameter p_{max} is used [1]. This gives the larger mean free path or less nuclear collisions ignoring the insignificant ones. Two criteria are used to determine the appropriate p_{max}, which are based upon deflection angle and energy transfer.

The final expression for p_{max} will be

$$P_{max} = \min (P_{max,0} , \max (P_{max,a} , P_{max,e})) \qquad (5.12)$$

where,

$p_{max,o}$ is the radius of the equivalent cell,

$p_{max,a}$ is the impact parameter which gives the deflection angle of the moving atom θ_{min} ($\approx 1°$), all the collisions with a smaller deflection angle are neglected,

$p_{max,e}$ is the impact parameter at which the moving atom transfers the displacement energy E_d, all the lower energy transfer collisions are neglected, or equivalently:

$$\sigma_t = \min (N_t^{\frac{-2}{3}} , \max (\pi P^2_{max,a} , \pi P^2_{max,e})) \qquad (5.13)$$

In a surface region, however, sputtering is an important process resulted from the near-surface interactions, which is dominated by lower energy collisions. Hence, if the collision occurs within some distance from the surface, the most conservative approach is used, i.e.

$$P_{max} = P_{max,o} \quad \text{if} \quad z \leq n_{sl} N_t^{\frac{2}{3}} \qquad (5.14)$$

or

$$\sigma = N_t^{\frac{2}{3}} \quad \text{if} \quad z \leq n_{sl}\, N_t^{\frac{1}{3}} \tag{5.15}$$

where z is the position of the moving atom from the surface and n_{sl} is the number of atomic layers considered as surface region (≈ 8).

Particle scattering angle calculation

Particle scattering angles are simulated using two dimensional scattering angle table that is prepared beforehand as a function of ε (the reduced energy) and b (the reduced impact parameter) for a specific interatomic potential. The scattering angle is calculated at any ε and b from a 2-dimensional interpolation with the table. At very high energies or with a small impact parameter compared to energy, the simple coulomb potential is used, which gives the analytic expression for the scattering angle as

$$\theta_{coul} = 2 \tan^{-1} \left(\frac{1}{2 \varepsilon b} \right) \quad \text{if} \quad \varepsilon > 10^3, \text{ or } b < 0.05 \, (1 + \log \varepsilon) \tag{5.16}$$

The azimuthal scattering angle φ of both interacting particles can be calculated from the assumption of the azimuthal symmetry, which yields

$$\varphi_1 = 2 \pi R \tag{5.17}$$

$$\varphi_2 = \pi - R \tag{5.18}$$

where R is a random number.

New directional cosines

For scattering angles θ and φ, the new directional cosines a_x, a_y, and a_z in terms of the old directional cosines a_{x0}, a_{y0}, and a_{z0} are given as:

$$a_x = \sqrt{1 - a_{x0}^2} \sin\theta \cos\phi + a_{x0} \cos\theta \tag{5.19}$$

$$a_y = \frac{-a_{x0}\, a_{y0} \sin\theta \cos\phi + a_{z0} \sin\theta \sin\phi + a_{y0} \sqrt{1 - a_{x0}^2} \cos\theta}{\sqrt{1 - a_{x0}}} \tag{5.20}$$

$$a_z = \frac{-a_{x0}\, a_{z0} \sin\theta \cos\phi + a_{y0} \sin\theta \sin\phi + a_{z0} \sqrt{1 - a_{x0}^2} \cos\theta}{\sqrt{1 - a_{x0}}} \tag{5.21}$$

Displacement model

A modified Kinchin-Pease model is used for the defect production mechanism by moving particles. Whenever an energy in excess of E_d is transferred to the target atom, it is assumed to be displaced. The projectile is allowed to continue the simulation if its energy is greater than E_c which is the cutoff energy at which the particle trajectory is terminated (0.5 Mev in case of neutrons and 1 eV for ions). An expression developed by Robinson [1] is used for the defect production because the higher order recoils have lower energies and do not penetrate a long distance from their creation points. The following expression is used:

$$\nu(T) = 0.8 \frac{E_\nu}{2 E_d} \quad \text{if} \quad 2 E_d \le E_\nu \tag{5.22}$$

, where

$$E_\nu = \frac{T}{1 + K_d\, g(\varepsilon_d)} \tag{5.23}$$

$$K_d = 0.1334\ Z_2^{2/3}\ M_2^{-1/2} \tag{5.24}$$

$$g(\varepsilon_d) = \varepsilon_d + 0.40244\, \varepsilon_d^{3/4} + 3.4008\, \varepsilon_d^{1/6} \tag{5.25}$$

$$\varepsilon_d = 0.01014\, Z_2^{-7/3}\ T \tag{5.26}$$

5.2.7 Diffusion calculations

The radiation enhanced diffusion due to the high point defect concentration and the radiation induced segregation caused by coupling of defect and atom fluxes can be described by the diffusion equation. In one dimension this will be:

$$\frac{\partial C_v}{\partial t} = K_o - L_{vd} - L_r - \sum_j d_{vj} \left(\frac{\partial}{\partial x} \left(C_v \frac{\partial C_j}{\partial x} \right) - \frac{\partial}{\partial x} \left(C_j \frac{\partial C_v}{\partial x} \right) \right) \tag{5.27}$$

$$\frac{\partial C_i}{\partial t} = K_o - L_{id} - L_r - \sum_j d_{ij} \left(\frac{\partial}{\partial x} \left(C_i \frac{\partial C_j}{\partial x} \right) - \frac{\partial}{\partial x} \left(C_j \frac{\partial C_i}{\partial x} \right) \right) \tag{5.28}$$

$$\frac{\partial C_j}{\partial t} = d_{ij} \left(\frac{\partial}{\partial x} \left(C_i \frac{\partial C_j}{\partial x} + C_j \frac{\partial C_i}{\partial x} \right) \right) + d_{vj} \left(\frac{\partial}{\partial x} \left(C_v \frac{\partial C_j}{\partial x} + C_j \frac{\partial C_v}{\partial x} \right) \right) \tag{5.29}$$

where $j = 1, \ldots, n$

with

$$L_{vd} = \frac{2\pi\rho d}{\ln(R_d / R_0)} (C_v - C_v^{eq}) \sum_j d_{vj} C_j \tag{5.30}$$

$$L_{id} = \frac{2\pi\rho d}{\ln(R_d / R_0)} C_i \sum_j d_{ij} C_j \tag{5.31}$$

$$L_r = 4\pi C_v C_i \sum_j \left(\frac{6(d_{ij} + d_{vj})}{\lambda_j^2 Z_j} C_j\right) \tag{5.32}$$

and

$$d_{vj} = \frac{\lambda_j^2}{6} Z_j \nu_{vj} \exp\left(-\frac{E_{vj}^m}{kT}\right) \tag{5.33}$$

$$d_{ij} = \frac{\lambda_j^2}{6} Z_j \nu_{ij} \exp\left(-\frac{E_{ij}^m}{kT}\right) \tag{5.34}$$

where, v, i, and j denote vacancy, interstitial, and j th element in n-component target respectively, C's are concentrations, K_0 is the defect production rate, L_{vd} and L_{id} are vacancy and interstitial loss rate to dislocations, L_r is v-i recombination loss rate, d_{vj} and d_{ij} are partial diffusivities, λ_j and Z_j are the jump distance and coordination number of the jth element, ν_{vj} , ν_{ij} , E_{vj}^m , E_{ij}^m and are the vibrational frequencies and energy of motion for the vacancy and interstitial of the jth alloy component, ρ_d is the dislocation density, R_d is the spacing between dislocations, R_0 is the dislocation core radius, and C_v^{eq} is the equilibrium vacancy concentration. This diffusion equation is numerically solved simultaneously, along with the collisional part as follows [1]. First, the total irradiation time is appropriately divided with a global time step Δt_g. Next, the corresponding number of neutron histories are followed without diffusion, creating defects and modifying the target by only collisional processes. Then, the resulting target profile is used as an initial condition to solve the diffusion equation from time=0 to time=Δt_g. The defect production rate is assumed to be constant during diffusion, which is

$$K_0(x) = \frac{\Delta C_d(x)}{\Delta t_g} \tag{5.35}$$

where, Δc_d is the depth-dependent defect concentration resulted from the collisional simulation in Δt_g. The concentration profile obtained from the diffusion equation will then be used as an initial target configuration for the next collisional simulation, and so on. To solve the diffusion equation, MINIR uses 'methods of lines', in which the space variable x is discritized while leaving the time t continuous. The resulting system of ordinary differential equation is solved with an ODE solver (LSODE) in Crays along with boundary conditions.

5.2.8 Biasing techniques

Splitting

To improve the statistics of the Monte Carlo code, several biasing techniques were used. The first one is the splitting and Russian Roulette technique. As particles migrate in an important direction, they are increased in number to provide better sampling, but if they head in the opposite direction, they are killed in an unbiased manner to avoid wasting time on them. When a particle of weight W passes from a region of importance I to one of higher importance I', the particle is split into a number of particles of lower weight according to the following recipe. If I'/I is an integer (e.g. 10), the particle is split into n identical particles, each weighing W/n. Thus, weight is preserved in the integer splitting process.

Russian Roulette

If a particle of weight W passes from a region of importance I to one of lower importance I', so that I'/I < 1, Russian roulette is played and the particle is killed with probability 1-(i'/I), or followed further with probability I'/I and weight W*I/I'.

Forced collisions

Since the thicknesses of coatings used in the fusion field ranges from several micrometers (in case of chemical vapor deposition coatings) to few millimeters (in case of plasma sprayed and brazed coatings), it is important to be able to simulate the damage

produced by neutrons in such small thicknesses. On the other hand, the average mean free path of a fast neutron is of the order of few centimeters. A special variance reduction method is adopted to force more neutron collisions in such small distances. In the method of forced collisions [6], whenever the neutron enters the volume of interest (the interface region in our case), we split the neutron into two smaller weight particles, the first of which passes through the volume without colliding, and the second of which is forced to collide. The neutron that survives without collision has a weight

$$w_e = w\, e^{-\Sigma u} \tag{5.35}$$

and the neutron that collides has a weight

$$w_c = w\,(1 - e^{-\Sigma u}) \tag{5.36}$$

where u is the distance the neutron has to move before exiting the volume of interest. Then, we generate x, the distance travelled before a collision from the random number R to be

$$x = -\frac{1}{\Sigma} \ln\left\{(1 - R\,(1 - e^{-\Sigma u})\right\} \tag{5.37}$$

5.2.9 Other features of the Monte Carlo code

Vectorization (parallel calculations): the vectorized algorithm may be described as an "event-based" algorithm versus the conventional "history-based" algorithms of scalar Monte Carlo codes. In a vectorized code, a given number of particles are followed simultaneously, continuously adding the generated recoil atoms in the particle stack until all of the particles are deleted from the stack by one of the termination mechanisms.

Grouping of recoils concept is used. The incident PKA is designated as group 0. The secondary recoils will have the group index 1, and so on. This is done for the purpose of efficient use of the program to a given specific problem.

The concept of dynamic memory is used because the actual memory size necessary to store the particle information depends on the specific problem. Since the size of an executable program strongly depends on the memory size used, the appropriate use of the dynamic memory allocation increases the efficiency of the program.

Neutron cross sections

The proper assessment of the neutron simulation technique depends to a large extent on the neutron data library. The ENDF/V library was used for the evaluation of the neutron cross sections in the energy range .5 MeV to 14.1 MeV. Detailed data on the (n,2n) reaction were obtained from the JENDL-(3) library. As mentioned before, the reaction is treated as two process. The first neutron is considered to be emitted via inelastic reaction. The angular distribution is sampled from the given probability density function (after integrating them to cumulative density functions). The second neutron is assumed to be emitted isotropically and its energy is sampled from the given probability density functions. In each case, the energy and angle of the recoil target atoms are calculated.

5.3 Parametric study of RIM along the interface of a Be/Fe bonded structure

Many candidate duplex structures were proposed for the International Thermonuclear Experimental Reactor (ITER) [7]. It is obvious that the damage along the interfaces should be a key factor in the acceptance of any candidate system. Depleted zones, change in composition, and helium concentration along interfaces are among the factors that may affect the adhesion, and ultimately the performance, of any duplex structures.

The case study was taken as a duplex structure of 10 μm Beryllium on a semi-infinite layer of iron. A parametric study of the intermixing along the interface was carried out for different fluences as well as different thicknesses of the Be coating.

5.3.1 Effect of neutron fluence

Four runs were made for fluences 10^{19} to 10^{22} n/cm^2. Results are shown in Figures 5.3 and 5.4 for the Be and Fe concentrations. As was expected, the higher the fluence is, the larger the atomic mixing along the interface. It can also be noticed that appreciable mixing occurred at the higher fluence (10^{22} n/cm^2) that extended to about 1500 angstroms around the interface. This has a profound implication for near-term devices exposed to higher fluences.

As was mentioned in chapter 4, Radiation Induced Segregation (RIS) is an important phenomena for candidate fusion structures because the segregation of certain elements to surfaces, grain boundaries and interfaces do influence physical as well as mechanical properties. RIS could have deleterious effects on the creep-rupture, fatigue crack growth rate or ductile to brittle transition temperature of the involved materials. RIS also affects other irradiation mechanisms. Because of the sensitivity of void nucleation to segregation-induced bias modifications, one must inevitably conclude that void formation and swelling is to a large degree dependent on, if not entirely determined by, the radiation-induced segregation and precipitation. This conclusion lends much support to the empirically derived hypothesis by Garner that microchemical evolution is one of the major factors which controls the onset of swelling in austenitic stainless steels, and perhaps other alloys.

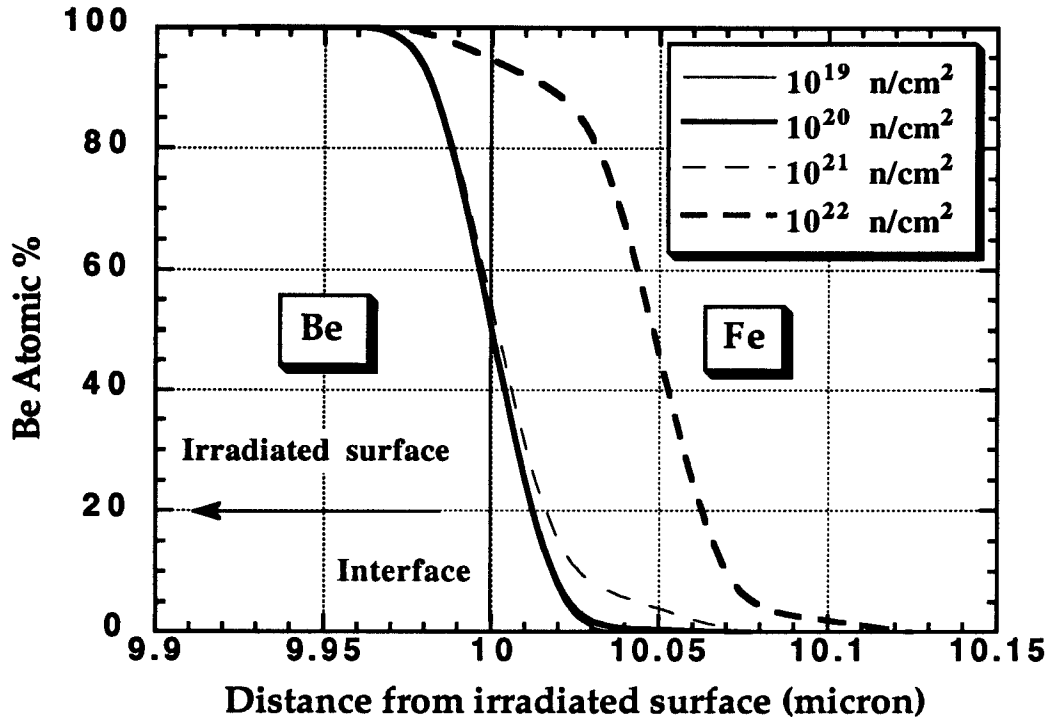

Figure 5.3: Effect neutron fluence on the beryllium atomic concentration along the interface of a Be/Fe joint.

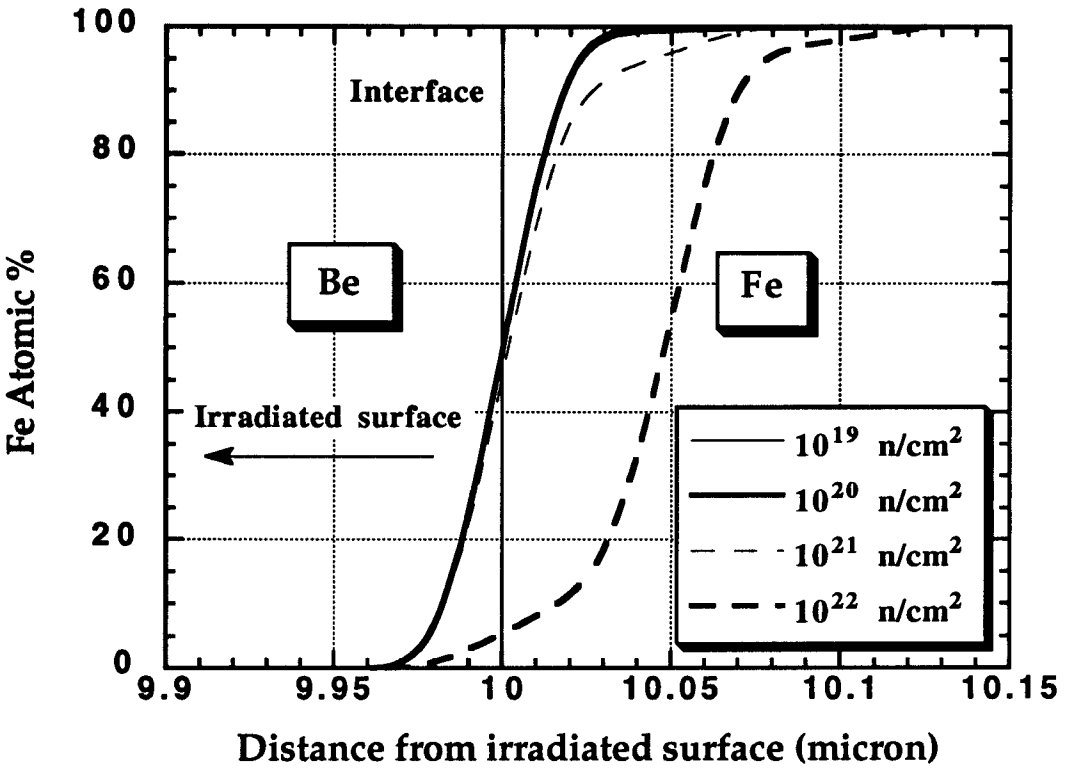

Figure 5.4: Effect neutron fluence on the iron atomic concentration along the interface of a Be/Fe joint.

The effects of RIS could be especially large when continual films of a phase, which may not even be present in the alloy under equilibrium conditions, would start to be formed at interfaces. It is quite obvious from Figures 5.3 and 5.4 that RIM induce changes similar to those expected due to RIS. Due to the small thickness of the coatings used, and the large mean free path for the 14.1 MeV neutrons, larger mixing is induced in the substrate (iron in our case) compared with the coating (beryllium in the case under study). This has serious implications as it may affect the microchemical conditions for swelling. Since this occurs in a very thin layer just beyond the interface, local unpredicted swelling in this area is deleterious to the proper function of the coating and its adhesion. Thus, the RIM phenomena is especially important when analyzing the swelling behavior of substrate alloys such as austenitic stainless steels.

5.3.2 Effect of Be thickness

Three cases were considered: 5, 10, and 20 micrometer thick Be coating on a semi-infinite iron substrate. Be and Fe concentrations are shown in Figures 5.5 and 5.6. Due to the high energy of the incident neutrons, the smaller the thickness, the more its probability not to be affected by the neutrons. As the thickness increases, the back-scattered atoms are increasing in number. This accounts for the increase in the beryllium concentration along the interface. For thicker coatings, more atoms will be displaced away from the interface, resulting in large number of secondary knock-on atoms along the interface, increasing the level of atomic mixing there.

As was mentioned in chapter 2, erosion is the primary issue that drives coating fabrication requirements in the fusion field. Since the accuracy of erosion predictions cannot be adequately evaluated on the basis of existing experimental data, the only prudent course of action is to continue to develop technology to apply thicker coatings of plasma side materials.

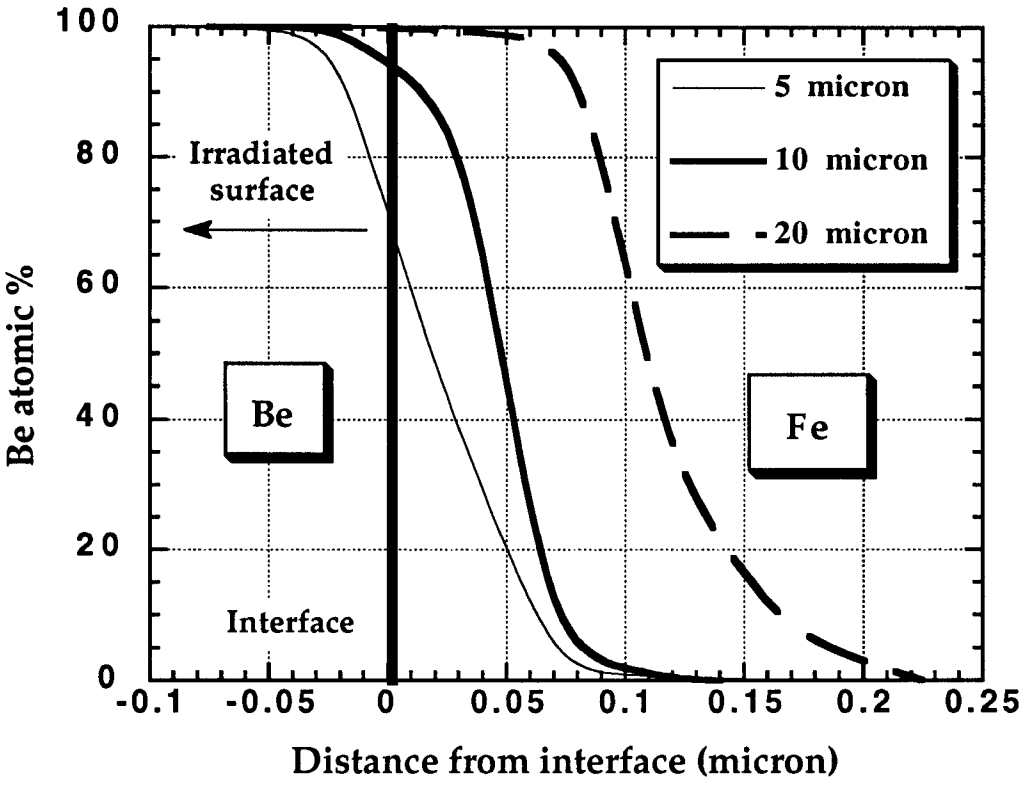

Figure 5.5: Effect of coating thickness on beryllium mixing along the interface of a Be/Fe joint exposed to a neutron fluence of 10^{22} n/cm^2

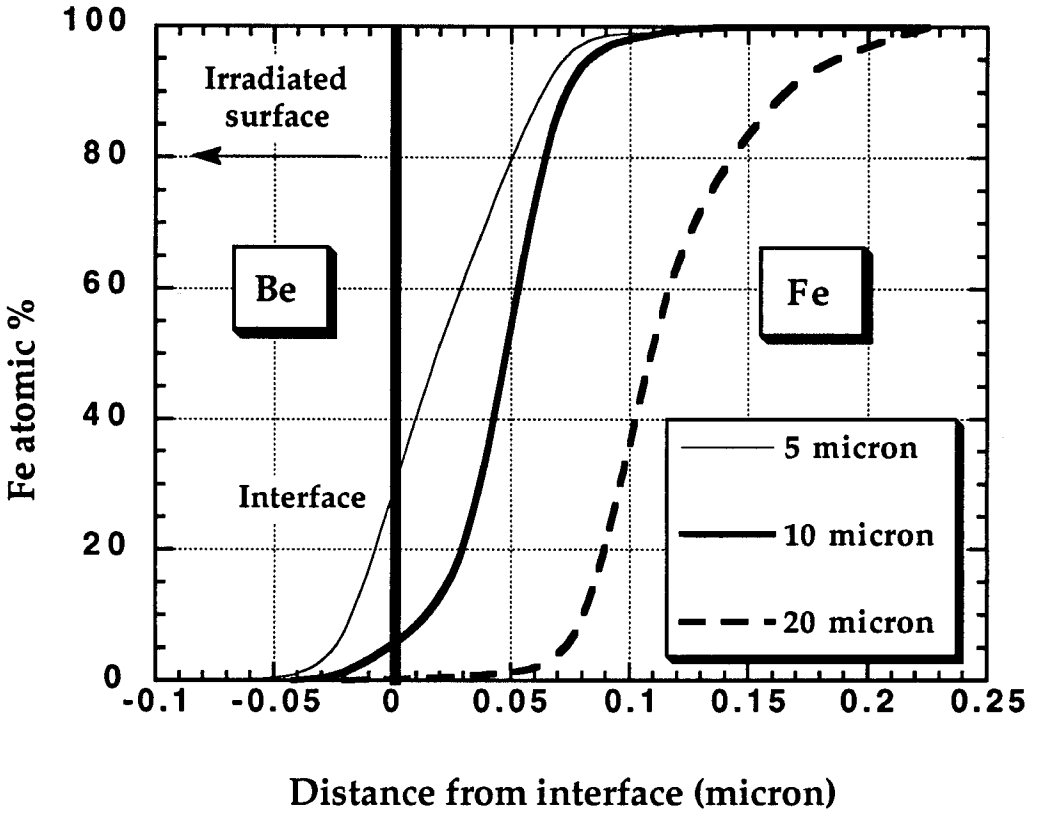

Figure 5.6: Effect of coating thickness on the iron mixing along the interface of a Be/Fe joint exposed to neutron fluence of 10^{22} n/cm^2

Thus, it can be concluded that this approach not only aggravates the thermal stresses in coated materials, but it also has serious implications on increasing the radiation induced mixing along the interfaces.

5.4 RIM along Be/Fe joint in the ITER environment

To investigate the impact of RIM in an actual fusion design, the Be coating on the Fe first wall structural material of the ITER design exposed to a wall loading of 2 MW/m^2 (i.e., $2.79*10^{21}$ n/cm^2) was investigated. This represents the 14.1 MeV neutron current incident on the first wall [10]. To reduce the run time, only 10 microns were simulated for the beryllium (instead of the expected thickness of 1000 micron [10]). Results are shown in Figure 5.7. It is clear that the mixing layer extended to about 0.1 micron (i.e., 1000 angstroms) along the interface.

The effect of RIM in ITER has many implications on the thermophysical and elastic properties along the interface which are of special importance for the behavior of the first wall. As shown in Figure 5.8, the atomic mixing significantly smoothed the transition in Young's modulus values between the Be coating and the iron substarte. Bulk values were obtained from references 11 and 12. It is to be noted that the mixing layer at the average operating temperature (i.e. 500 °C [10]) will be broadened due to thermal and irradiation diffusion. Figure 5.8 is calculated for the two different loading cases [13], isostrain (where the load is applied parallel to the interface) and isostress (where the load is applied perpendicular to the interface). Of course, the actual loading conditions will be a combination of both cases.

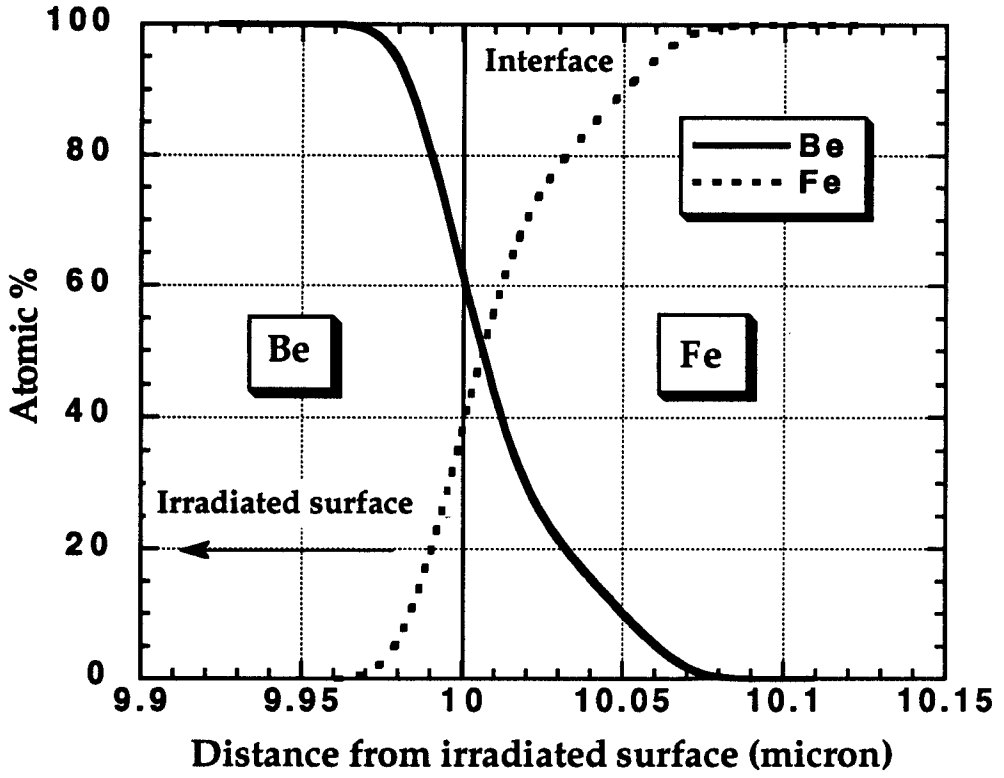

Figure 5.7: Atomic concentration along the interface between beryllium and iron for ITER first wall exposed to wall loading of 2 Mw/m^2 ($2.79*10^{21}$ n/cm^2).

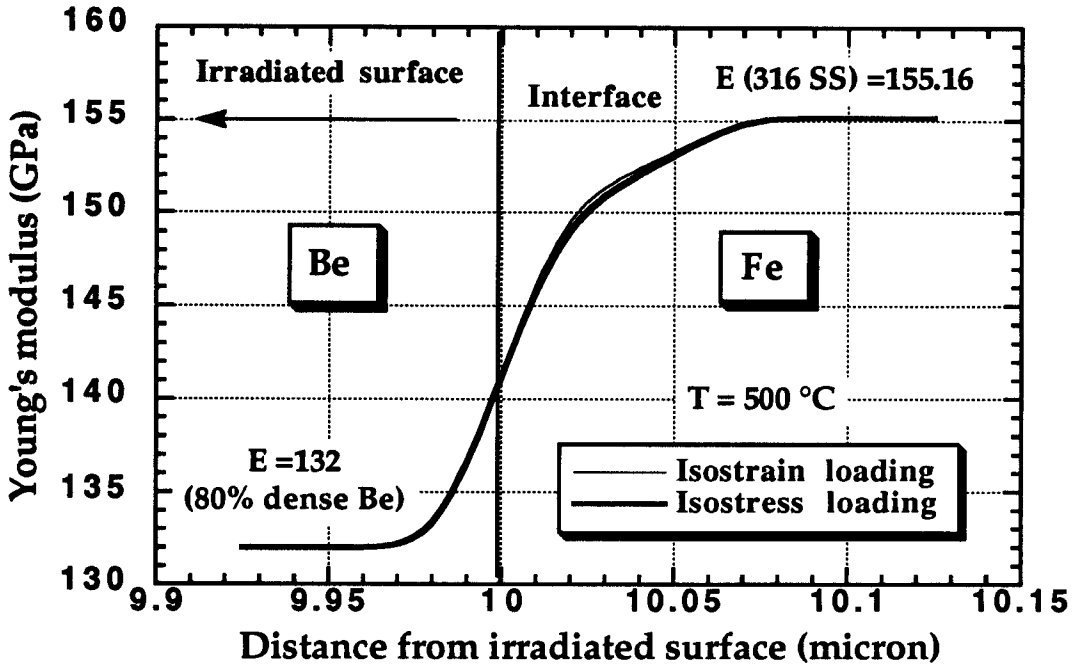

Figure 5.8: Smmothing of the Young's modulus mismatch between Be coating and iron substarte for ITER first wall structure due to Radiation Induced Mixing.

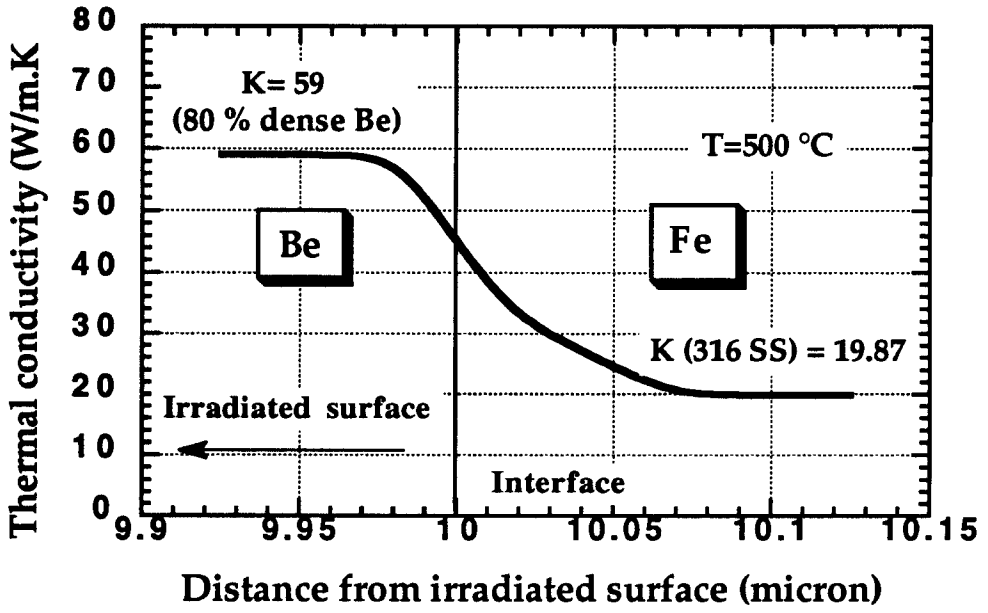

Figure 5.9: Reduction in thermal conductivity along the interface between Be coating and iron substrate for ITER first wall structure due to Radiation Induced Mixing.

RIM is expected to alter the thermophysical properties that depend on composition. In Figure 5.9, the induced changes in thermal conductivities along the interface due to RIM is calculated according to the principles of thermal conductivities for heterogeneous solids [14]. Regardless of the fact that the thermal conductivity acquired smoother transition, its value for the Be coating is reduced along the interface which may affect the heat conducted to the substrate. As shown, the reduction amounts to nearly 22% of its bulk value.

5.5 Conclusions

1. Radiation Induced Mixing (RIM) along interfaces of bonded structures proved to be a significant phenomena for fusion reactor environments. Mixing layer of hundreds angstroms thick were formed between Beryllium and iron joint structure.

2. For ITER first wall (10 micron beryllium thick coating) exposed to a wall loading of 2 MW/m^2, a mixing layer of about 0.1 micron was formed along the interface. This reduced the thermal conductivity of the Be coating at the interface to 78% of its bulk value. It also caused a smooth transition in the Young's modulus values along the interface between the coating and the substrate.

3. The higher the fluence is, the larger the atomic mixing along the interface. Thus, it is expected that RIM will have more impact on near and far term fusion devices exposed to high fluences.

4. RIM induces changes similar to those expected due to Radiation Induced Segregation (RIS). Due to the small thickness of the coatings used, and the inherent forward-scattering nature of the scattering cross sections in the MeV region, larger mixing will be induced in the substrates compared with the coatings. This has serious implications as it may affect the chemical conditions for swelling. Since this occurs in a very thin layer just beyond the interface, the RIM phenomena should be taken into consideration when analyzing the swelling behavior of substarte alloys such as 316 SS. RIM could also have deleterious effects on mechanical properties that are dependent on the microchemical constituents of the materials involved such as the creep-rupture, fatigue crack growth rate or ductile to brittle transition temperature.

5. Thick coatings will result in an appreciably thicker mixing layer compared with thin coatings. Since thick coatings (of the order of few millimeters) are assumed for current

designs, it is apparent that high values of RIM will be induced in such designs regardless of the low expected fluences

6. Experimental verification of RIM using the techniques for RIS analysis is needed to quantify the mixing induced. The impact of RIM on radiation induced phenomena, like swelling and change in mechanical properties, also need to be evaluated.

7. Taking the thermal as well as the irradiation diffusion into consideration is expected to broaden the mixing layer along the interface. This is an important area that needs to be investigated. However, lack of diffusion data, especially for Plasma Facing Components materials, is a serious drawback that limit the prediction of the behavior of bonded structures.

5.6 References

[1] S. Han, University of Wisconsin report **UWFDM 789** (1988).

[2] R. W. Conn, et al., UCLA PPG-815 (1984).

[3] F. Davarya, et al., J Vac Sci. Techn. **A 1 (2)**, 467 (1983)

[4] M. L. Roush, et al., Nucl. Inst. Meth. **194**, 611 (1982).

[5] D. M. Goebel, et al., PPG-1125 UCLA-ENG-88-02 (1988).

[6] E. E. Lewis and W. F. Miller, Computational methods of neutron transport, John Wiley & Sons (1984).

[7] R. T. McGrath, et. al., SAND89-0901 (1989).

[8] Final report on Coating and surface modifications, Division of Materials sciences, US DOE (1984).

[10] Dr. A. Hassanein, ANL, Private communication, May 1993.

ANL/FPP/TM-86 (1986).

[11] R. F. Mattas, Austenitic stainless steel bulk property considerations for fusion reactors, ANL/FPP/TM-86 (1986).

[12] M. C. Billone and S. Majumdar, Thermomechanical analysis of the U.S.-ITER driver blanket, 9th topical meeting on the technology of fusion energy (poster session), Oak Brook, Illinois, October 7-11 (1990)

[13] C. R. Barrett, et al., The Principles of Engineering Materials, Prentice-Hall, inc. (1973).

[14] J. E. Parrott and A. D. Stuckes, Thermal conductivity of solids, Pion limited (1975).

Chapter 6.

Theoretical Impact of Swelling-Creep-Stress Relationship on Bonded Structure Behavior

6.1 Introduction

Duplex structures (i.e., coatings or thin films on a substrate structure) are likely to be used for high heat flux components in both near-term and commercial fusion reactors. The bonding of these structures leads to complicated stress fields which must be understood in order to evaluate the probability of failure for the device [1]. Radiation damage will be a major factor in the design of the different duplex components and the synergistic effects of high heat fluxes, high dpa (displacement per atom) levels, and high primary stresses must be taken into consideration. While radiation-effects data on (as well as modelling for) individual fundamental phenomena can be correlated to structural effects, the uncertainty in synergistic effects could jeopardize the success of the final design [2].

The mechanisms of irradiation damage at the interface of bonded structures are not well understood. Although the damage mechanisms which occur in metallic materials should also apply to coatings (e.g., swelling or differential swelling). Of greatest concern are the fatigue/crack propagation properties and the effects of irradiation on swelling and embrittlement of the materials [3].

Swelling due to radiation-induced voids is a major concern for the first wall of fusion devices at temperatures above 400 °C and has been the focus of considerable alloy development effort since 1970's [4]. Researchers have typically used end of life limits on

swelling of 2-10% volumetric swelling [5]. Stress is also known to reduce the incubation period for swelling (see section 2). Since one probable mechanism of failure of bonded structures is, in fact, the level of differential swelling [6], it is obvious why an understanding of swelling (and the effect of stress on it) is critical to the design of successful bonded structures.

Irradiation creep and swelling have a common source and hence there is a possibility that an interrelationship between both phenomena exists [7]. There would be many practical consequences of such coupling. Flinn et al., [8] indicated that if no competing mechanism existed (swelling-enhanced creep for example), the residual stresses due to differential swelling could build up with exposure to a level where a component could yield or fracture. Thus, if irradiation creep and swelling are proportional to each other, many of the problems generated by differential swelling would be minimized through the relaxation mechanism of the swelling-enhanced creep. Daenner and Raeder [9] indicated that it would be dangerous to regard swelling and creep separately. They also proved that it is dangerous to see the stress/strain analysis isolated from the materials behavior. Figure 6.1 is a schematic of the relationships that exist between swelling, creep, and stress, together with the different systems involved in the analysis. The heavy lines indicate the areas that are examined in this work.

For ITER and beyond, experimental data on the effect of stress on swelling, and the relationship between radiation creep and swelling are badly needed [10]. One of the major concerns for 316 SS, for example, is the differential swelling in 400-500 °C range [11]. This is the range where stress-enhanced swelling was first noticed. While extensive stress analyses have been carried out for plasma facing components made of single materials such as 316 stainless steel, stress analysis for bonded structures is only in its early stages of

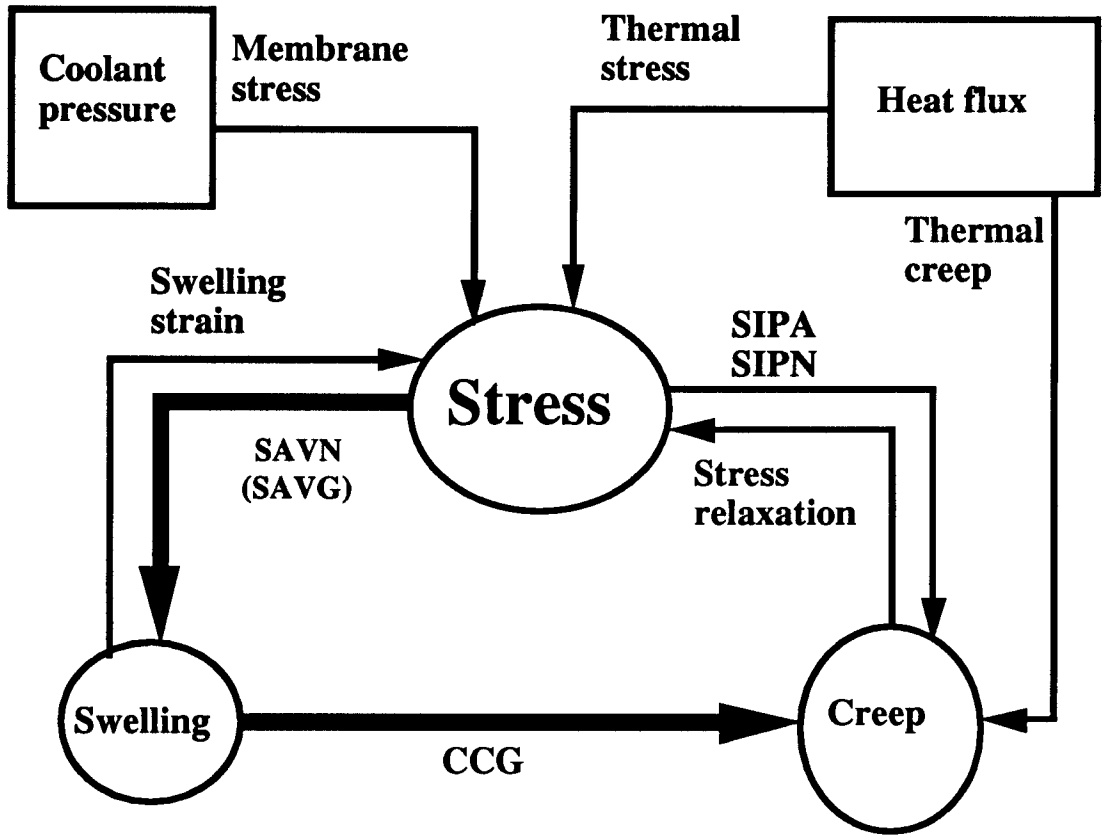

SIPA : Stress Induced Preferential Absorption
SIPN : Stress Induced Preferential Nucleation
SAVG : Stress-Assisted Void Growth (possibly)
SAVN : Stress Assisted Void Nucleation
CCG : Climb-Controlled Glide

Figure 6.1: Relationship between Swelling-Creep-Stress in a radiation environment

development [12]. The major work in this area is mainly from Mattas [10,13,14], Glasgow [15], and Blanchard [1,16]. None of these previous studies, as well as the few inelastic stress analyses that included radiation effects [5,9,17-23], have incorporated the effect of stress on the swelling. Only Mattas [10] took the interrelationship between creep and swelling into consideration.

6.2 Stress-enhanced swelling phenomena

The effect of stress on swelling was first recognized in 1967 when Cawthorne and Fulton [24] reported that "there is no doubt that stress and strain during irradiation will influence void growth". Since that time, it has become obvious, from the substantial amount of available data that stress plays a major role in the onset (and possibly) the rate of void growth in AISI 316 stainless steel in a variety of metallurgical conditions [18,24,25-34]. A more limited set of data on AISI 304 [35], Deutsches Institut fur Normung DIN 1.4970 and 12RN72 [36] as well as Nickel [37-41] shows that the effect of stress on void swelling is not limited to 316 stainless steel.

Much of the early work on stress-swelling interactions, in the absence of adequate irradiation effects data, involved theoretical modelling. In general, it was predicted that a tensile stress will enhance and a compressive stress will retard the operation of mechanisms associated with the swelling phenomena [42-46]. Most of these predictions were based on the stress effect on dislocations bias for vacancies (see section 6.3.1). Bates and Gilbert [25] described stress-enhanced swelling in AISI Type 316 stainless steel fuel cladding and showed experimentally that an apparently linear relationship exists between tensile stress and swelling in both annealed and cold-worked material, provided the yield strength of the material is not exceeded. That was confirmed by other investigators who studied the swelling behavior of

stressed cladding and compared that with unstressed capsules (see Figure 6.2) as well as work on pressurized tubes (Figure 6.3) [24,25-32,47]. It was later shown that this linear relationship was misleading and that the principal effect of stress was that of shortening the transient regime of swelling [33]. Since the late seventies, the effect of stress has been studied using pressurized tubes (where the stress states were not purely hydrostatic but involved strong shear stresses). Recently, however, irradiated foils were also studied to assess the effect of compressive as well as tensile stress [33,48-51].

The results of stress effects on void swelling are summarized to discriminate between various mechanisms as follows:

1. External stresses reduce the incubation period for void formation [17,33,36,53-56]. For the case of austenitic steels, this behavior is linear for applied stresses up to the proportional elastic limit of the material. Stresses in excess of the proportional elastic limit can extend the incubation time [25,31,32,56]. Thus, annealed material will show greater sensitivity to stress [57].
2. Both the incubation period and the growth rate are indifferent to reversion of stress from uniaxial tension to compression, indicating a possible effect of deviatoric components of the stress, as well as the hydrostatic component [33,48-51].
3. The total void density established during the nucleation stage may increase [38,54] or decrease [48] with stress. However, as the steady state swelling is reached, the total void density is insensitive to the applied stress [48,58]. Also, the increase in void density is compensated partially by a downward shift of the mean void size, particularly at higher stresses [7].
4. The void growth rate is unaltered by external stresses. The observed increase of void size with increasing stress at a given dose in some experiments is explained as

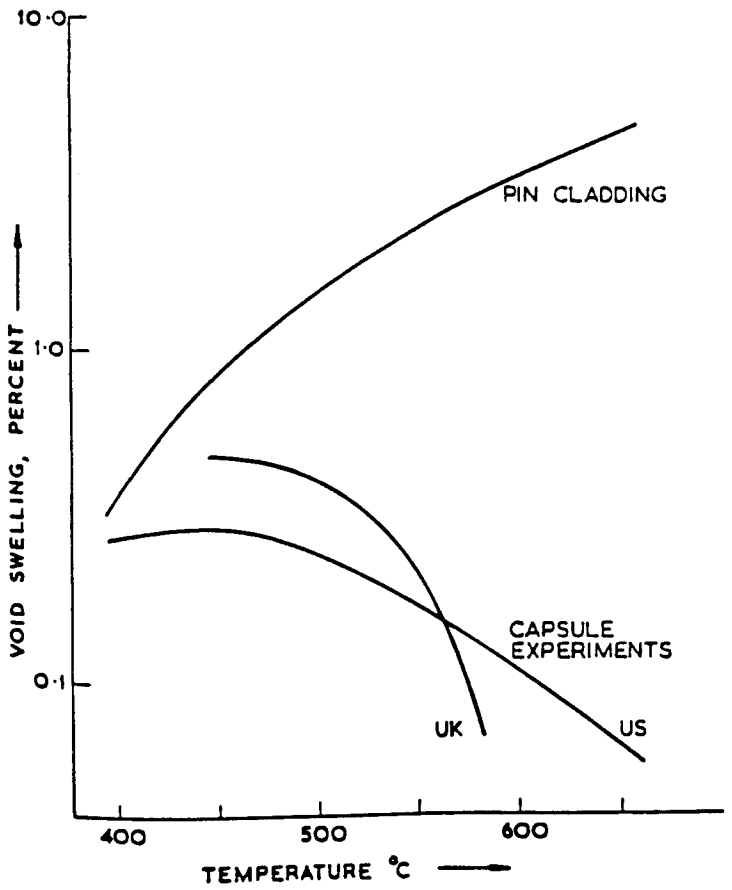

Figure 6.2: Swelling-temperature relationships on a SA 316 steel irradiated as cladding and capsule experiments at Dounreay Fast Reactor after 16 dpa [52]

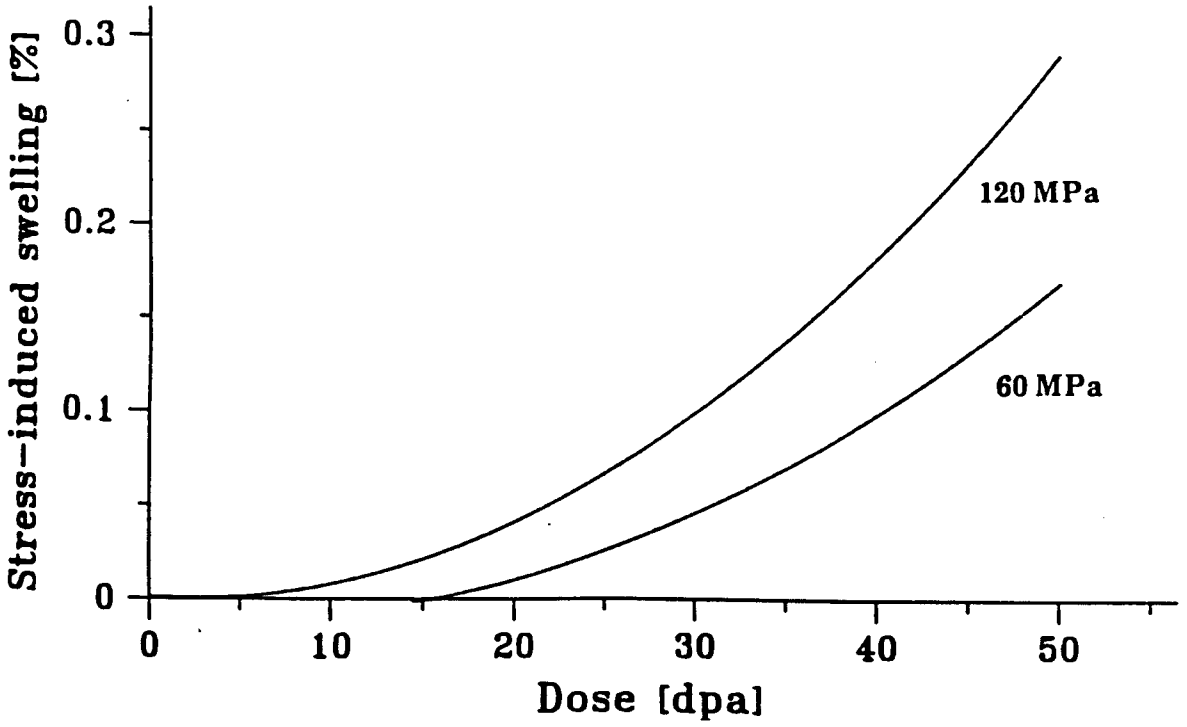

Figure 6.3: Reduction of swelling incubation dose due to stress at 420 °C for DIN 1.4970 steel after 52 dpa [36]

resulting from the reduced incubation time with stress. However, the possibility of stress effects on the growth rate is not totally overruled [59].

Stress-affected swelling spans the entire temperature range applicable to fast reactors (350-650 °C), but it appears that more than one mechanism is involved, one which dominates at relatively low temperature and another which controls at higher temperatures (>550°C) [59]. Generally speaking the effect of stress on void nucleation at temperatures below 400 °C may be negligible [59-60]. Thus, it is difficult to observe the phenomena at low temperature [59], particularly in materials with short incubation periods [35]. However, at higher temperatures, the influence of stress is more pronounced [53].

At lower fluences and flux levels, the effect of stress on swelling is difficult to recognize, especially if the temperature is low [35,47]. It should also be clear that the effect of stress on swelling is a transient one, which is not repeated when the stress is removed, since it affects the incubation dose. Applied stresses probably cannot completely eliminate the incubation period. Porter and Garner [35] showed that a tensile-shear stress applied during neutron irradiation cannot shorten the transient duration of AISI 304 below nearly 10 dpa minimum characteristic of the Fe-Cr-Ni and Fe-Cr-Mn systems. The magnitude of the enhanced swelling is very sensitive to dose rate. The effect of stress at low irradiation temperatures is more pronounced at the higher displacement rates where void nucleation is more difficult and the transients are longer.

6.3 Stress-enhanced swelling mechanisms

Externally applied stresses do not operate in a mechanical sense directly on the void surface [42]. The microscopic mechanism for the stress enhancement of the swelling rate is

that the growth rate for each individual void is the same but a greater number of voids is nucleated when a stress is applied. However, a faster growth rate under stress for each individual void, with the same number of voids as in unstressed material, or a combination of both effects, is not totally overruled. The difference between the two effects is depicted in Figure 6.4. Since it is possible to envisage a large number of processes that would produce an interaction between stress and swelling, the different mechanisms will be briefly reviewed according to temperature domains.

6.3.1 Low temperature regime

The low temperature regime exhibits a stress effect with little or no temperature dependence [59]. It is important to note that the Q value approach used to describe the reduction of the incubation period with stress (see section 6.4) is essentially constant at low irradiation temperature but it increases sharply above 600 °C as is shown in Figure 6.5 [59]. At temperatures below the peak swelling temperature (550 °C for 316 SS), the explanation probably is related to the effect of stress on the evolution of dislocation density and the impact that it has on the nucleation period of swelling.

Before discussing the proposed model, it is interesting to note that one of the early models presented to explain the stress-enhanced swelling at low temperatures analyzes the effect of stress on the different capture efficiencies of voids for vacancies and interstitials [25,37,38,48,55,57,58,62-65]. In this model, as the void grows larger (> 100 A) the shear stress, which is ineffective for small voids, may increase the bias again, thereby reducing the swelling rate. Based on this model, the mechanism is only weakly dependent on temperature [37,38]. Also, a stress effect on void nucleation rates is predicted at all temperatures. If the nucleation rate for the stress-free case is already very large and the incubation period rather short, a further reduction by stress may not be observable [25,65]. Hence, the effect of

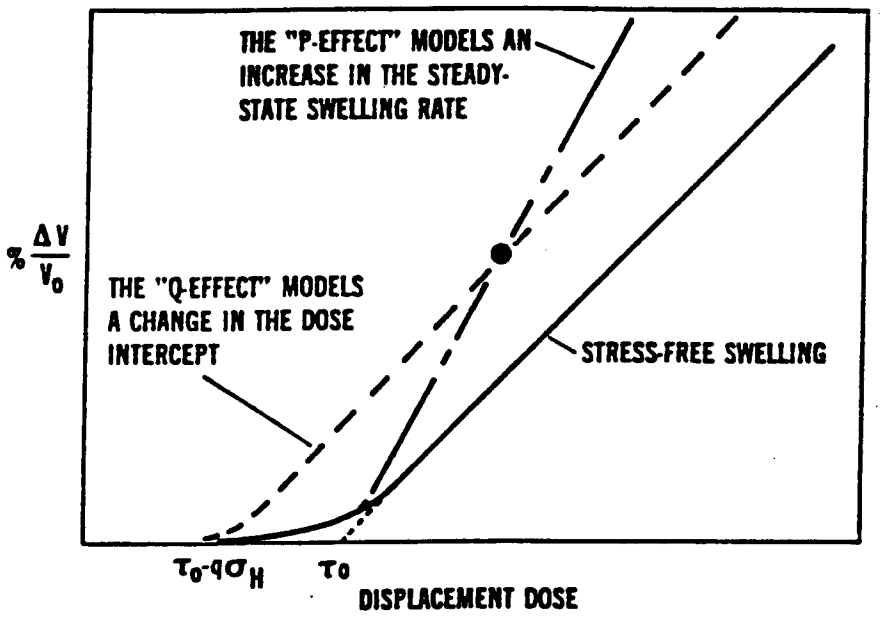

Figure 6.4: Schematic representation of the proposed models of stress-enhanced swelling [59]

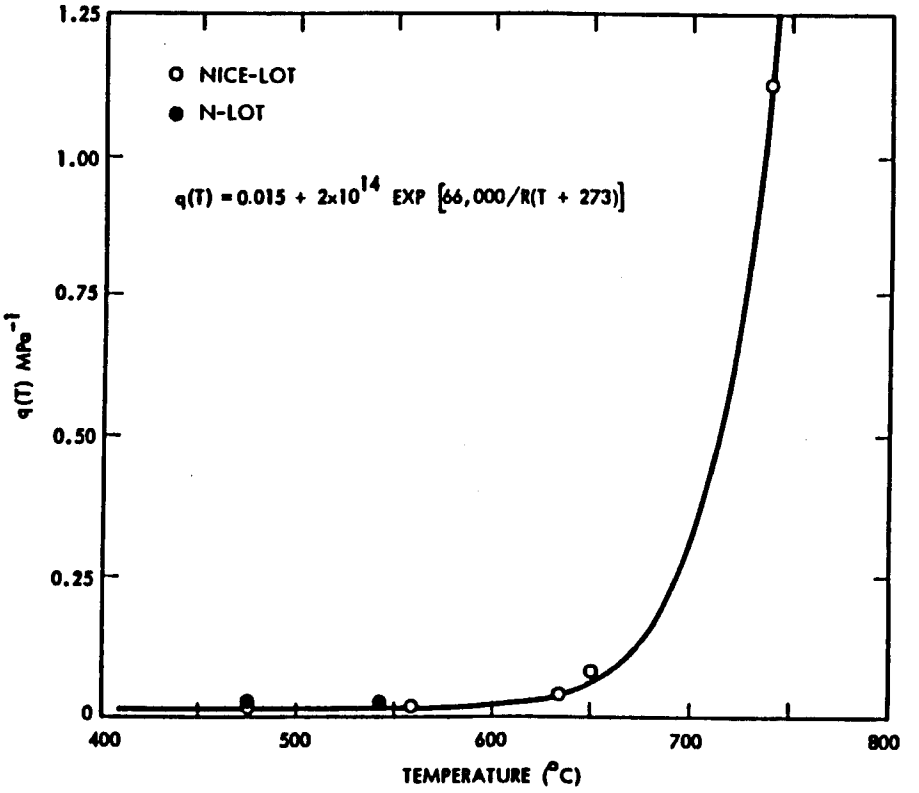

Figure 6.5: Temperature and heat dependence of the q-coefficient for 20% CW AISI 316 pressurized tubes irradiated at EBR-II [61]

stress on void nucleation at temperatures below 400 °C may be negligible. However, such an effect may be substantial at a temperature of 500 °C. Regardless of the success of this model to account for many of the manifestations of the phenomena, it was recently rejected because it predicts lower swelling under compressive hydrostatic stress and this contradicts recent findings [33,48-51].

Since the void nucleation rate depends on the dislocation density, the enhanced nucleation rate may reflect the acceleration of dislocation development with stress. An observable void density is produced in areas where dislocation loop densities were formed in the early stage of irradiation. This indicates the possibility that initial dislocation loops act as the nucleation sites of voids and such a hypothesis was used to formulate a successful model for the stress-enhanced swelling phenomena at low temperatures. The model predicts a shortening of the incubation period for swelling under stress by an accelerated development of the irradiation-induced loop structure [48-49,65]. The origin of this phenomenon may arise from the extraordinarily high strain field near the dislocation loop, thereby strongly enhancing the nucleation of voids [65]. Under stress, the enhanced growth of favorably oriented loops increases the average bias of the system and thus may induce a vacancy supersaturation and promote void nucleation. During void growth, the bias of the system is dominated by voids and dislocations, while the effect of stress may become of secondary importance.

This mechanism also depends on the shear component of the external stress and therefore works equally well under tension and compression [59]. It also accounts for the earlier nucleation in the partially annealed alloy reported in the literature when compared to the cold worked material, where the irradiation-induced loops have to compete with the network dislocations in this case [48]. Also, the model exhibits a weak dependence on temperature.

As for the extension of the incubation period after the stress reaches its proportional elastic value, it is related to the introduction of additional dislocations (i.e., the plastic yielding of the material) [25,32,56]. Also, if an effect of stress on the steady-state swelling rate exists, it will probably arise due to the increased Frank loop density [60].

It should be noted that the importance of loops as nucleation sites may be dominant if there are no precipitates or other sinks that could act as nucleation sites [65]. Thus, the previous mechanism needs more analysis for materials other than stainless steels. In the case of copper, it was reported that the evolution of voids and dislocations occurs in such a segregated form that the areas containing dislocations contain no voids and the areas containing voids contain practically no dislocations [66]. Similar heterogeneity in void distribution has also been observed in aluminum [66].

6.3.2 High temperature regime

Stress may have pronounced effects due to different mechanisms at high irradiation temperatures [67]. The observation of two swelling peaks in unstressed solution-treated 316 steel is consistent with this view that low and high temperature swelling are controlled differently. Also, there are significant changes at around 525 °C in the temperature dependencies of void size, void concentration and dislocation density observed at the Dounreay reactor which all may be associated with the change of controlling mechanism (Figures 6.6 and 6.7) [67]. Some of the 550 °C data at the highest stresses showed a marked increase in void size and decrease in number density, indicating the possibility that a different, or additional, stress effect exists.

6.3.2.1 Stress enhanced-vacancy thermal re-emission from dislocations

One of the possible effects is the effect of stress on the thermal vacancy concentrations at the various sinks (by altering the free energies of formation). Ultimately this may affect the

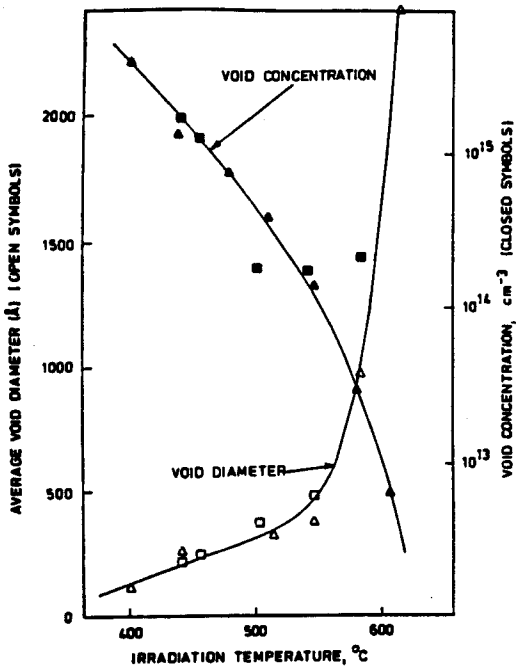

Figure 6.6: Average void diameters and void concentration in cold-worked M316 fuel pin cladding at Dounreay reactor for two different burnups [67].

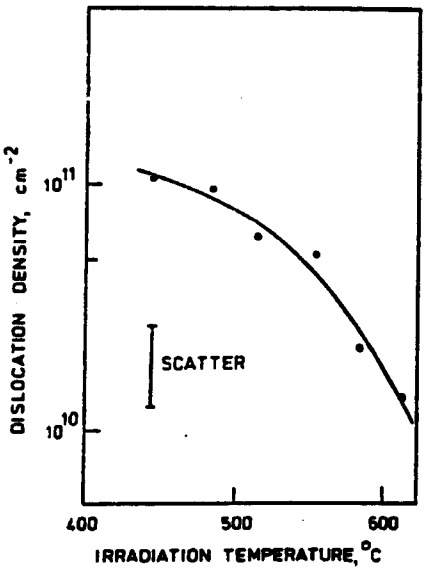

Figure 6.7: Dislocation density in V1294 cold-worked M316 cladding at Dounreay reactor [67]

thermal emission of vacancies from dislocations [45,53,55,58-60,56]. The process is temperature dependent. It was found to be too small at 500 °C to account for the sensitivity of the void density to stress. At higher temperatures, however, this mechanism gains in importance. At these temperatures, the thermal supersaturation of vacancies is low and the increment in the supersaturation due to stress can be significant. This would lead to a reduced critical cavity size and hence a reduced incubation time [66].

6.3.2.2 Stress enhanced-vacancy currents to voids

One effect of stress on void growth is expected to be the alteration of the free energies of migration for the point defects, with resultant changes in defect mobility [44,68-70]. In the general triaxial case, the presence of a void leads to a modulation of the local hydrostatic stress over the void surface with deviations above and below the level of hydrostatic stress present in the undisturbed matrix. This modulation then leads to altered point-defect diffusivities and currents and generates nonuniform concentration gradients and fluxes across the void surface. Void growth within grains can thus be enhanced due to stress-motivated point-defect currents. It is important to note that the biased flow of interstitials to voids (due to the stress gradients generated around voids by the external stress) is negligible [45,70]. There is a sharp dependence on temperature because the temperature dependence of the defect diffusivities dominates the temperature behavior (normally, at temperatures above 0.3 T_m all the single radiation-produced point defects (vacancies and interstitials) are mobile [67]). The diffusivities contain exponential terms in temperature, the effect of which overshadows that of other effects.

6.3.2.3 Stress Assisted Void Nucleation-Microchemical mechanism

The possibility exists that the required mechanism for stress enhanced swelling (at least in the case of AISI steels) is microchemical in nature [53,54]. However, this does not

preclude the possibility that the previously proposed microstructural mechanisms are also operating but not dominant under certain conditions. A plausible explanation of the stress effect [54] is that the degree of microchemical segregation required for swelling to commence is merely decreased by the application of a volumetric stress or the associated application of strain energy to the system. Such an effect may be manifested in a reduction in the effective stacking fault energy for dislocation loops or increases in defect mobilities. This microchemical mechanism is not anticipated to respond to compressive or cyclic stresses in the same manner as would the microstructurally-based mechanisms. As long as experimental constraints prevent a detailed study of phase evolution during low dose irradiation, the importance of this mechanism cannot be identified.

6.3.2.4 Effect of helium generation

Above 525°C the gas generation rate becomes important for swelling of steels [67]. It is only in this higher temperature regime that stress effects would be expected to become significant [67]. However, at these temperatures, stress may act only synergistically [65]. If the gases are produced during irradiation, stresses will then reduce the amount of gas needed to initiate void formation. If the gas is already present at the start of the irradiation, stresses may no longer influence the incubation dose. It is also to be noted that at high doses, gas-driven swelling rates may also exceed the bias-driven swelling rates at low doses [52] which supports the conclusion of a gas generation effect on the stress-enhanced swelling phenomena. This effect must be understood in the context that the effect of He/dpa ratio on stress-free swelling is non-monotonic and the incubation period could actually be a minimum for helium generation rates characteristic of fusion [71].

6.3.2.5 Other mechanisms

Other mechanisms have also been proposed throughout the literature to explain the stress-enhanced swelling phenomena. It was proposed that tensile stress promotes void growth by opposing the surface tension forces tending to minimize void size [28]. It was proven that the stress must be high (on the order of 370 MPa) and the void diameter large (>200 A) if stress is to exert a significant effect on void growth. Only at high temperatures, where void diameters are high, should stress then significantly accelerate void development. Thus, this mechanism should be thoroughly investigated especially in the context of the expected high stress fields as well as high dose levels in fusion reactors.

It is also very possible that enhanced irradiation creep under high temperature conditions promotes a coalescence of some of the smaller voids, thus accounting for the observed increase in void size in some experiments [54]. This may prove to be the case, taking into consideration the effect of stress on the void shape. In one study [72], this was taken into consideration by assuming that voids have an ellipsoidal shape. The change in equilibrium shape is negligible for small voids and small stresses; however, as larger voids (i.e., higher temperatures) and higher stresses are considered, the ellipticity ratio for equilibrium increases, eventually leading to spontaneous collapse of the void at a rate determined by the diffusion mechanism (dominant at high temperatures).

It is interesting to note that the growth of grain boundary cavities or helium bubbles under stress was considered in the early stages of the investigations to be the mechanism for the stress-enhanced swelling [42,44]. However, it was concluded that at typical LMFBR operating temperatures, the mechanism is not expected to yield significant density changes since intergranular failure will occur before significant density changes occur due to growth of grain boundary bubbles [42,44].

6.4 Modelling of stress-enhanced swelling

Bates and Gilbert [25], based on experimental data, developed the relationship between stress (σ) and swelling (S) for annealed steel of the form (Figure 6.8):

$$S_T = S_\circ \left[1 + P\,(\sigma - \beta \ln \sigma/\sigma_p) + \beta \left(\frac{1}{\sigma} - \frac{1}{\sigma_p}\right) \right] \qquad (6.1)$$

where;

S_T is the total swelling, $S_\circ$ is the stress-free swelling, P is a coefficient (apparently independent of fluence), σ_p is the stress at maximum swelling, and β is another coefficient. The above equation should be used only for stresses less than the unirradiated value of the proportional elastic limit.

Harbourne [73] developed an empirical model for the effect of stress on cladding swelling deduced from the experimental data. This was put on the form

$$\ln (\Delta V / V) = A + (n_0 + K \overline{\sigma})\ \ln (\phi\, t) \qquad (6.2)$$

where K is a constant, which may be determined from the experimental data. The values of K obtained in the study were fitted to an Arrhenius temperature function over the range 480 to 670 °C. This equation is a modification of the stress-free swelling equation [73].

Brager et al. [17,58] formulated the effect of stress on void nucleation as:

$$\rho_v(\sigma_H) / \rho_v(0) \approx \exp (n\, \Omega\, \sigma_H / kT) \qquad (6.3)$$

where ρ_v is the void number density, n is the number of vacancies in the critical nucleus, Ω is the atomic volume, and σ_H is the hydrostatic stress. The sign convention employed here implies that the application of a tensile stress enhances the probability of void nucleation.

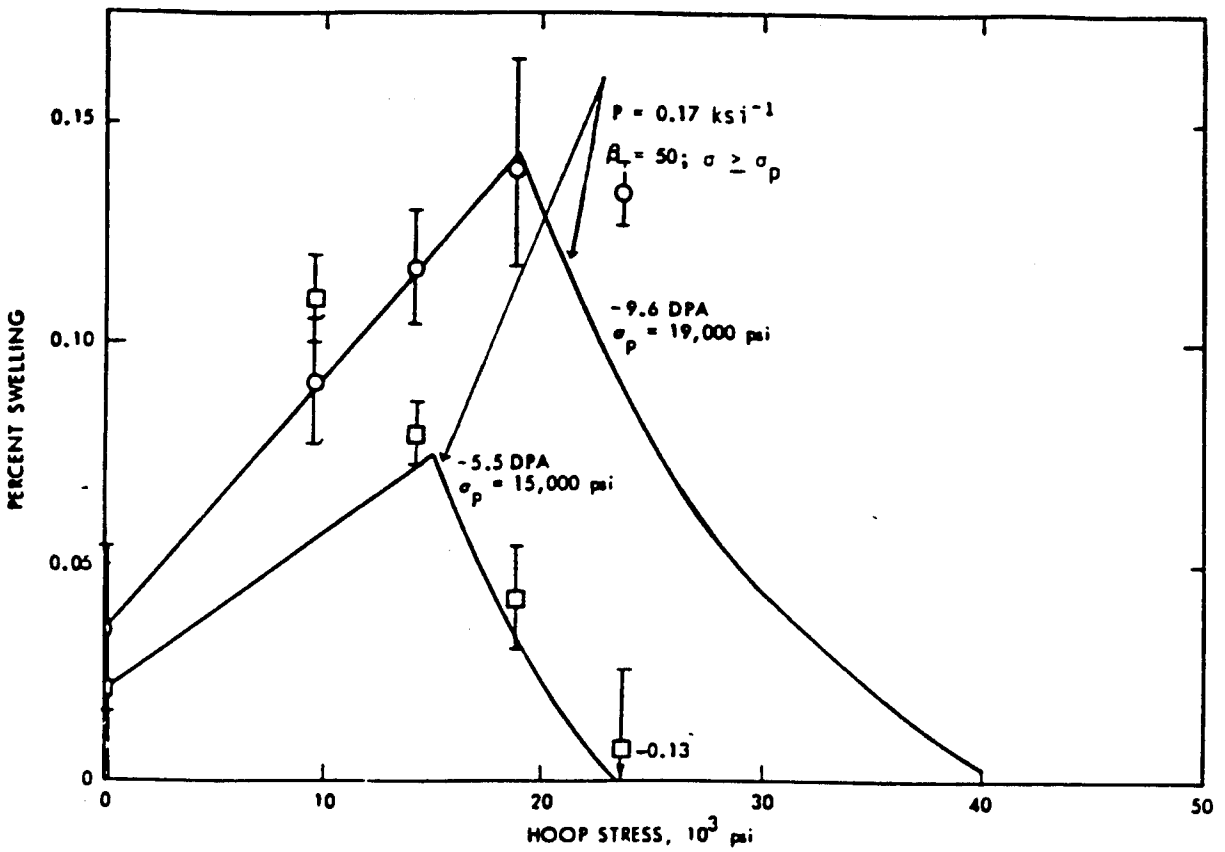

Figure 6.8: Effects of stress on swelling in annealed 316 SS pressurized tubes at 5.5 and 9.6 dpa (500 °C) [25].

Another equation was formulated [25,31,32,74] for the linear part of solution annealed steel and for the entire range of cold-worked steels:

$$S/S_0 = 1 + P\sigma_{hyd} \tag{6.4}$$

where σ_{hyd} =hydrostatic stress = $\frac{1}{3}(\sigma_1 + \sigma_2 + \sigma_3)$; S = total swelling (%); S_0 = stress-free swelling (%); and P = a constant. Of course, this equation suggests a stress modification of the swelling rate, not the incubation period.

An empirical constitutive equation for the stress effect on swelling incubation dose is given as the larger of [59]:

$$\tau_e = \tau - q(T)\,\sigma_h \tag{6.5}$$

$$\tau_e = 0.5 \tag{6.6}$$

where T is the temperature in units of °C,

σ_h is the hydrostatic stress in units of MPa, $\sigma_h = \frac{1}{3}(|\sigma_x| + |\sigma_y| + |\sigma_z|)$,

τ_e is the incubation parameter in units of 10^{22} n.cm^{-2} (E > 0.1 MeV),

q(T) expressed in the units of 10^{22} n.cm^{-2}. MPa^{-1} is calculated [159] from

$$q(T) = q_0 + \exp[\,a - Q'/(T + 273)\,] \tag{6.7}$$

where $q_0 = 0.013$, $a = 51.4$, $Q' = 50{,}000$ in units of °C^{-1}.

Straightforward use of the stress effect on incubation dose in fusion designs is complicated by the presence of time-varying stress histories. A formalism, called the Incubation Averaged Fluence (IAF) technique [27,32], has been developed so that this behavior can be included in calculations of the stress effect on incubation dose. The IAF, f(t), is defined as [50,55]

$$f(t) = \int_0^t \frac{\phi(t')}{\tau_e(t')}\,dt' \tag{6.8}$$

In this equation the effective incubation fluence τ_e depends on time through the time variation of the hydrostatic stress σ_H. The value of σ_H is used in calculating τ_e from the above equation describing the dependence of incubation dose on stress. The condition for swelling to remain in the incubation phase is now $f(t) < 1$, while the condition for steady state swelling is $f(t) > 1$.

6.5 Irradiation creep and its dependence on swelling

Irradiation creep is caused when external non-hydrostatic stresses are applied during irradiation. In a temperature regime where thermal creep and irradiation creep compete, the picture is that at high stress levels, thermal creep dominates. At low stress levels (<150 MPa) the deformation shows a linear stress dependence [166]. In a temperature/stress region (300-550 °C), where thermal creep can be neglected, irradiation creep is weakly temperature dependent. As for dose rate, a linear correlation of creep with the damage rate is observed. This may not be true for very low irradiation temperatures [75].

6.5.1 Climb-Controlled Glide creep

There are a number of theoretical approaches proposed in the literature to explain the phenomenon of irradiation creep [see for example 75-77]. Of the different mechanisms, the mechanisms of stress-induced loop nucleation or alignment (SIPN) and stress-induced preferential absorption (SIPA) have a common feature that the formation or growth of interstitial loops or the absorption of defects at existing dislocations depends upon their orientation with respect to the external stress and therefore cause a macroscopic creep strain. The application of the SIPN model is restricted to materials with low dislocation densities, e.g, solution-annealed materials at low neutron fluences [75]. On the other hand, SIPA creep dominates at high dislocation densities and low stresses [75].

In the previous models, glide processes are neglected. Models which include dislocation glide (Climb-Controlled Glide, CCG) as a further strain contribution are of especial interest in cases where the linear stress-dependence of creep deformation is no longer valid or where the creep rate increases at the onset of swelling [75]. The contribution of strain due to dislocation glide is difficult to analyze. During the random climbing of the network certain segments find themselves able to glide. This glide occurs and thereby gives an increment to the irradiation creep strain. The segment is then left in a low stress locality and further glide of that and other potentially glissile segments have to wait until further climb creates the appropriate conditions. The major creep strain comes from the glide and not from the the intermediate climb [78]. In conclusion, the climb-controlled glide of dislocations past obstacles is indeed an important mechanism for irradiation creep for low fluences at all temperatures or for all fluences at high temperatures [79]. Early theoretical models proposed were heuristic in nature and, depending on the assumptions, yield a variety of stress-dependencies [76].

6.5.2 Modelling of stress-enhanced radiation creep

In a number of recent reports, the creep-swelling relationship has been investigated for annealed AISI 304L [80,81,82] and various thermomechanical treatments of AISI 316 stainless steel [61,83-88,89]. These studies were conducted in EBR-II and showed a remarkable consistency in results. It was found that that at most temperatures of interest, irradiation creep could be described as a combination of several minor contributions (precipitation-related dimensional changes and transient relaxation of cold-worked-induced dislocations) and two major contributions [90]. The major contributions were associated with the creep compliance, a quantity unrelated to void swelling, and a swelling-driven creep component. Other similar studies have also been conducted on the Prime Candidate Alloy (PCA) in FFTF [91] and for the ferritic/martensitic alloys HT9 and 9Cr1Mo [92] which

showed the same trend. It has been proposed [75,90-93] that the creep rate $\dot{\varepsilon}$ at any relevant temperature is linearly dependent on stress and related to the swelling rate $\dot{S}$ by the following relation:

$$\frac{\dot{\varepsilon}}{\sigma} = B_0 + D_0 \dot{S} \qquad (6.9)$$

The creep compliance B_0 has been shown to be approximately equal to 10^{-6} MPa^{-1} for a wide range of austenitic steels. The swelling-enhanced creep coefficient D_0 is likewise thought to be relatively constant ≈ 0.01 MPa^{-1} over a wide range of steels and temperatures. This relationship ignores the short transient usually observed in cold-worked alloys [94]. If we accept the proposed insensitivity of B_0 and D_0 to composition and starting microstructure, then the sensitivities of swelling will dominate the creep behavior at high fluence (where, as shown later, the effect of stress on swelling is more pronounced). Note that Equation (6.9) requires a swelling rate of greater than 0.01%/dpa (which is generally the case) to give dominance to the second term over the first one, i.e., to make the swelling behavior dominating the irradiation creep behavior [94]. It is clear that due to the stress dependence of swelling, an apparent deviation from the linear stress dependence of the creep should be anticipated at high swelling rates (>0.01% per dpa). This was reported for 1.4981 type stainless steel [75].

It has been commonly accepted that the irradiation-induced creep rate accelerates with the onset of swelling and that it will continue at a rate proportional to that of the swelling. However, some research indicated that the creep rate in AISI 316 stainless steel subsequently declines as swelling approaches levels in excess of 5% (For dpa < 50, and at 550 °C) [83,95]. It is not yet clear whether the cessation of creep arises as a direct consequence of large swelling levels or whether other late-term microstructural developments are responsible [95]. The increase in the stress-enhanced swelling with temperature as well as the observed

cessation of irradiation creep may have deleterious effects on the performance of bonded structures.

6.6 Effect of void swelling on elasticity

The behavior of bonded structures (especially along the interfaces) should be dependent on the inherent mechanical properties of both the substrate as well as the coating. Changes in microstructure, as well as microchemical changes, are also known to affect elastic moduli. For the design of a next step large fusion device the influence of neutron irradiation on elastic moduli is of particular interest [96]. Also, a high value of the thermal strength factor $M = (\lambda * \alpha)\ (\sigma_u / G)$ (λ = thermal conductivity, α = thermal expansion coefficient, σ_u = ultimate strength, G = elastic modulus) is an important parameter to indicate material suitability for heat sink materials in duplex structures [97].

As was mentioned in Chapter 4, Marlowe and Appleby [98] measured the reduction in Young's modulus due to swelling for 316 stainless steel using a dynamic resonance technique. The following relation was reached:

$$(E / E_0)_{316} = [\ 1.086 - 4.435\ S\ ] \qquad (6.10)$$

at the 95% confidence level for the coefficients, where the E_0 's are the moduli of the fully dense materials, and S is the volume fraction swelling.

6.7 Stress analysis of bonded structures

The effect of stress history on the development of swelling in bonded structures and the role played by stress-enhanced swelling in irradiation creep calculations has been incorporated into the TSTRESS code [99] in its latest version GTSTRESS [100]. The code

uses the method of the boundary integral method formulated for time dependent plastic deformation in one-dimension.

In the case of plasma facing components for fusion, the boundary integral method reduces to a one-dimensional integration of the plastic strain components throughout the thickness. The 1-D analysis is a reasonable approximation because the stress gradient through the components is typically much greater than the gradient along the surface, for thin-walled components with large radii of curvature [101]. Four different sources of stress were initially considered: (1) membrane loads from internal coolant pressures, (2) temperature gradients through the wall caused by steady-state heat fluxes, (3) irradiation induced differential swelling gradients through the wall, and (4) residual stress gradients caused by both thermal and irradiation creep-induced stress relaxation.

The code was modified to incorporate models for the stress-enhanced swelling. The modification of the irradiation creep due to the stress-enhanced swelling and the effect of swelling on the young's modulus were also taken into consideration. The ability of the code to produce the swelling distribution throughout the thickness of the first wall (as well as in its coating) allows for the proper assessment of the swelling behavior especially near the interfacial area between the coating and the substrate. This gives an excellent chance to investigate the impact of differential swelling on the bonding of duplex structures.

The thin-walled shell element that will be used represents a flat section of the first wall and is assumed to be constrained from bending, but not from expansion. The model is, therefore, applicable to spherically and cylindrically shaped first walls whose radii of curvature are large when compared to the wall thickness. The basic structure will be the

numerical solution of N coupled initial value problems using Euler's method, with automatic selection of the time step interval.

The physical model of the first wall which will be used is a thin shell element, as shown in Figure 6.9. The element is loaded with externally applied in-plane membrane loads N_X and N_Y. Also, the element is subjected to time independent temperature loads and time-dependent swelling loads which are assumed to vary only along the Z-direction. In addition, the stresses are allowed to relax as a function of time due to the combined influence of thermal and irradiation creep. The elastic properties are temperature dependent and the neutron flux is assumed to remain constant through the wall's thickness. In most first wall designs these assumptions are reasonably well satisfied. Since the normal stress $\sigma_Z \cong$ - pressure, then it may be neglected because the in-plane stresses σ_X and σ_Y are typically found to be much larger than the internal coolant pressure.

The stress rate equations to be solved are:

$$\sigma_j^{n+1/2} = \Delta t_j^n \left(\frac{1}{h^n} \sum_j \left[F_j^n + \psi_j^n \sigma_j^{n-1/2} \right] \Delta Z_j^n - F_j^n - \psi_j^n \sigma_j^{n-1/2} \right) + \sigma_j^{n-1/2} \qquad (6.11)$$

and

$$\tau_j^{n+1/2} = \Delta t_j^n \left[\left(\frac{1}{h^n} \sum_j \Phi_j^n \Delta Z_j^n \tau_j^{n-1/2} - \right) - \Phi_j^n \tau_j^{n-1/2} \right] + \tau_j^{n-1/2} \qquad (6.12)$$

where

$$\sigma(z) \equiv \frac{1}{2} [\sigma_X(z) + \sigma_Y(z)] \qquad (6.13)$$

and

$$\tau(z) \equiv \sigma_x(z) - \sigma_Y(z) \qquad (6.14)$$

$\psi(z)$ and $\phi(z)$ are related to the creep compliance by

$$\psi(z) = \mu \left(\frac{1+\nu}{1-\nu} \right) \varphi(z) \qquad (6.15)$$

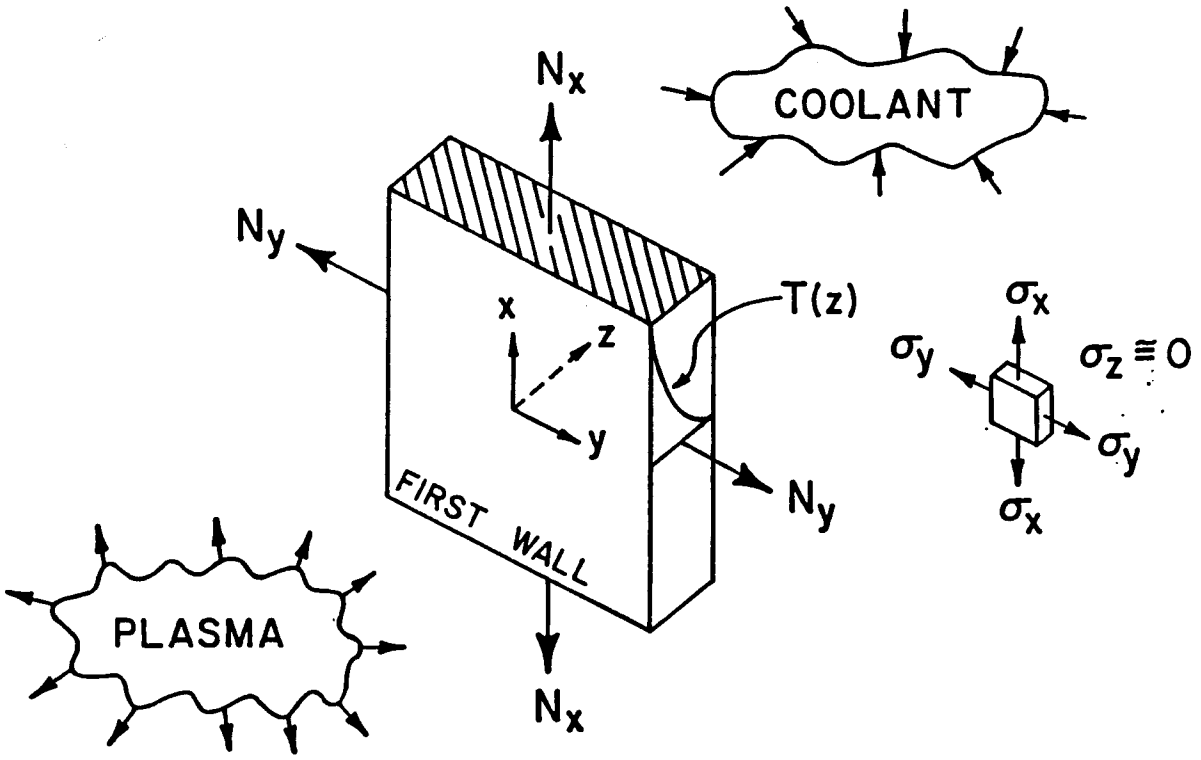

Figure 6.9: Thin walled shell element model of the first wall [15].

and

$$\phi(z) = 3\mu\varphi(z) \tag{6.16}$$

while F(z) is a function of expansion and swelling,

$$F(z) = \mu\left(\frac{1+\nu}{1-\nu}\right)\left\{2\alpha T(z) + \frac{2}{3}S(z)\right\} \tag{6.17}$$

6.7.1 Parametric study of the stress-enhanced swelling phenomena

The behavior of 20% cold-worked 316 stainless steel plate free to expand but not to bend (an ideal simulation for first wall structures) and subject to different irradiation, stress, as well as thermal conditions was first investigated (Figure 6.10). The attempt was to determine an envelope for the behavior of the stress-enhanced swelling phenomena, and the impact of the swelling on the irradiation creep. The choice of 316 stainless steel was made since it is the only material on which the effect of stress on swelling has been studied and modeled. The upper temperature (525 °C) was chosen since this is upper temperature limit for stress to have an impact on the swelling rate as well as the incubation period. Also, the effect of gas generation would become important above this temperature. Since the impact of stress on swelling is small below 400 °C, most calculations were limited to above 400 °C. In the following discussion, volumetric swelling is shown for three conditions of interest to the behavior of bonded structures: at the surface, using the average over the first millimeter, and using the average over the whole thickness. Also, in the following results, stress always refers to σ_x. It is apparent from the different results that the stress-enhanced swelling phenomena complicates the prediction of the irradiation behavior of bonded structures and will have a major role on their performance at the interfaces.

6.7.1.1 Effect of plate thickness

Four different thicknesses were used in the calculations; 3, 5, 7, and 9 mm as shown in Figure 6.11. The same temperature range was maintained (400-525 °C). In this case,

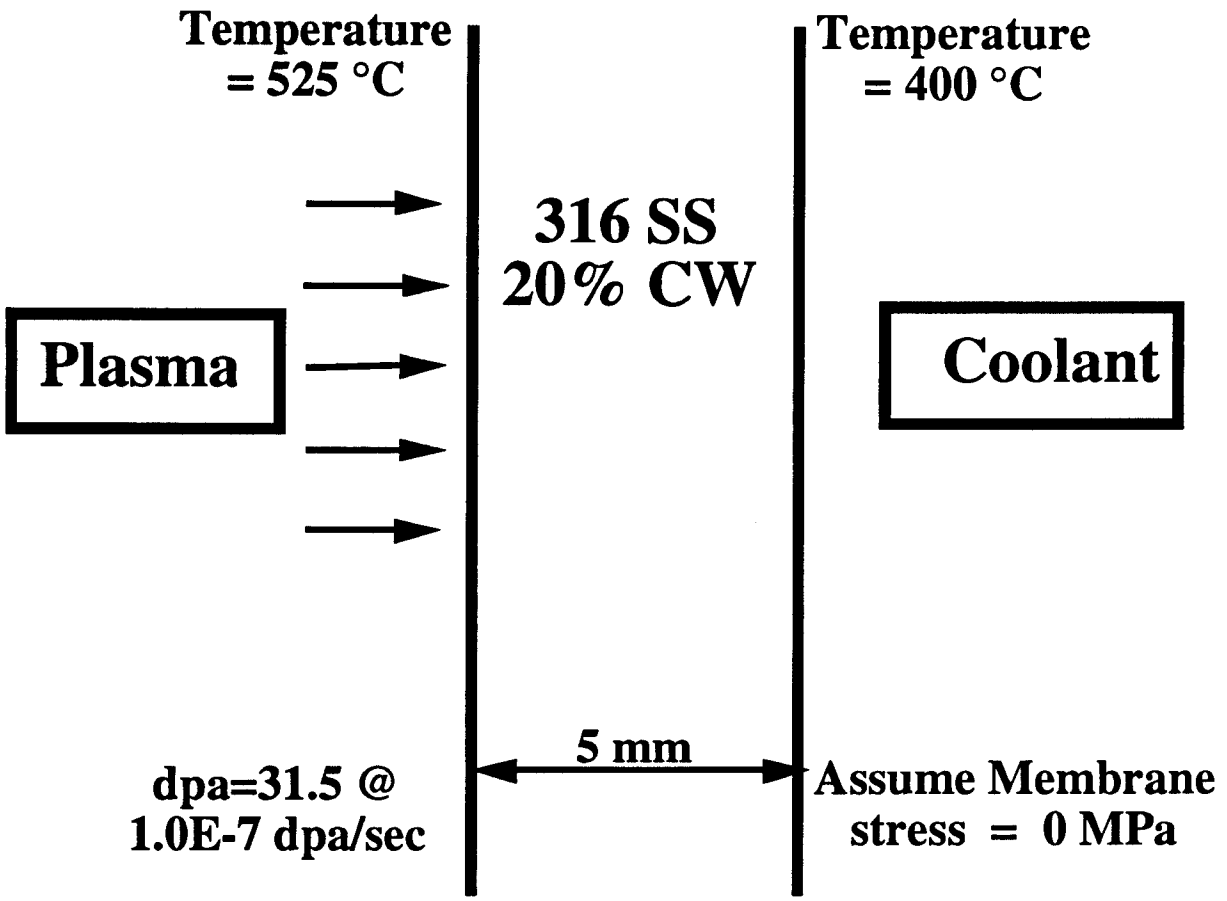

Figure 6.10: Schematic of the plate used for the analysis of the stress-enhanced swelling and its influence on irradiation creep

varying the 316 plate thickness had little effect on surface swelling and the average swelling along the whole thickness. Since the first mm has a different temperature gradient in each case-being hotter for the large thickness (Figure 6.12), the 9 mm plate experienced the largest increase in swelling.

6.7.1.2 Effect of damage rate

Three different cases were investigated (5*E-8, 1*E-7, and 5*E-7 dpa/sec) at an accumulated dose of 15.75 dpa as shown in Figure 6.13. The stress-enhanced phenomena played a major role as the damage rate increases. This will have an impact for the DEMO as well as commercial reactors.

6.7.1.3 Effect of membrane stress

As shown in Figure 6.14, the stress-enhanced swelling is decreased with the increase in membrane stress. The trend will be reversed as the stress level increases. This is explained for a simple stress distribution in Figure 6.15. As the membrane stress increases, the stress on the surface as well as in the first millimeter will first decrease in value, then it will increase once more, thus increasing the stress-enhanced swelling. One has to keep in mind that what is important is the absolute value of the stress. The importance of the membrane stress effect on swelling should be considered along with the future trends of using high temperature, high pressure coolants that generate high membrane stresses.

6.7.1.4 Effect of temperature range

As shown in Figure 6.16, the impact of the phenomena is highest for the 400-525 °C temperature range. It is important to note that this trend only reflects the increased stress levels rather than the enhancement of the stress-assisted swelling with temperature (in this temperature range, the stress-enhanced phenomena is an athermal process). This is also clear

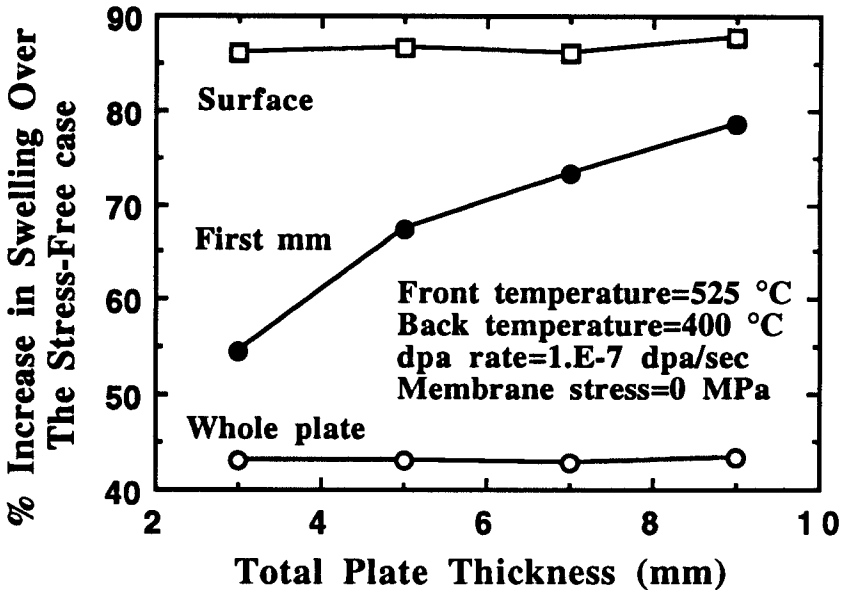

Figure 6.11: Effect of plate thickness on the stress-enhanced swelling of 316 SS plate after 31.5 dpa

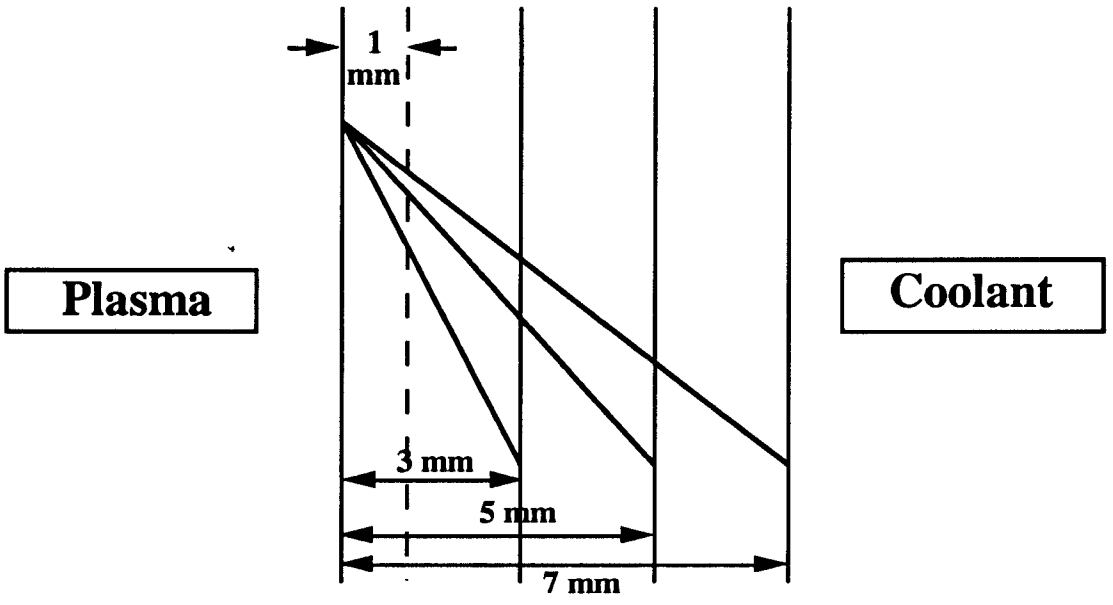

Figure 6.12: temperature gradients for different thicknesses and fixed surface temperatures.

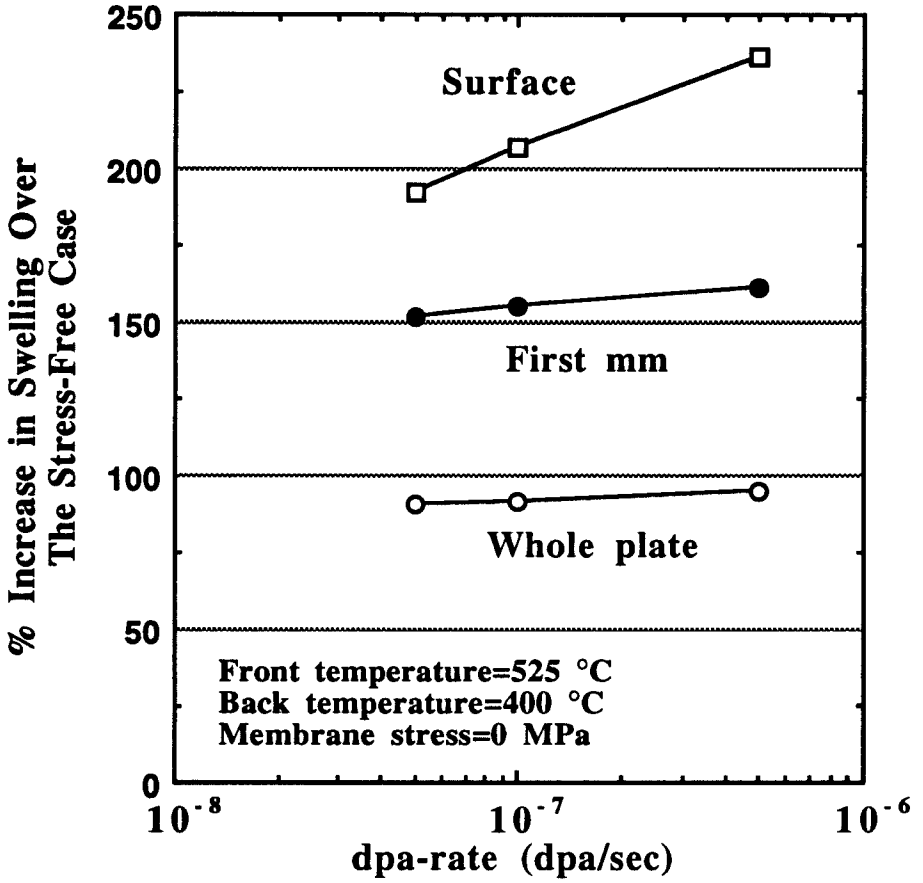

Figure 6.13: Effect of dpa rate on the stress-enhanced swelling behavior of 5 mm 316 SS plate after 15.75 dpa.

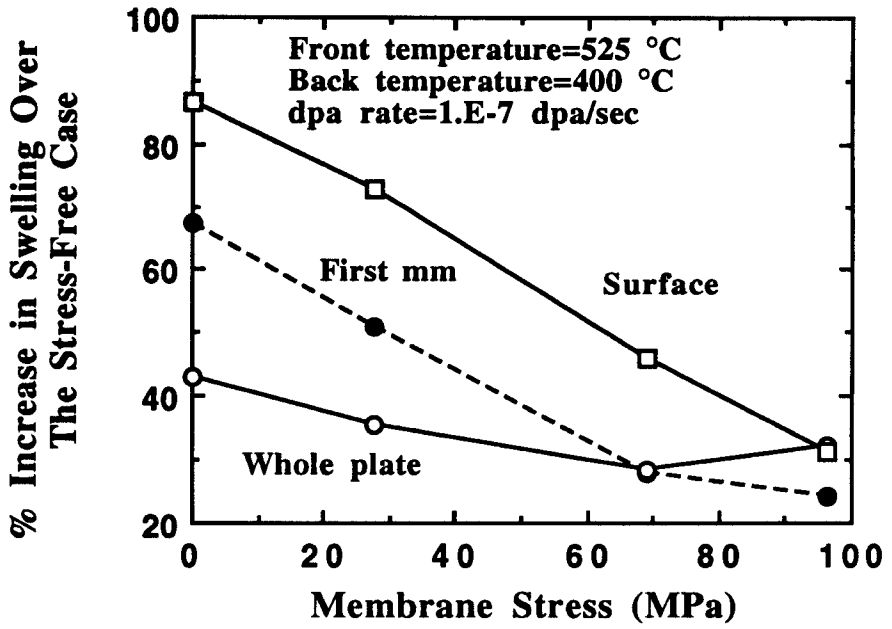

Figure 6.14: Effect of membrane stress on the stress-enhanced swelling of a 5 mm 316 SS after 31.5 dpa.

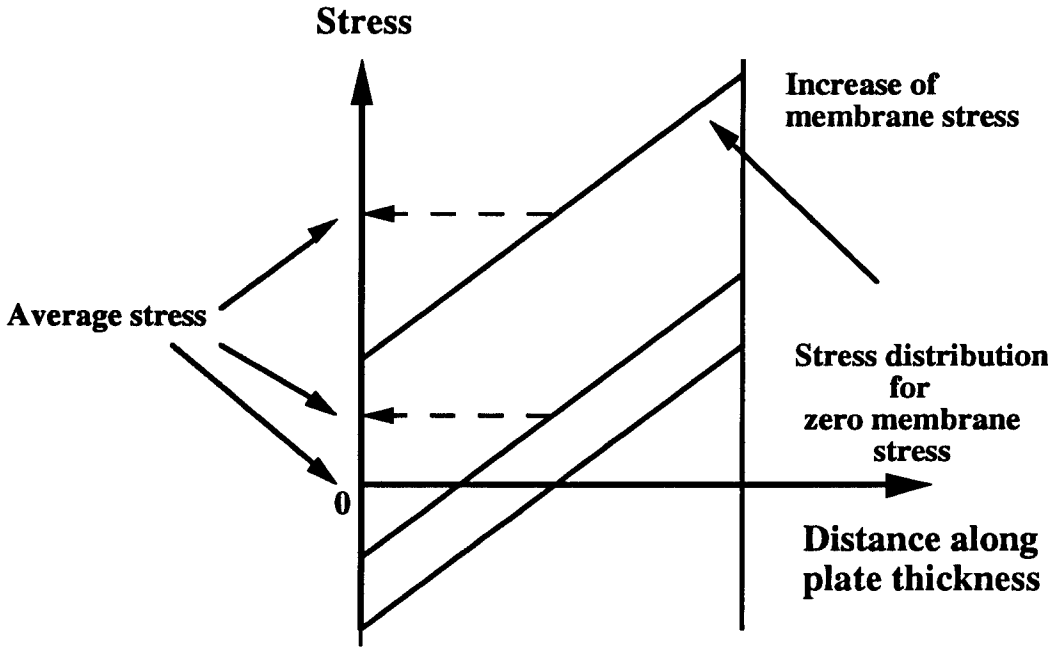

Figure 6.15: Stress distribution in a plate subject to simple membrane stress. Initial stress distribution is assumed symmetric.

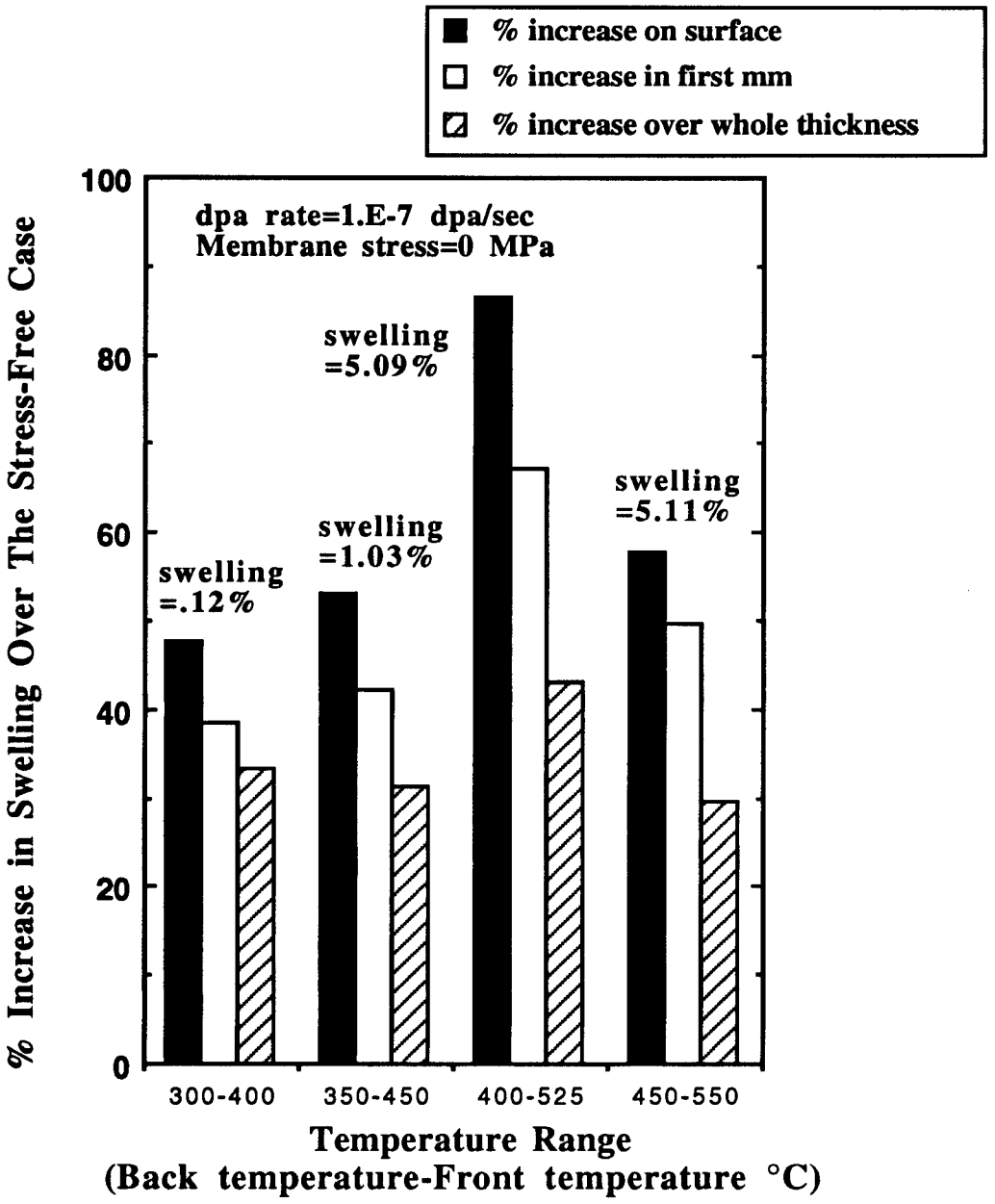

Figure 6.16: Effect of temperature range on the stress-enhanced swelling behavior of a 5 mm 316 SS after 31.5 dpa.

by noting that the reduction in stress-enhanced swelling as the temperature gets higher because the thermal creep begins to be effective in reducing stress levels.

6.7.1.5 Swelling evolution with time

As shown in Figure 6.17, the stress-enhanced swelling will have a major role in the beginning of life (regardless of the low swelling value). This is expected since in the beginning, before the creep begins to redistribute the stresses, the stress levels will be high. This will have an impact on the the early performance of bonded structures.

6.7.1.6 Stress distribution

The time dependence of the stress distribution is shown in Figure 6.18. A remarkable deviation from linearity is observed, especially on the surface (i.e., at the coating). To investigate the roots of this behavior, both the swelling and the creep evolution were plotted in Figures 6.19 and 6.20. It is quite obvious that the stress-enhanced swelling is the key factor behind the resultant stress distribution. This is even more obvious when the stress-enhanced swelling is used to enhance the irradiation creep. The stress relaxation due to creep is more effective on the surface as a result of the dominant effect of the stress-enhanced swelling in this area. It is also worth mentioning that, in all the above calculations, the stress level did not exceed the proportional elastic limit of the 20% CW stainless steel. Thus, swelling always increased with stress.

6.7.2 Effect of stress-swelling-creep coupling

As shown in Figures 6.21 and 6.22, the creep-swelling coupling has a major impact on the swelling distribution, as well as on the stress evolution. As a result, the stress-enhanced swelling will be reduced by as much as 40%. It is important to note that the creep relaxation of stress on the surface will have an important effect on the generation of intrinsic

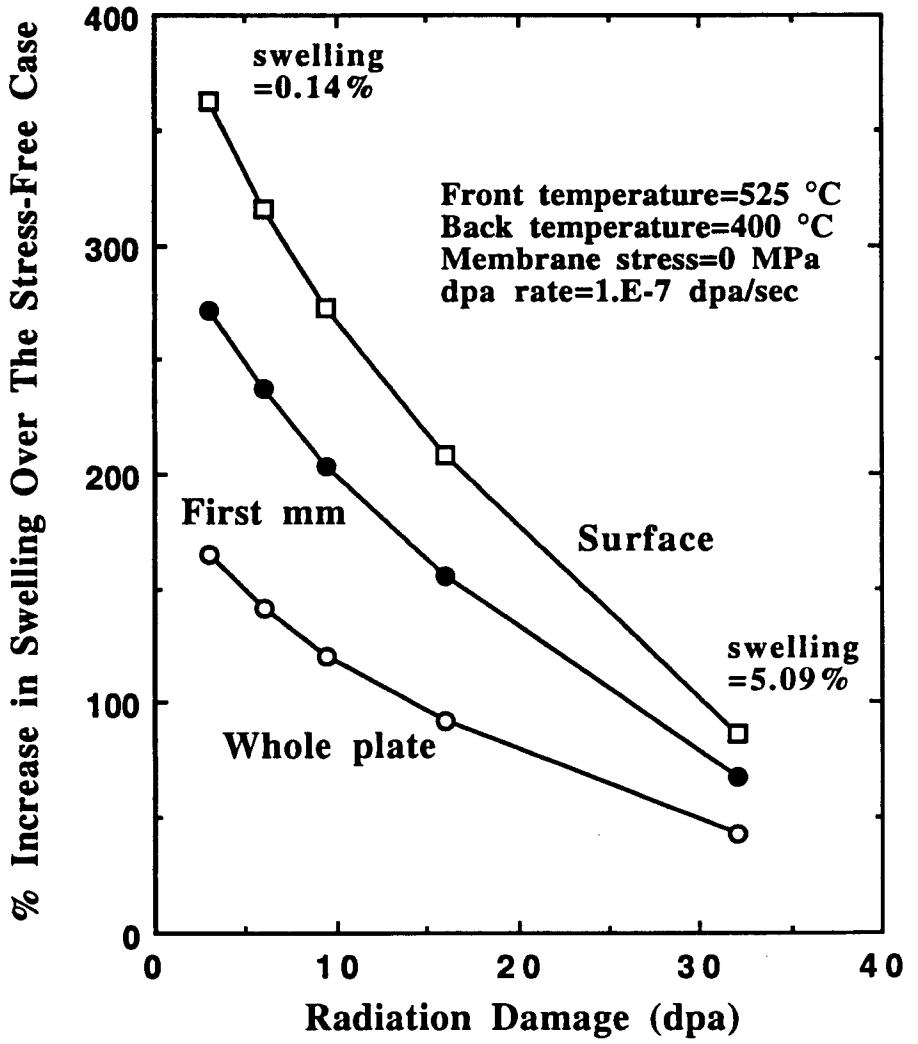

Figure 6.17: Effect of radiation damage (dpa) on the stress-enhanced swelling behavior of a 5 mm 316 SS after 31.5 dpa.

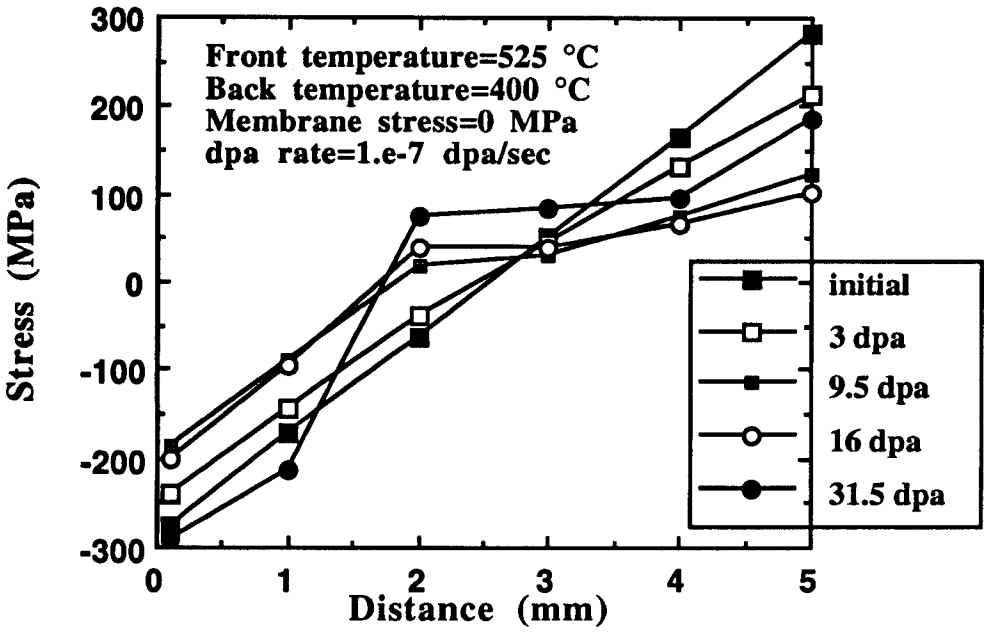

Figure 6.18: Evolution of stress as a function of dpa for a 5 mm 316 SS plate.

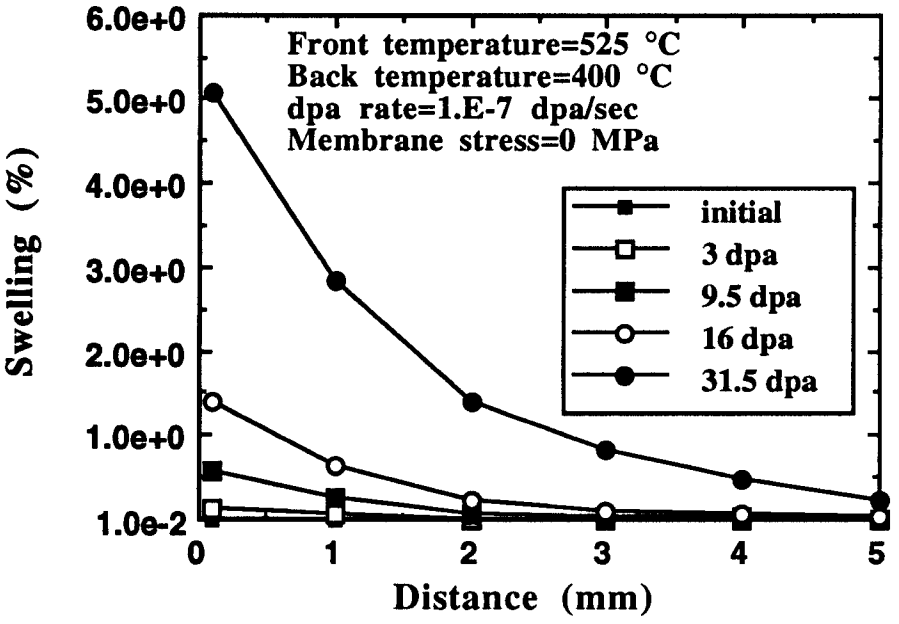

Figure 6.19: Evolution of the stress-enhanced swelling distribution as a function of dpa for a 5 mm 316 SS plate.

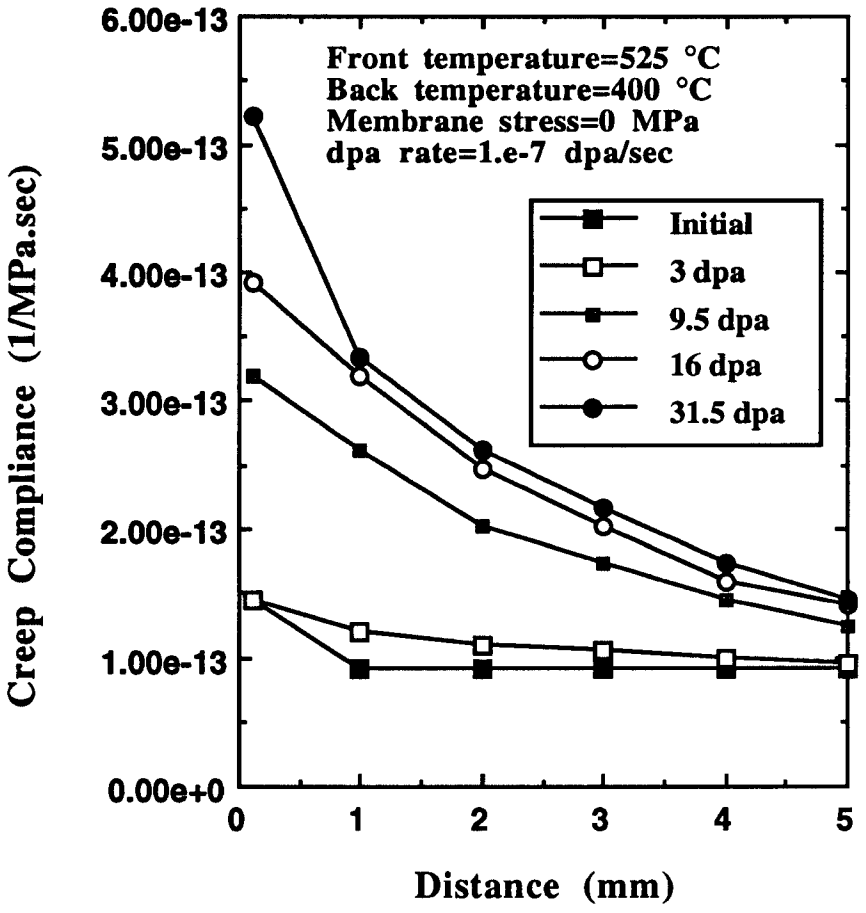

Figure 6.20: Evolution of creep compliance as a function of dpa for a 5 mm 316 SS plate.

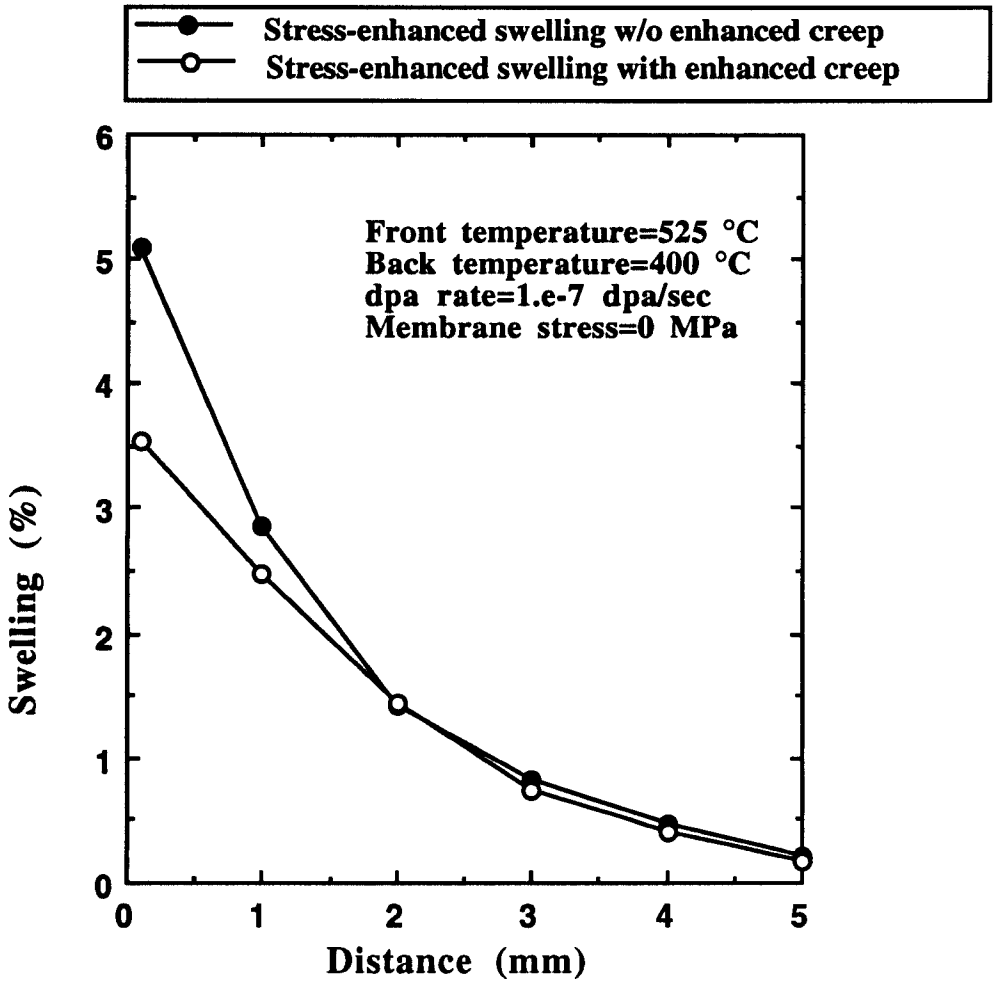

Figure 6.21: Effect of (stress-enhanced swelling)-enhanced creep on the swelling of a 5 mm 316 SS plate after 31.5 dpa.

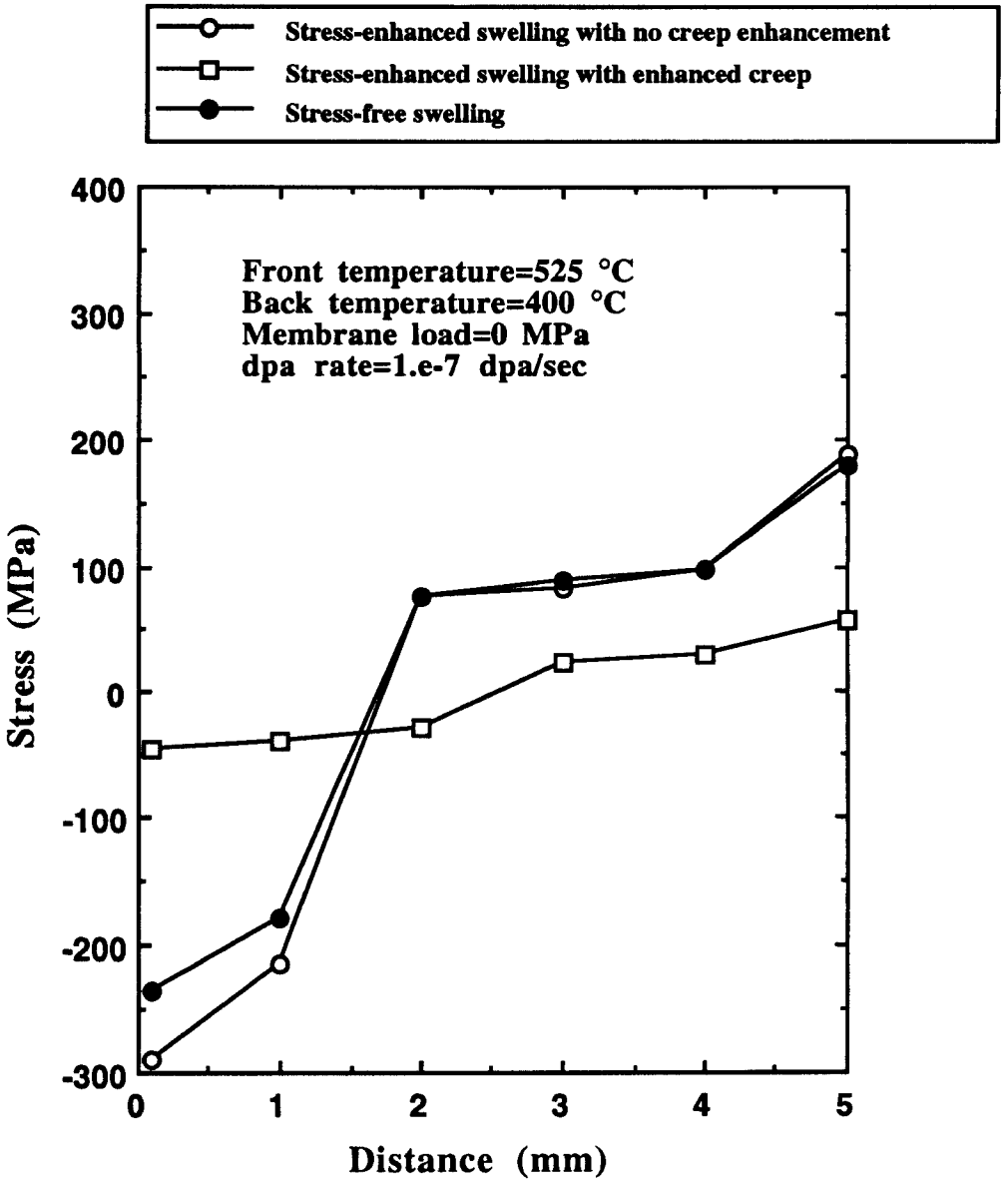

Figure 6.22: Effect of (stress-enhanced swelling)-enhanced creep on the stress in a 5 mm 316 SS plate after 31.5 dpa.

stresses along the interface if a coating is applied. It is thus obvious that the effect of stress-enhanced swelling should be taken into consideration. Otherwise, an overestimation of swelling, especially along interfaces, may result. One complication is the cessation of irradiation creep at high values of swelling (5%) that was reported earlier [95].

6.7.3 Effect of swelling on the elastic modulus

As a result of the dependence of the elastic modulus on swelling, it is expected that the stress-enhanced swelling may reduce the modulus even further than in the stress free case. This is shown in Figure 6.23 where it is shown that the reduction in Young's Modulus values may reach 15% on the surface (twice the reduction in case of stress-free swelling). A low value of Young's modulus indicates a greater elastic accommodation and smaller permanent damage. Also, this reduces the force required to develop the strain compatibility between the coating and the substrate. (note that the effect of swelling on Young's modulus was not taken into consideration in sections 6.1 and 6.2).

6.7.4 Be/SS structure for the DEMO design

To simulate an actual case of a duplex structure that uses stainless steel, the parameters of the first wall of a DEMO reactor were used (Figure 6.24) [102]. These were:

Neutron wall loading	2.1 MW/m^2
Thickness of Be (70% TD) tiles	2 mm
Thickness of 20% CW 316 SS	4 mm
Surface temperature	730 K
Interface temperature	725 K
Back temperature	670 K
Coolant temperature	653 K
Membrane load	50 MPa

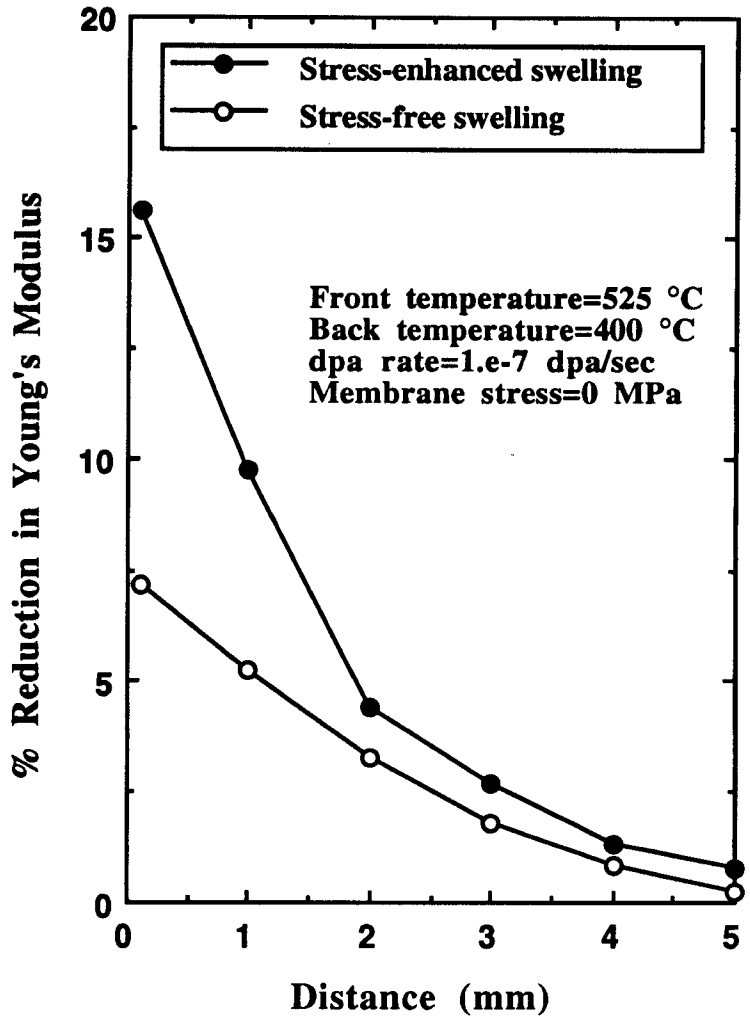

Figure 6.23: Effect of stress-enhanced swelling on the Young's modulus in a 5 mm 316 SS plate after 31.5 dpa.

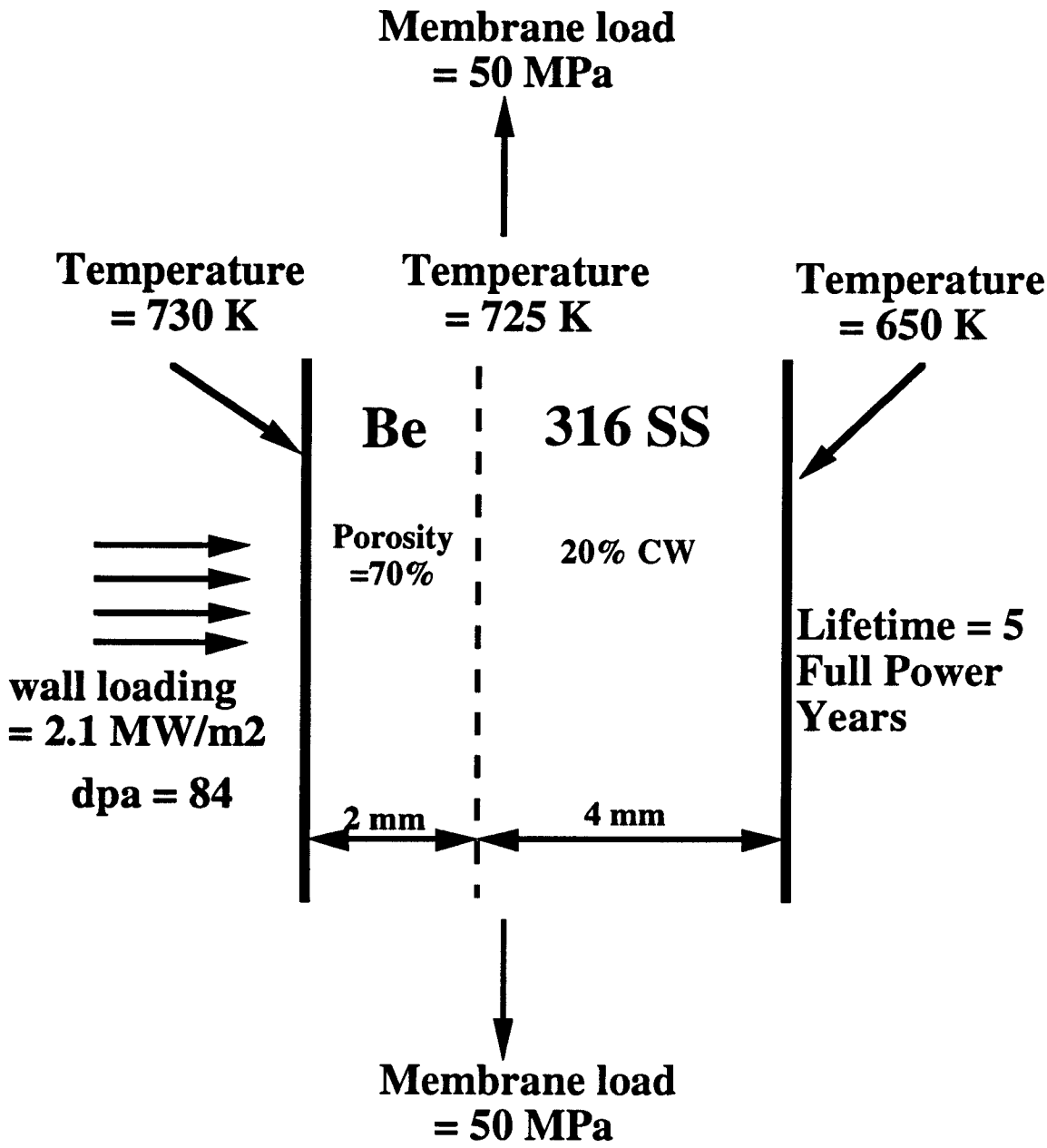

Figure 6.24: Model for DEMO Bonded Structure

Life time	10 years
Availability	50%
Damage level	84 dpa
Gas generation rate in Be	6405 appm/year

Since the stress-enhanced swelling phenomena is negligible below 300 °C, all the temperatures used above are in fact 100 degrees higher than those in the original design. Recent data for Be [103] were taken into consideration to account for the gas induced swelling as well the irradiation creep. The end of life swelling distribution in the steel structure (the substrate) is shown in Figure 6.25. The percentage increase in swelling due to stress is shown in Figures 6.26 and 6.27 as a function of thickness as well as averaged over certain thicknesses. Because of the way stress redistributed in steel (Figure 6.28), the increase in swelling is more pronounced at the back end of the substrate, eventually reaching a value of 20% over the stress free value. It should be noted that at the back end of the substrate the low temperature should result in low swelling values. It is obvious that the stress-enhanced swelling increased the swelling level at the back of the substrate more than it affected the swelling level at the interface (as would have been anticipated from results of section 6.1). Thus, the impact of stress-enhanced swelling should be evaluated in the relevant stress environment. Coupling between swelling and creep was not taken into consideration in these figures to single out the impact of stress-enhanced swelling. It is expected that if this coupling is taken into consideration, the increase in swelling at the back will be reduced since creep will be enhanced more in that region.

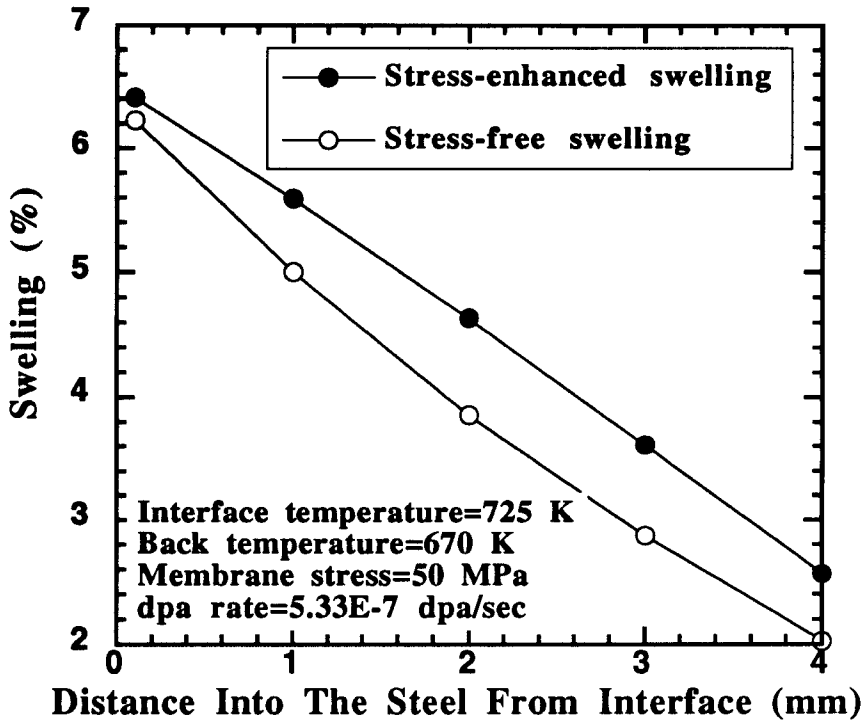

Figure 6.25: End of life swelling distribution in a 20% CW 316 SS substrate coated with 2 mm of Be

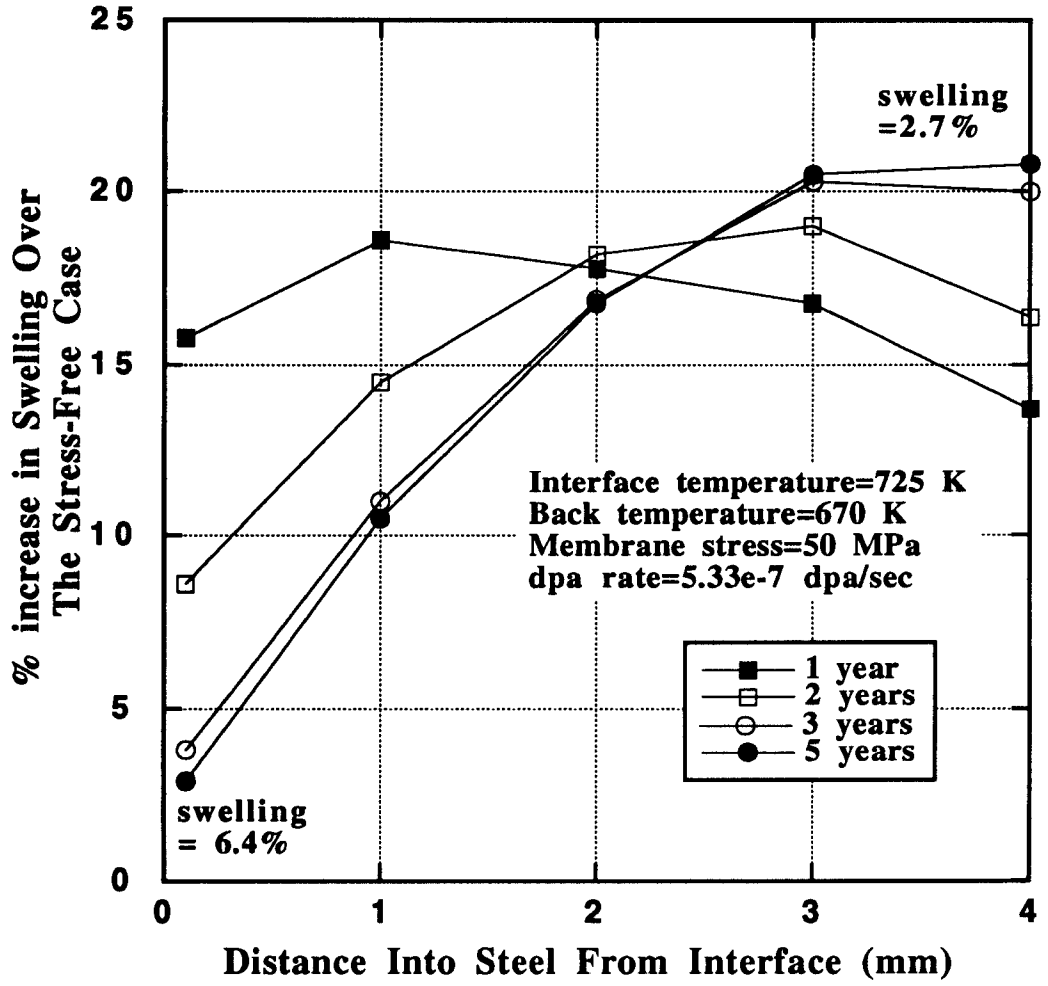

Figure 6.26: Percentage increase in swelling over the stress-free case for a 20% CW 316 SS substrate coated with 2 mm of Be

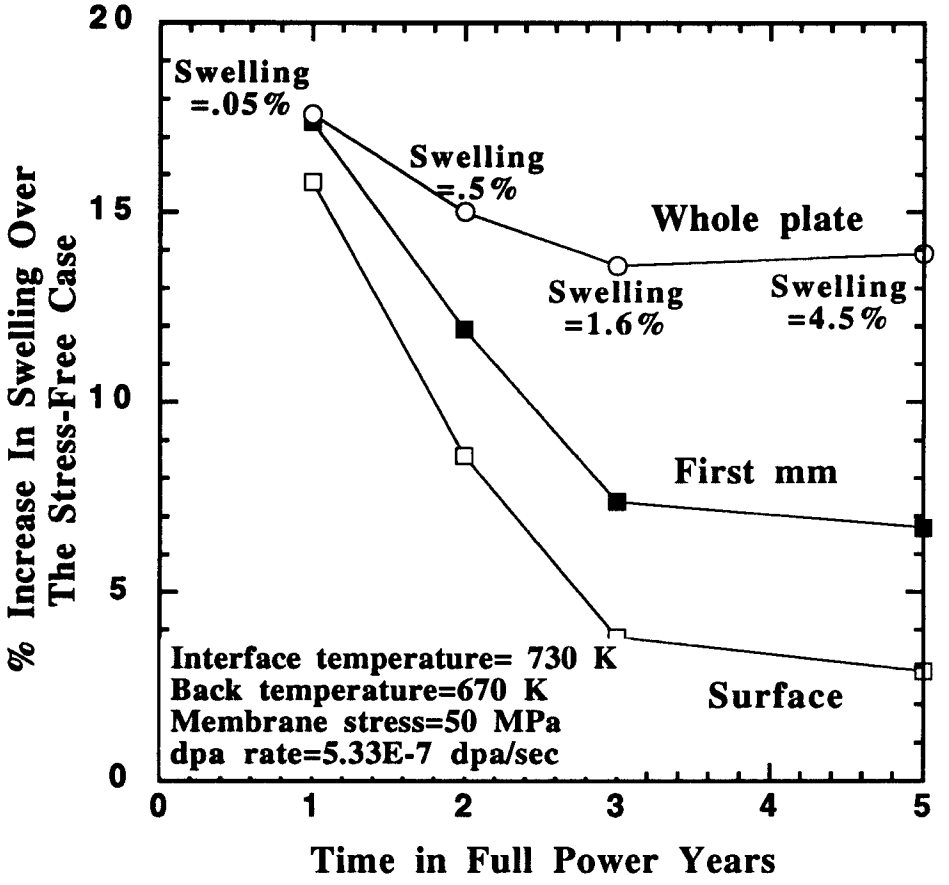

Figure 6.27: Percentage increase in swelling over the stress-free case for a 20% CW 316 SS substrate coated with 2 mm of Be

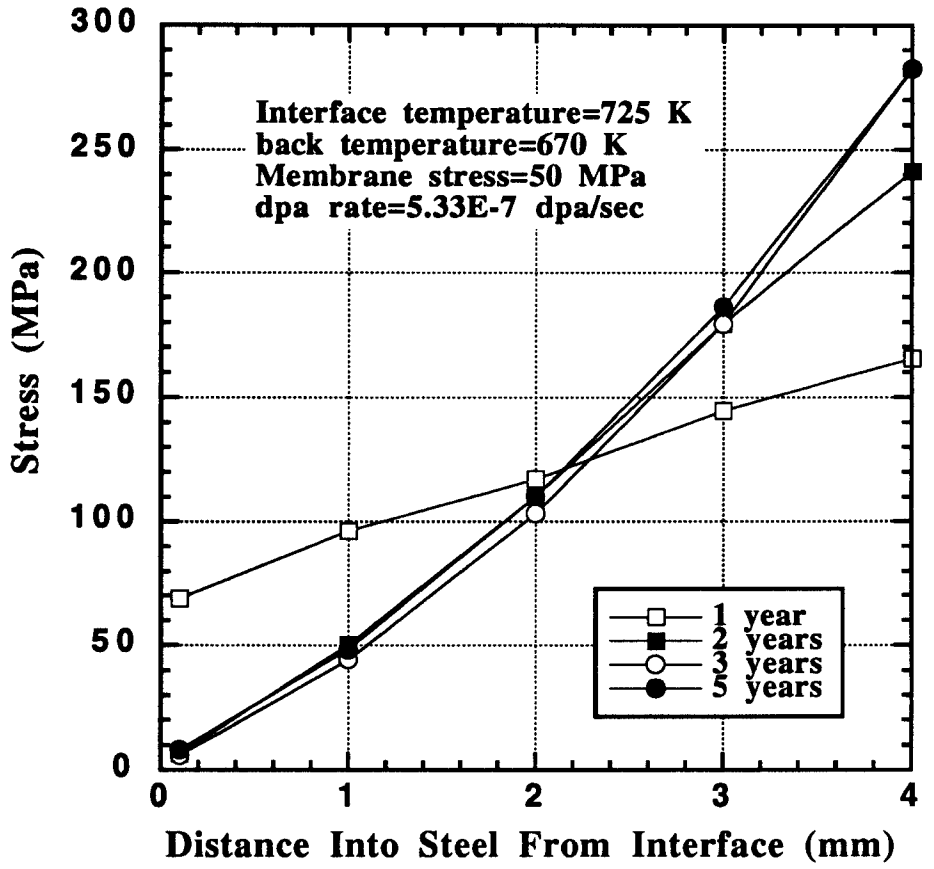

Figure 6.28: Stress distribution in a 20% CW 316 SS substrate coated with 2 mm of Be

6.8 Conclusions

1. The impact of stress on the incubation period for swelling should be taken into consideration for the analysis of fusion reactors, especially those experiencing high dose levels and using high temperature coolants and pressures (i.e., high primary stress levels).

2. The phenomena proved to be especially important early in the component life before the redistribution of stress due to thermal as well as irradiation creep.

3. The stress-enhanced swelling is important in the temperature range where thermal creep is negligible resulting in high level of stresses.

4. The phenomena proved to be the key factor that determines the redistribution of stress with time. When the interrelationship between (stress-enhanced) swelling and creep was taken into consideration, the stress-enhanced swelling was reduced by as much as 40% on the plasma side of the structure where large values of stress as well as high temperature enhanced the swelling resulting in a greater enhancement of the irradiation creep.

5. Because of the way stress redistributed in the substrate of the DEMO design (Figure 6.29), the increase in swelling was more pronounced at the back end of the substrate, eventually reaching a value of 20% over the stress free value. It is to be noted that at the back end of the substrate, the low temperature should normally result in low swelling values. Thus, the stress counteracted the impact of temperature, producing high values of swelling in areas that were considered to be in the low swelling regime due to the low temperature. It is to be concluded that the impact of stress-enhanced swelling should be evaluated in the relevant stress environment and that it is of a special importance for the analysis of bonded structures because of the magnitude of differential swelling expected in these structures (Figure 6.30).

6. The reduction in elastic moduli along the interfaces of bonded structures due to stress-enhanced swelling could be as high as twice the reduction in case of stress-free swelling. This has profound impact on bonded structures since low value of Young's modulus

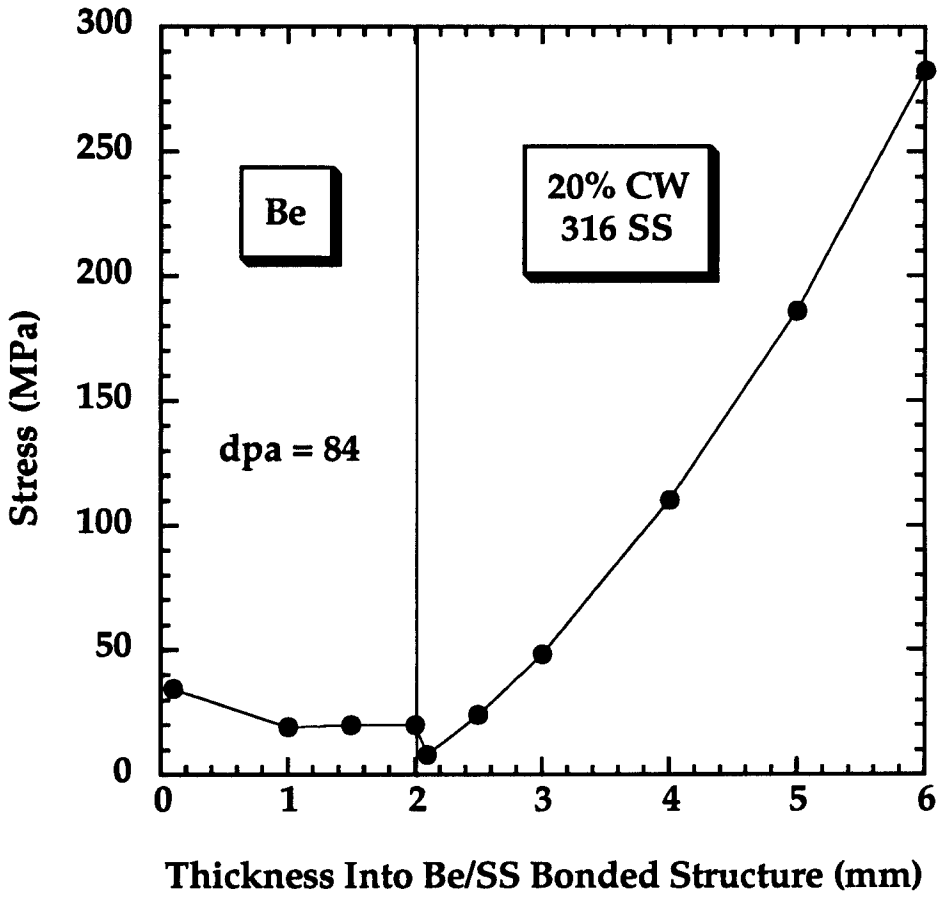

Figure 6.29: Different stress distributions on the two sides of the interface of a Be/SS structure

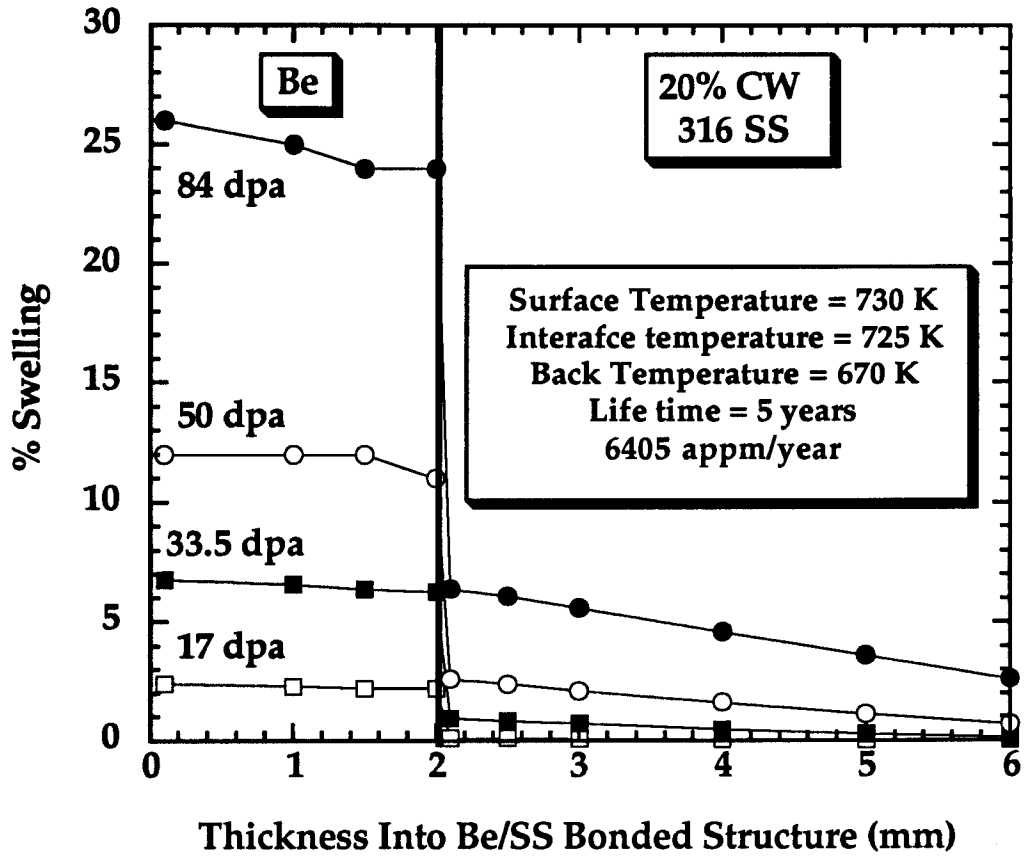

Figure 6.30: Swelling evolution with time for a Be/SS bonded structure

indicates a greater elastic accommodation and smaller permanent damage. Also, this reduces the force required to develop the strain compatibility between the coating and the substrate.

7. Many questions concerning the stress-enhanced swelling phenomena are still to be answered. Further experimental, as well as theoretical, work is necessary to assess and model the effect of stress on cavity density, the observed enhanced void growth especially at high temperatures. The role played by the shear component of the stress, as well as the synergistic effects of temperature, damage rate, gas generation rate, and stress still need to be more fully understood so before the influence of the different variables relevant to fusion applications can be assessed.

6.9 References

[1] J. P. Blanchard and N. M. Ghoniem, J. Nucl. Mat. **172**, 54 (1990).

[2] N. M. Ghoneim and J. B. Whitley, J. Fusion Energy **8**, 157 (1989).

[3] R. F. Mattas, et al., J. Nucl. Mat. **122/123**, 66 (1984).

[4] G. L. Kulcinski, Contemp. Phys. **20**, 417 (1979).

[5] J. P. Blanchard and N. M. Ghoneim, Nucl. Eng. Desi./Fusion **2**, 19 (1985).

[6] R. W. Conn, et al., UCLA PPG-815, (1984).

[7] H. R. Brager, et al., J. Nucl. Mat. **66**, 301 (1977).

[8] A. E. Walter and A. B. Reynolds, Fast breeder reactor, Pergamon Press, New York, (1981).

[9] W. Daenner and J. Raeder, Proc. 3rd Top. Meeting on the Technology of Contr. Nucl. Fus., p. 347, Santa Fe', New Mex., USA (1976).

[10] R. F. Mattas, Fusion tech. **19**, 1487 (1991).

[11] D. L. Smith, Blanket and Shield Design Meeting, ANL, November 6 (1991).

[12] R. D. Watson, et al., J. Nucl. Mat. **103**, 97 (1981).

[13] R. F. Mattas, Fusion Tech., 637 (1990).

[14] R. F. Mattas, ANL/FPP/TM-160 (1982).

[15] B. B. Glasgow and W. G. Wolfer, Fusion Tech. **8**, 596 (1985).

[16] J. P. Blanchard, Analysis of singular stress fields in fusion components, Ph.D. thesis, UCLA (1988).

[17] B. M. Ma, Nucl. Eng. Des. **28**, 1 (1974).

[18] W. Daenner and J. Raeder, J. Nucl. Mat. **85/86**, 147 (1979).

[19] W. Daenner, J. Nucl. Mat. **103/104**, 121 (1981).

[20] R. D. Watson, R. R. Peterson, and W. G. Wolfer, UWFDM-433 (1981).

[21] R. D. Watson, R. R. Peterson, and W. G. Wolfer, J. Pressure Vessel Tech. **105**, 144 (1983).

[22] S. D. Harkness and B. Cramer, J. Nucl. Mat. **85/86**, 135 (1979).

[23] H. Oomura, et al., Fusion Tech. **8**, (1985).

[24] C. Cawthorne and E. J. Fulton, Nature **216**, 576 (1967).

[25] J. F. Bates and E. R. Gilbert, J. Nucl. Mat. **59**, 95 (1976).

[26] J. I. Bramman, et al. in: Proc. Intern. Confs. on Radiation effects in breeder structural materials, Scottsdale, AZ, 479 (1977).

[27] R. A. Weiner and A. Boltax, J. Nucl. Mat. **68**, 141 (1977).

[28] K. Q. Bagley, et al. in: Proc. on Voids Formed by Irradiation of Reactor Materials BNES, p. 1, Harwell (1971).

[29] R. J. Jackson, et al., Trans. Am. Nucl. Soc. **22**, 184 (1975).

[30] R. A. Weiner and A. Boltax, Stress Effects on The Void Swelling Incubation Period, WARD-OX-3045-22, Westinghouse Advanced Reactors Division (1976).

[31] J. F. Bates and E. R. Gilbert, J. Nucl. Mat. **71**, 286 (1978).

[32] J. F. Bates and E. R. Gilbert in: Proc. Int. Conf. on Structural Mechanics in Reactor Technology, Vol. C, Berli, Germany, 4/1 (1979).

[33] T. Lauritzen et al.: Proc. on Effects of Radiation on Materials, ASTM 870, p. 221, Williambsburg, VA. (1984).

[34] J. L. Staralsund, in: Proc. Intern. Confs. on Radiation effects in breeder structural materials, p. 191, Scottsdale, AZ (1977).

[35] D. L. Porter, et al.: Proc. on Effects of Radiation on Materials, ASTM 870, p.212, Williambsburg, VA. (1984).

[36] K. Herschbach et. al., ASTM STP **1046**, 570 (1990).

[37] J. E. Harbottle, J. Nucl. Mat. **66**, 258 (1977).

[38] J. E. Harbottle in: Proc. Intern. Confs. on Radiation Effects in Breeder Structural Materials, p. 455, Scottsdale, AZ (1977).

[39] J. E. Harbottle and A. Silvent, in proc: Irradiation behavior of metallic materials for Fast Breeder Reactors, p. 391, France (1979).

[40] S. Ya. Lebedev, et al., Phy. Met. Metall **54**, 164 (1982).

[41] P. J. Barton and P. H. Hunter, Proc. on Voids Formed by Irradiation of Reactor Materials, BNES, p. 45, Harwell (1971).

[42] F. A. Garner, et al. in: Proc. on Radiation Induced Voids in Metals, CONF 710601, p. 841, Albany (1971).

[43] J. L. Straalsund, et al. in: Proc. on Effects of Radiation on Structural and Mechanical Properties of Metals and Alloys, ASTM 529, p. 247, Los Angeles, California (1972).

[44] R. G. Anderson et al., Oxide fuel element development quarterly report, WARD-4210T3-8 (1971).

[45] R. G. Anderson, et al., AERE report R-6891 (1971).

[46] J. L. Straalsund and G. L. Guthrie, Nucl. Tech. **16**, 36 (1972).

[47] A. E. Walter and A. B. Reynolds, Fast breeder reactor, Pergamon Press, New York (1981).

[48] H. Ullmaier, Rad. Eff. **101**, 147 (1986).

[49] H. K. Shau and P. Jung, J. Nucl. Mat. **136**, 154 (1985).

[50] T. Lauritzen, et al., DAFS report, DOE/ER-0046/21, 83 (1985).

[51] T. Lauritzen, et al.: Proc. on Radiation Induced Changes in Microstructure, ASTM 955, p. 101, Seattle, WA. (1986).

[52] P. J. Barton et al., J. Nucl. Mat. **67**, 181 (1977).

[53] F. A. Garner, Damage Analysis and Fundamental Studies, U.S. Department of Energy, Office of Fusion Energy, 198 (1981).

[54] D. L. Porter, et al., J. Nucl. Mat. **116**, 272 (1983).

[55] W. G. Wolfer, et. al., in:Properties of Reactor Structural Alloys After Neutron or Particle Irradiation, ASTM STP 570, 233 (1975).

[56] R. E. Stoller, et al., J. Nucl. Mat. **155/157**, 1328 (1988).

[57] A. Boltax, et al., J. Nucl. Mat. **65**, 174 (1977).

[58] H. R. Brager, et al. in: Proc. Intern. Confs. on Radiation effects in breeder structural materials, p. 727, Scottsdale, AZ (1977).

[59] F. A. Garner, et al. in: Proc. on Effects of Radiation on Materials, ASTM 725, p. 680, Savanah, Ga (1980).

[60] F. A. Garner, et al.: Proc. on Effects of Radiation on Structural Materials, ASTM 683, p. 160, Richland, Washington (1978).

[61] D. L. Porter and F. A. Garner, J. Nucl. Mat. **159**, 114 (1988).

[62] F. A. Garner, et al.: Proc. on Effects of Radiation on Structural Materials, ASTM 683, p. 160, Richland, Washington (1978).

[63] S. K . Khera, et al., J. Nucl. Mat. **92**, 299 (1980).

[64] W. G. Wolfer and M. Ashkin, J. Appl. Phys. **46**, 547 (1975).

[65] N. Igata, et al.: Proc. on Effects of Radiation on Materials, ASTM 870, p. 265, Williambsburg, VA. (1984).

[66] R. E. Stoller, Oak Ridge National Laboratory, Oak Ridge, Tennessee, Microstructural Evolution in Fast-Neutron-Irradiated Austenitic Stainless Steels, ORNL-6430 (1987).

[67] J. H. Gittus, Irradiation effects in crystalline solids, Applied Science Publishers LTD, England (1978).

[68] A. Boltax, et al. in: Proc. on Fast reactor fuel element technology, p. 157, New Orleans, Louisiana (1971).

[69] Che-Yu Li, et al. in: Proc. on Irradiation Effects on Structural Alloys for Nuclear Reactor Applications, ASTM 484, p. 347, Toronto, Ontario, Canada (1970).

[70] R. Bullough and R. C. Perrin in: Proc. on Voids Formed by Irradiation of Reactor Materials, BNES, p. 79, Harwell (1971).

[71] F. A. Garner, Symp. by Nuclear Metallurgy Committee at the winter meeting of the Metallurgical Society, p. 111, Los Angeles, CA (1984).

[72] R. A. Johnson and D. Kuhlmann-Wilsdorf in: Proc. on Radiation induced voids in metals, CONF 710601, p. 852, Albany (1971).

[73] B. L. Harbourne, et al., J. Nucl. Tech. **16**, 156 (1972).

[74] W. G. Wolfer, et al., ASTM **570**, 233 (1974).

[75] K. Ehrlich, J. Nucl. Mat. **100**, 149 (1981).

[76] R. Bullough and M. H. Wood, J. Nucl. Mat. **90**, 1 (1980).

[77] F. A. Garner and D. S. Gelles, J. Nucl. Mat. **159**, 286 (1988).

[78] W. G. Wolfer, J. Nucl. Mat. **90**, 175 (1980).

[79] W. G. Wolfer and A. Boltax, BNES, 283 (1972).

[80] D. L. Porter, F. A. Garner and G. D. Hudman, DOE/ER-0313/7, 133 (1989).

[81] J. P. Foster, et. al., J. Nucl. Eng. Desgn. **31**, 117-127 (1974).

[82] R. A. Weiner, et. al., in: Proc. Intern. Confs. on Radiation effects in breeder structural materials, p. 865, Scottsdale, AZ (1977)..

[83] F. A. Garner, D. L. Porter and B. J. Makenas, J. Nucl. Mat. **148**, 279 (1987).

[84] D. L. Porter and F. A. Garner in Influence of Radiation on Material Properties, ASTM STP 956 (F. A. Garner, C. H. Henager, Jr. and N. Igata, eds.) 11 (1987).

[85] F. A. Garner and D. L. Porter, J. Nucl. Mat. **155/157**, 1006 (1988).

[86] D. L. Porter, E. L. Wood, and F. A. Garner, DOE/ER-0313/5, (1989).

[87] F. A. Garner, DOE/ER-0313/8, (1990).

[88] R. W. Clark, A. S. Kumar and F. A. Garner, J. Nucl. Mat. **155157**, 845 (1988).

[89] D. L. Porter, et. al., ASTM STP 1046, 551-569 (1990).

[90] M. B. Toloczko, F. A. Garner and C. R. Eiholzer, DOE/ER-0313/9, 160 (1991).

[91] F. A. Garner and R. J. Puigh, DOE/ER-0313/7, 140 (1991).

[92] F. A. Garner and R. J. Puigh, DOE/ER-0313/7, 114 (1991).

[93] F. A. Garner, J. Nucl. Mat. **122**, 459 (1984).

[94] F. A. Garner, J. Nucl. Mat., 122&123, 459 (1984).

[95] D. L. Porter and F. Garner, ASTM 956, 11 (1986).

[96] H. Nickel, Discussion session in: Proc. 4th Int. Conf. on Fusion Reactor Materials (ICFRM4), J. Nucl. Mat. **179/181**, 1231 (1991).

[97] G. M. Kalinin, J. Nucl. Mat. **179/181**, 119 (1991).

[98] M. O. Marlowe and W. K. Appleby, Trans. Am. Nucl. Soc. **16**, 95, (1973).

[99] R. R. Peterson, University of Wisconsin report UWFDM 382 (1980).

[100] R. R. Peterson, personal communication, June (1989).

[101] R. D. Watson et al., Trans. ASME 105, 144 (1983).

[102] M. Abdou et al., A Demonstration Tokamak Power Plant Study (DEMO), ANL/FPP/82-1 (1982).

[103] M. C. Billone and S. Majumdar, Thermomechanical Analysis of the U.S.-ITER Driver Blanket, ANL (1990).

Chapter 7.

Experimental measurement of Mechanical Properties Along Interfaces of Bonded Structures

7.1 Introduction

A fusion material characterization program should focus on the following points [1]:

1. Extracting information from small test volumes.
2. Fission-fusion correlations.
3. Modelling and analysis of microstructure/properties and properties/failure limits.
4. High energy irradiations to verify analytical/experimental procedures.

The major problems with the existing irradiation facilities are that the fission reactors have average neutron energies more than an order of magnitude below the 14.1 MeV for fusion, the irradiation space is severely limited and costly in high energy facilities (few cm^3 in RTNS.II); and also for the small irradiation volumes available, large flux gradients, and relatively low flux levels exist.

A Miniaturized Specimen Technology had to be developed to account for smaller irradiation volumes, lower post irradiation testing doses to personnel, etc. Certain features of this technology can easily be identified: The increased difficulty in handling, testing, data reproducibility, and relationship of the data to bulk properties. Information can be provided directly or data has to be interpreted either by empirical correlations or analytical procedures. Also, the microstructure characterization (average and maximum grain sizes, average and maximum particle sizes, and degree of anisotropy) should be taken into consideration.

Finally, analyses should be done to determine minimum volume and smallest dimension for continuum criteria. Above all, it should be ensured that this volume is practical for an experimental program. A wide variety of tests have been developed for determining strength, ductility, and fracture-related data [1]. Table 7.1 shows some of these small-specimen tests and their characteristics [2].

7.2 Mechanical properties along interfaces of bonded structures

Measurement of mechanical properties of interfacial zones is very complicated and requires the support of mathematical micromechanical models [3]. Adhesion tests based on fracture mechanics principles are the most likely source of quantitative data. Fracture mechanics methods also exhibit several attractions. First, an adhesion parameter, such as the interface fracture resistance (or toughness) K_c^{inter} can be defined. Secondly, the potential exists for developing sound, theoretically based, measurements of interface toughness. Finally, fracture mechanics provides a mathematical framework for using the fracture toughness as a design parameter. However, currently available tests are of restricted application and are too complex for most purposes [4].

7.2.1 Hardness

Despite the difficulty of predicting the serviceability of a coating from its hardness value, it is probably the mechanical property most often measured [5]. When dealing with small volume of materials and certain structures like interfaces, it is understood that microhardness techniques; rather than the conventional hardness; will be used. Conventional microhardness has several characteristics that make it attractive for mechanical property characterization in small specimens [6]. Primarily, the volume of material "sampled" during the test is small ; while this volume varies with material and applied load, a nominal value of

Table 7.1: Small-Specimen Tests and Characteristics [2]

Test	Approximate Avg. Specimen vol. (mm^3)	Nature of raw data	Type of properties*	Nature of analysis
Tensile	15	Load-displacement	$\sigma=f(\varepsilon)$	direct
Microhardness				
conventional	1.7	load/area	strength	empirical
Ball	1.7	load/area	$\sigma=f(\varepsilon)$	semi-empirical
Punch				
Ball	1.7	load-displacement	ductility	analytical
			$\sigma=f(\varepsilon)$	analytical
			strength	semi-empirical
Shear	1.7	load-displacement	strength,ductility	empirical
Bend	10	load-displacement	strength	analytical
Fracture	370	load-crack growth	fracture toughness	direct
Impact	200	load-time-temperature	energy absorbed	direct
Fatigue				
S-N	1000	load-cycles	S-N	direct
FCP	245	crack length-cycles	crack growth-ΔK	direct
Pressurized tube	350	diameter-time	creep rate	direct
			rupture time	direct

* σ=stress, ε=strain, ΔK=stress intensity range, S-N=stress vs. number of cycles to failure

$\approx 1 cm^3$ can be taken as the amount of material plastically deformed around an indenter in a medium strength steel for a 200 g load. To date, however, conventional microhardness data have been related to mechanical properties of the test material, such as ultimate tensile strength, largely by empirical means. This is generally achieved with equations of the form $H \approx C\,\sigma$, where H is some measure of the microhardness, σ the mechanical property of interest, and C a constant (or function of some material property or set of properties). Yet, the indentation process is dictated by the basic flow properties of the material; thus there should be information in the process of indentation or in the indentation itself which, if extracted properly, should be related to these basic properties. It should be noted that conventional microhardness testers require direct imaging of the indentations to obtain hardness, large errors are introduced due to measurement of the diagonal lengths, especially when the indentations are small [7].

As indicated above, Tabor [8] has shown that the Vickers hardness of many metals is proportional to the yield stress, the proportionality constant being found experimentally to be close to the theoretical value of three for ideal plastic materials. For ductile metals and other similar materials, this relationship works well. But, indentation experiments with highly elastic materials, have shown that the elastic and plastic strains associated with indentations are of the same order of magnitude and the linear relationship does not apply. Johnson [8] indicated that for the case of an elastic-plastic material, the hardness is not only a function of yield stress but also a function of the parameter E/σ, where E is the Young's modulus of the material.

7.2.2 Elastic properties

Elastic properties along interfaces are very important for several reasons. First: modelling of bonded structure behavior is very complicated since some of the critical input

parameters such as bond strength and interface compliance are not well known and the lab testing of these properties is believed to be even more critical than it would be for simple structure [9]. Second: fabrication techniques, like brazing or plasma spray, do not produce sharp interfaces, and a certain degree of elemental mixing along the interfaces take place. Elastic properties are known to depend on the composition [10], especially along interfaces where elemental mixing may be promoted. There are two extreme cases to consider for bonded structures. At the one extreme, a stress is applied transverse to the interface and the other, the load is applied parallel to the interface. Figure 7.1 shows how the modulus of the substrate varies with its volume fraction for these two extreme cases. We have to keep in mind that many bonded structures will deform by a combination of the two cases.

Radiation damage in bonded structures is expected to induce certain changes in elastic properties. As mentioned in chapter 6, swelling can reduce the elastic properties by up to 2% for every 1% swelling in AISI 316 Stainless Steel. Designers usually use a swelling limit of 5-10%. Based on this figure, we may expect a 10-20% reduction in Young's modulus by the end of the component life time. Detecting changes in Young's modulus from small material volumes along interfaces thus becomes a necessity to forecast the irradiation behavior of certain structures especially interfaces of bonded structures. Collisional mixing due to neutron irradiation may also cause elemental mixing along interfaces of bonded structures (as explained in Chapter 5). These changes need to be quantified and measured.

7.3 The Nanoindenter

An automated system with the ability to evaluate the mechanical response of a sample with submicron spatial resolution has an extremely wide range of applications. A testing system must have certain characteristics to be considered a Mechanical Properties Microprobe

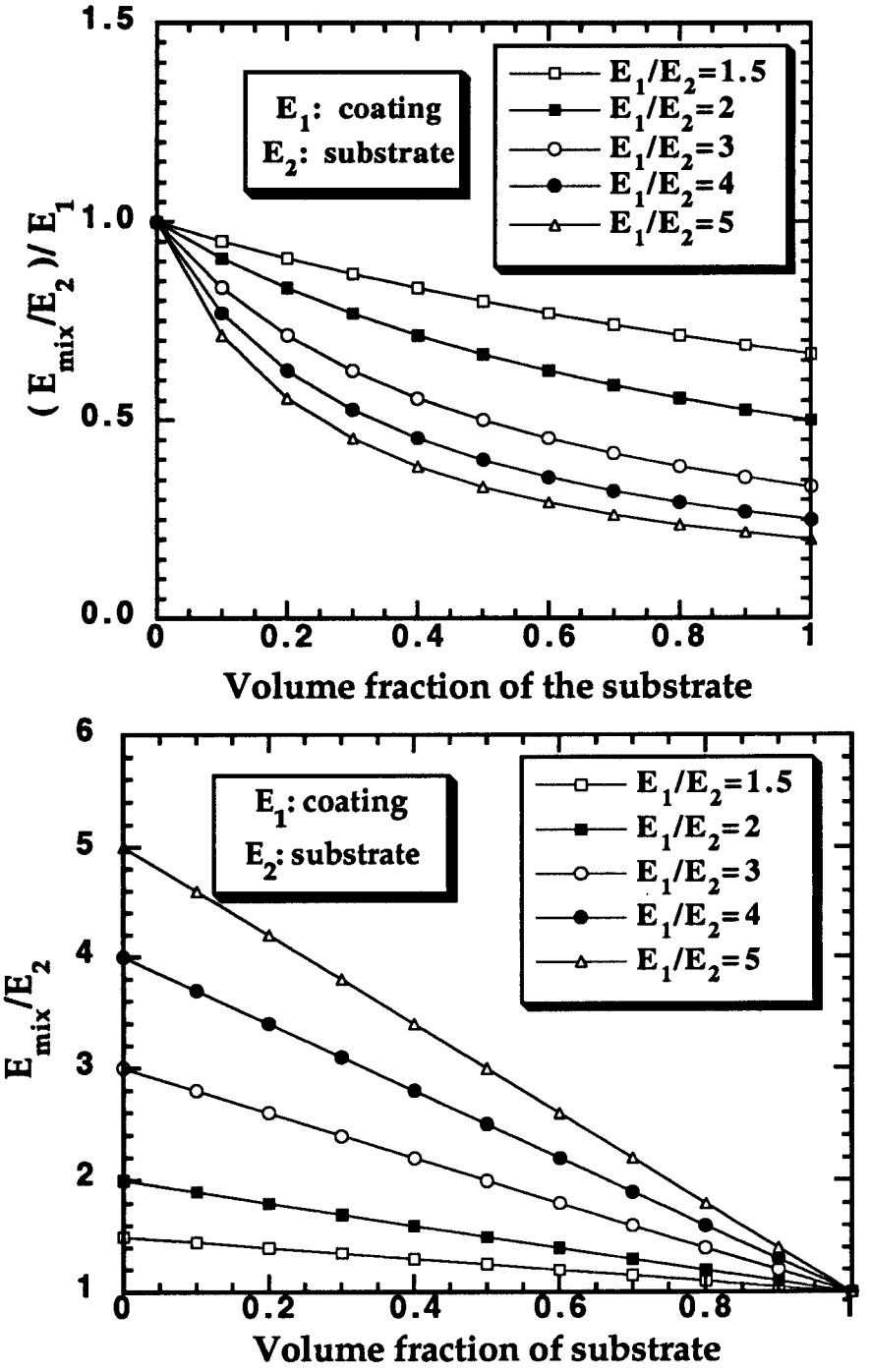

Figure 7.1: Variation of substrate Young's modulus with type of loading as a function of its volume fraction: (a) Isostress case $E_{mixture} = \frac{E_1 E_2}{V_{f2}E_1 + (1-V_{f2})E_2}$, (b) Isostrain case

$E_{mixture} = E_2 V_2 + E_1 (1-V_2)$

(MPM) [11]. It can measure the required properties from volumes of material at least as small as one micron in diameter. Ideally, the system could determine a constitutive equation for that volume of material; hence, it must measure both the elastic and plastic mechanical properties. To do this reproducibly, the system must control or measure all the parameters affecting such properties. These parameters include the strain, strain rate, temperature, stress, and the environment. Finally, the system must take these measurements with reasonable precision and with reasonable investment of time and effort.

At the present time, only one type of mechanical test can potentially satisfy all of the above requirements [11]. Properly instrumented and controlled, a (depth sensing) microindentation test can accomplish many of these goals. During an indentation test, both elastic and plastic strains are generated. For many materials the strains from both fields are of sufficient magnitude to be measured. The test can be scaled down so that submicron volumes of materials are sampled. Microindentation tests have been used to measure an extremely wide variety of material properties: yield strength, creep resistance, stress relaxation, modulus, fracture toughness, and even fatigue tests. In addition, because the material being tested is close to a surface, environmental effects can be measured. With the proper combination of microindentation tests, a nearly complete constitutive equation of the sample's mechanical response can be mapped.

A schematic of a commercially available ultralow force indentation system; the Nanoindenter, is shown in Figure 7.2 [7]. The indenter is a triangular pyramid shaped diamond with the same area to depth ratio as the traditional Vickers pyramid. The capacitance displacement gauge permits one to detect displacement changes of 0.2-0.3 nm. The force application system has two ranges: 0-20 mN and 0-120 mN with resolutions of 300 nN and 1.8 μN. A typical test involves moving the indenter to the surface of the material and

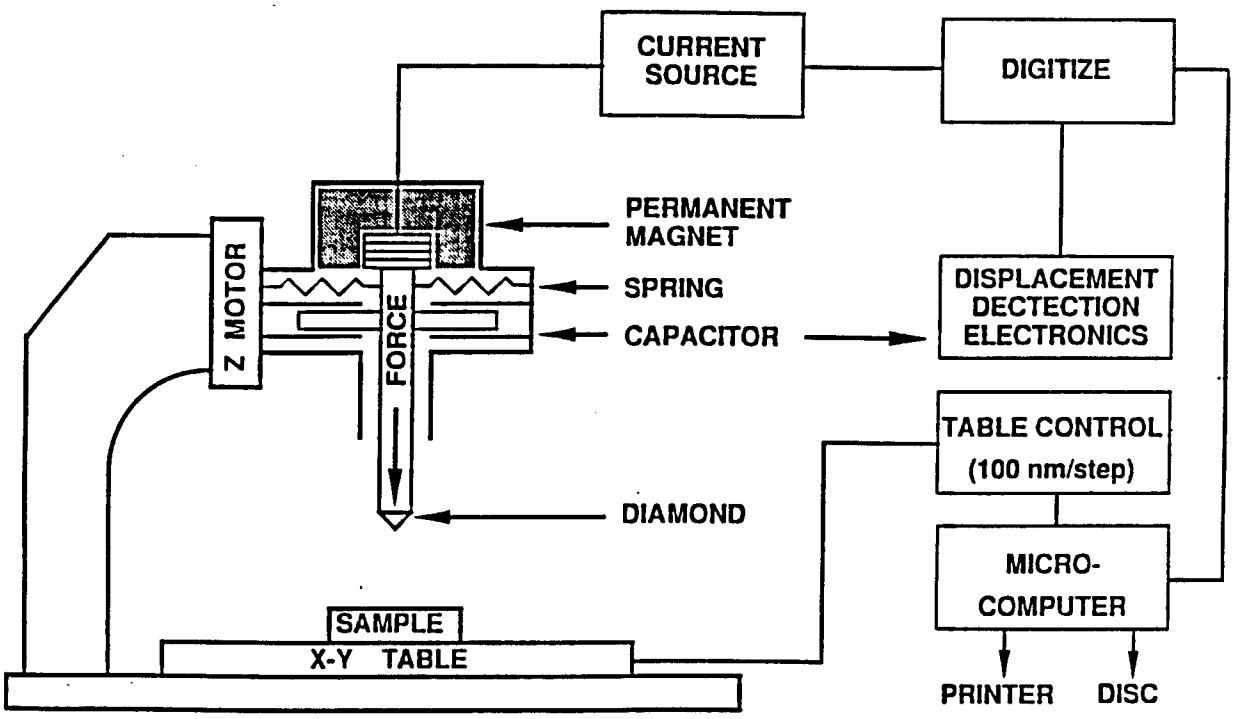

Figure 7.2: Schematic diagram of the Nanoindenter [12]

measuring the forces and displacements associated with the indentation process. The surface is located for each indentation by lowering the indenter at a constant rate against the suspending springs and detecting a change in velocity on contact with the surface. In the testing mode, the load is incremented in order to maintain a constant velocity, although other schemes, such as a constant strain rate, can be implemented. A typical testing rate is about 3 nm/s. A typical loading curve is shown in Figure 7.3. The depth plotted represents the total displacement of the indenter relative to the initial position of the surface. It is composed of both elastic and plastic deformation (Figure 7.4). An inherent complication of the Nanohardness unit is that the stresses and strains produced by indentation are nonuniform within the test sample. Therefore, only nominal values of the stresses, strains, and strain rates can be determined in such tests [13].

It should be noted that the Nanoindenter is currently limited to ambient temperatures because the displacement measured is sensitive to the thermal expansion of the load application system. This is particularly important when displacements are being measured to a fraction of a nanometer. The interest in varying the temperature of the indentation test is high, but the mechanical difficulties involved with precise thermal control are significant if the resolution of the experiment is to be maintained.

Some observations concerning the Nanohardness unit are worth mentioning [13]:

1. The tip of the indenter is usually sharp enough to cause plastic flow to occur from the very beginning of the test so that an elastic-plastic transition typical of an ordinary tensile test is not observed.

2.The slope of the loading curve increases with depth of indentation because the indenter makes increasing contact with the material during indentation.

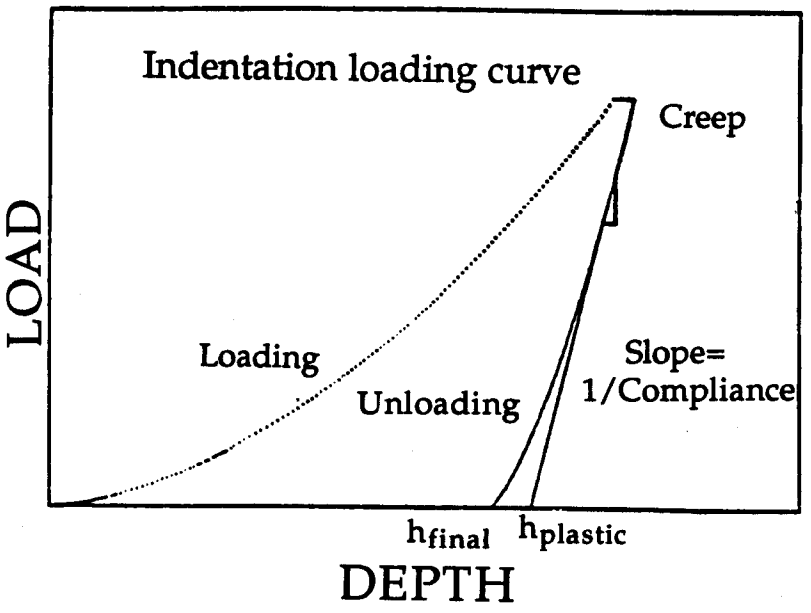

Figure 7.3: Typical load-displacement curve obtained using the Nanoindenter showing the difference between the plastic and final depth [7]

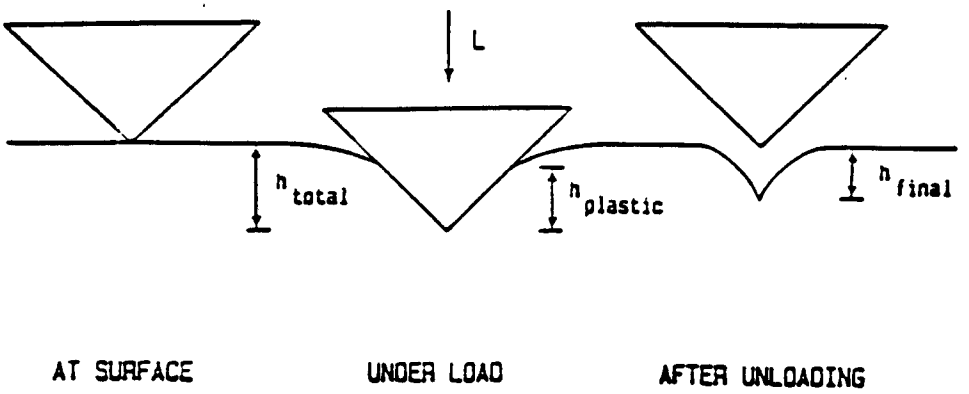

Figure 7.4: Schematic representation of the indentation process illustrating the decrease in indentation depth upon unloading [7]

3. If the load is held constant, the indenter will continue to sink into the material in a time-dependent manner as creep flow under the indenter occurs. This allows a study of the creep properties of very small volumes of material.

4. During unloading, the indenter is pushed back out of the material by the elastic restoring forces in the system.

5. For hard materials, the MPM gives moduli that are higher than expected. It is believed that this is caused partly by the high pressure under the indenter. Some densification may also sometimes occur. Also, the elastic modulus of the material just under the indenter may increase through nonlinear elastic effects.

7.3.1 Hardness measurement

Hardness is the equivalent of the average pressure under the indenter, calculated as the applied load divided by the projected area of contact between the indenter and the sample [7]. Since the depth measured during the indentation includes both plastic and elastic displacements, the elastic contribution must be subtracted from the data to obtain hardness. For the calculation of hardness under load, it is necessary to determine the plastic depth (h_p). As illustrated in Figure 7.3, the plastic depth is defined as the depth of the indenter in contact with the sample under load. With knowledge of the indenter geometry, the plastic depth can then be used to obtain the projected area in contact with the indenter. The plastic depth can be obtained from the loading curve as shown in Figure 7.3. This method assumes that during initial unloading the area in contact with the indenter remains constant. A constant contact area implies linear unloading which, for metals, is observed over most of the unloading range. The loss of contact with the indenter is a result of the change in shape of the indentation that occurs when the elastic displacements are recovered.

7.3.2 Elastic properties

The slope of the unloading curve can be used as a measure of the elastic properties of the sample. If the area in contact remains constant during initial unloading, the elastic behavior may be modeled as that of a blunt punch indenting an elastic solid. By equating the projected area in contact under the indenter to the area of the punch, we obtain for a Vickers indenter

$$\frac{dp}{dh} = \left(\frac{2}{\pi}\right)^{1/2} D\, E_r \tag{7.1}$$

where

$$\frac{1}{E_r} = \frac{1 - \nu^2}{E} + \frac{1 - \nu_o^2}{E_o} \tag{7.2}$$

and where dp/dh is the slope of the unloading curve, D is the Vickers diagonal length, E and ν are Young's modulus and Poisson's ratio for the sample, and E_o and ν_o are the same parameters for the indenter. If we assume that the indenter had an ideal pyramidal geometry and use the plastic depth h_p, instead of the diagonal length, we obtain

$$\frac{dh}{dp} = \frac{1}{2\, h_p} \left(\frac{\pi}{24.5}\right)^{1/2} \frac{1}{E_r} \tag{7.3}$$

where dh/dp is the reciprocal of the unloading slope, or the compliance. From equation 7.3, it can be seen that a plot of the measured compliance versus the reciprocal of the plastic depth should yield a straight line with slope equal to $0.179/E_r$. Young's modulus can then be calculated, provided Poisson's ratio is known.

7.4 Cross sectional measurement of mechanical properties along interfaces

There is a great need for the determination of hardness and elastic profiles along the interface of bonded structures as well as to probe certain microstructures like the intermetallic compounds formed in some of the brazing joints. If the specimen is prepared in cross

section, special machines like the Nanohardness unit, with its high accuracy in placement of indents, can be used to probe the mechanical properties along interfaces. Regardless of the fact that the measurement of hardness on cross sectioned samples was suggested early in the literature [14], there has been a substantial activity in this area only in the last few years as the use of coatings as well as composite materials has increased.

An automated microhardness testing procedure was applied to get a hardness profile across the welded zone of an alloy 2090-T8X (Al-2.7 Cu-2.2 Li-0.12 Zr) as well as along the heat affected zone [15]. Another indentation method was also used to evaluate the mechanical properties of welds. The use of 598 indentations (in this case) allows the complete hardness profile to be obtained. This technique gives an idea on how the hardness varies along the different welding regions as well as in the heat affected zone and the variation can be explained in terms of the microstructure of these areas. The determination of strength and modulus has also been successfully scaled down to submicron volumes for the welding joints of austenitic steel [16]. A Nanoindenter was also used to measure the elastic modulus of carbon beam implanted samples of Chemically Vapor Deposited Silicon Carbide/Nicalon composites [17,18]. Elastic moduli were seen to decrease significantly for the CVD material after 30 dpa at room temperature while the modulus for the fiber was increased.

A major point of concern for cross sectional measurements of mechanical properties; especially along interfaces; is how close successive indents can be to each other and how close an indent come to a material discontinuity such an edge or an interface, without interference. Standard specifications for macroindentations require that the center spacing of pyramidal indentations be at least three indentation diagonals (3D) [19]. The origin of this value seems to be lost in the early history of the development of hardness testing, and there

appears to be no modern published reports of experimental investigation to support the value of 3 [19].

Samuels and Mulhearn [20] experimentally quantified these limits using Vickers-pyramid and Brinell-ball indentations for 70:30 brass. Since the iso-strain contours below the indenter are independent of indenter geometry away from the plastic imprint, their results apply also to the Berkovich pyramid of the Nanoindenter [17]. Figure 7.5 shows the elastic-plastic boundaries for an infinite and semi-infinite material. The indenter geometry is that of the Berkovich pyramid which has an imprint diagonal to depth ratio of 6.5. From the figure it is apparent that for the infinite medium the elastic plastic-boundary is spherical for infinite material.

The knowledge that is available on the plastic zone associated with the indentations permits an assessment to be made of what should be an acceptable spacing. As a starting point, it might be said that the elastic-plastic boundaries of adjoining indentations should not overlap [19]. This criterion would permit a center spacing of about 3 D for metals of moderately low yield stress, and 1 D for metals of moderately high yield stress. But these would be conservative values because hardness is not sensitive to small plastic strains even in materials which work harden considerably. A more realistic criterion perhaps would be that the iso-strain boundaries for something approaching Tabor's equivalent strain should not overlap. To be on the safe side, one might require that the 5% iso-strain boundaries should not overlap. By this criterion, the indentations could nearly touch one another without error, except perhaps in the very softest of materials. As a guide, it can be assumed that a serious error has not been introduced if the shape of the preexisting indentation has not been distorted noticeably by the new indentation. This criterion is particularly likely to be acceptable with microindentations in which there is so many other experimental uncertainties [19].

The iso-strain contours are deformed significantly for indents close to the edge of a sample. From Figure 7.5 [17] it is seen that the elastic-plastic boundary for a semi-infinite sample is skewed such that the boundary contacts the edge of the sample at a distance/indenter depth ratio of 11.7. The minimum approach distance to an edge should therefore be 11.7 times the depth of the indent. While this would lead to the conclusion that the shallowest indents are the best, considerations of surface roughness must be addressed. A tradeoff must be made between decreased volume averaging below the indenter and the inaccuracy due to surface imperfections [21]. Once more, Samuels suggested that the standards are certainly excessively conservative for microindentation testing [19].

Another point of concern for the cross-sectional measurement of mechanical properties of bonded structures is the anisotropy of these properties [22]. For example, there is a typically crystallographic variation in Young's modulus. The reported values of elastic properties are usually average values taken from polycrystalline materials with a random orientations of the individual grains [10]. The question that is usually addressed is whether to average over the elastic constants (Voight averages) or over the elastic compliances (Reuss averages). The former is appropriate for a polycrystal in which the grains have the same state of strain; the latter for the case when they have the same stress [23]. If one is interested in probing the anisotropy along interfaces for bonded structures in fusion reactors; where the structures at the interfaces are subject to the same strain; the use of the Voight average is more suitable.

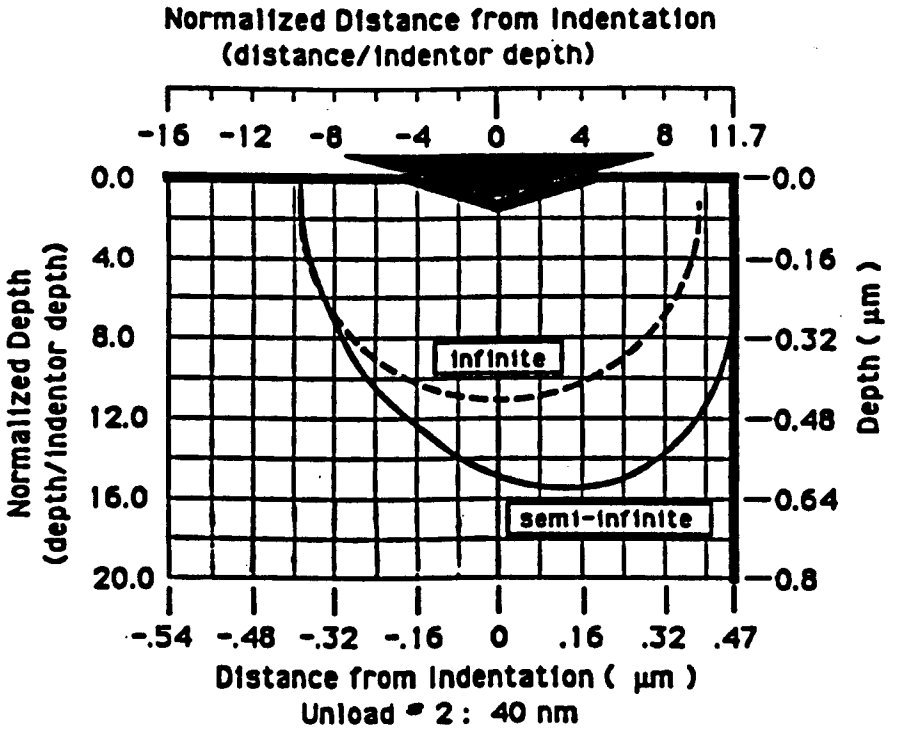

Figure 7.5: Elastic Plastic boundaries for indentations on infinite and semi-infinite media [17]

7.6 Mechanical properties along the interfaces of Be/Cu structures

The Mechanical Properties Microprobe (MPM) at the University of Wisconsin was used in measuring the mechanical properties along interfaces of Be/Cu structures fabricated at SANDIA National Lab. Samples of two fabrication techniques were studied:

1. Beryllium hipped (Hot Isostatic Pressed) to Oxygen Free High Conductivity (OFHC) copper.

2. Beryllium brazed to OFHC using a Silver based brazing alloy.

It is worth mentioning that the success of the beryllium program in Joint European Torus (JET) has enhanced interest in the beryllium for the Plasma Facing Components (PFCs) in future fusion devices. The idea of beryllium armor in the International Tokamak Thermonuclear Reactor (ITER) also appears to have merit [24]. Also, copper alloys have been used as heat sink materials for the limiters, wall armor, and divertor plates of today's tokamaks [25].

The samples were polished using 1 μm diamond paste. Hardness and Young's modulus were then measured using the Nanoindenter.

7.6.1 Be/Cu Brazed structure

Thirty two indentations were first made in two runs in Be and Cu bulks away from the interface to compare the bulk and interface values. Fifty indentations were then made starting from the Be side into the interfacial zone in two runs (20 and 30 indentations respectively). The large number of indentations is needed to assess the variation along the interface and also to increase the statistical certainty in the results. The high load range (0-120 mN) was used to obtain indentation depths of 500, 750, and 1000 nm. The minimum

spacings between indents were 53, 34 μm for the two runs respectively (> 30 times depth). The distance to the interface was approached at nearly 10 and 7 μm per indentation for the two runs respectively. As shown in Figure 7.6, indentations were made at an angle to the interfaces so that a proper assessment of the properties along the interface can be done (notice that indentations size reflects the different hardness values). Forty indentations were then made starting from the interfacial zone into the Cu side in two runs (20 each) at indentation depths 500, 1000, and 1500 nm. Minimum spacings of indentations in this case was 51 μm. The interface was approached at nearly 12 and 10 μm per indentation for the two runs respectively. Table 7.2 represent the indentations segments for both the Be-Interfacial zone and Interfacial zone-Cu regions.

7.6.2 Be/Cu hipped structure

The same techniques that were used for the brazed joint, were followed for the hipped structure. Indentations were first made in the Be and Cu bulk regions away from the interface to compare the bulk and interface values. In this case, a separate run had to be done for the interface since its thickness varies from 400 to 450 μm.

7.7 Results

Figures 7.7, 8, and 9 show the variation of hardness (H), Young's modulus (E), as well as L/S^2 (i.e. H/E^2) for indentation depth 1000 nm for the brazed structure. Several points can be observed:

1. The jump in the mechanical properties between the Be side and the interfacial zone is quite obvious compared with the smooth transition along the interface between the copper and the interfacial zone.

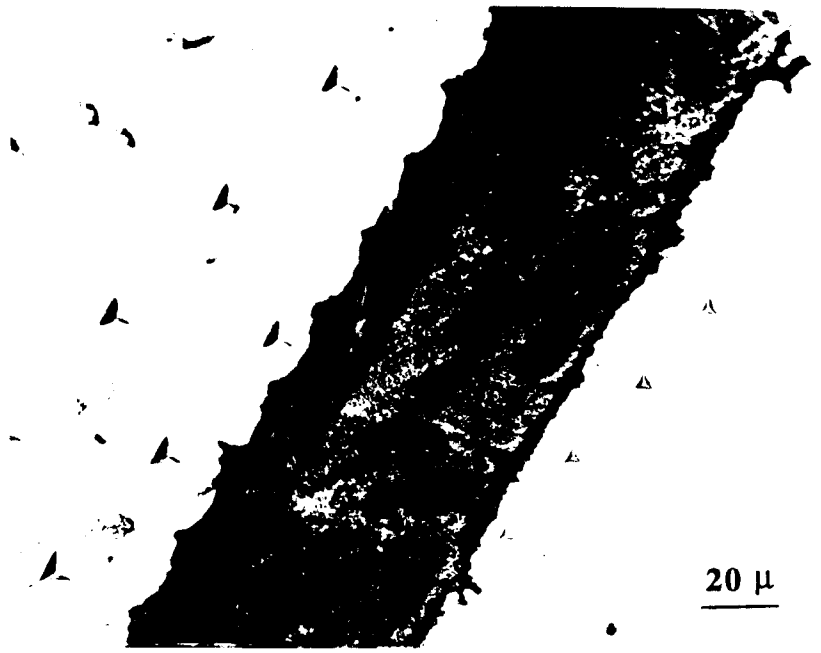

Figure 7.6: Indentation run along the border of the interfacial zone of a Be/Cu brazed joint.

Table 7.2: Indentation test configuration used for the Be bulk, Interfacial zone, and Cu bulk regions

Segment number	segment type	rate (nm/sec)	Depth limit (Loading segment) (nm)	Unloading (Unloading segment) (% of final load)
1	Approach	10	...	...
2	Loading	5	500	...
3	Hold	25 data points; 1 sec delay between logging points		
4	Unloading	50%	...	80
5	Loading	5	750 (1000)**	...
6	Hold	25 data points; 1 sec delay between logging points		
7	Unloading	50%	...	80
8	Loading	5	1000 (1500)**	...
9	Hold	25 data points; 1 sec delay between logging points		
10	Unloading	50%	...	80
11	Hold	100* data points; 1 sec delay between logging points		
12	Unloading	300	...	100

*For copper, a 25 min. Hold period was performed to avoid creep effects.

**Values between parentheses represent depth limits for Cu bulk and Cu-Interfacial zone interface.

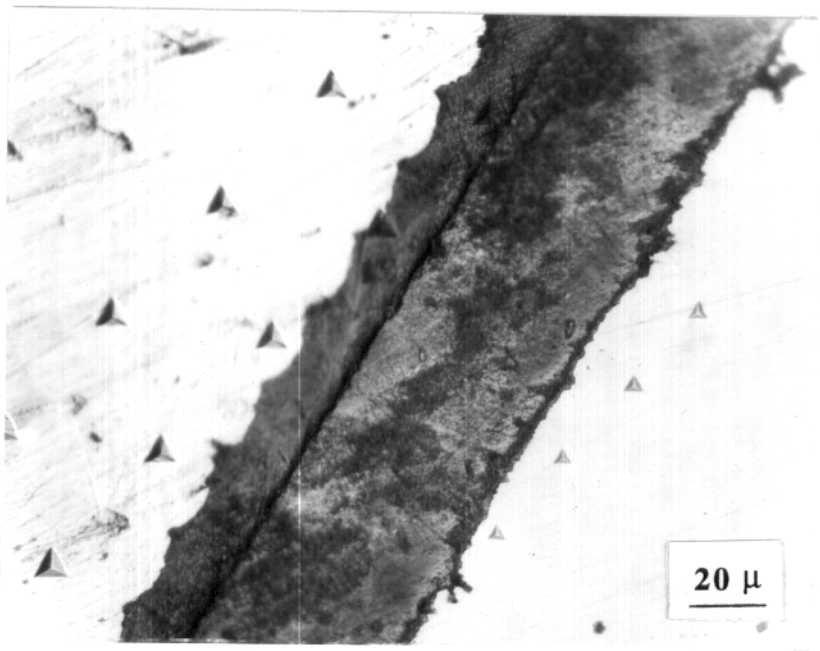

Figure 7.6: Indentation run along the border of the interfacial zone of a Be/Cu brazed joint.

Table 7.2: Indentation test configuration used for the Be bulk, Interfacial zone, and Cu bulk regions

Segment number	segment type	rate (nm/sec)	Depth limit (Loading segment) (nm)	Unloading (Unloading segment) (% of final load)
1	Approach	10	...	...
2	Loading	5	500	...
3	Hold	25 data points; 1 sec delay between logging points		
4	Unloading	50%	...	80
5	Loading	5	750 (1000)**	...
6	Hold	25 data points; 1 sec delay between logging points		
7	Unloading	50%	...	80
8	Loading	5	1000 (1500)**	...
9	Hold	25 data points; 1 sec delay between logging points		
10	Unloading	50%	...	80
11	Hold	100* data points; 1 sec delay between logging points		
12	Unloading	300	...	100

*For copper, a 25 min. Hold period was performed to avoid creep effects.

**Values between parentheses represent depth limits for Cu bulk and Cu-Interfacial zone interface.

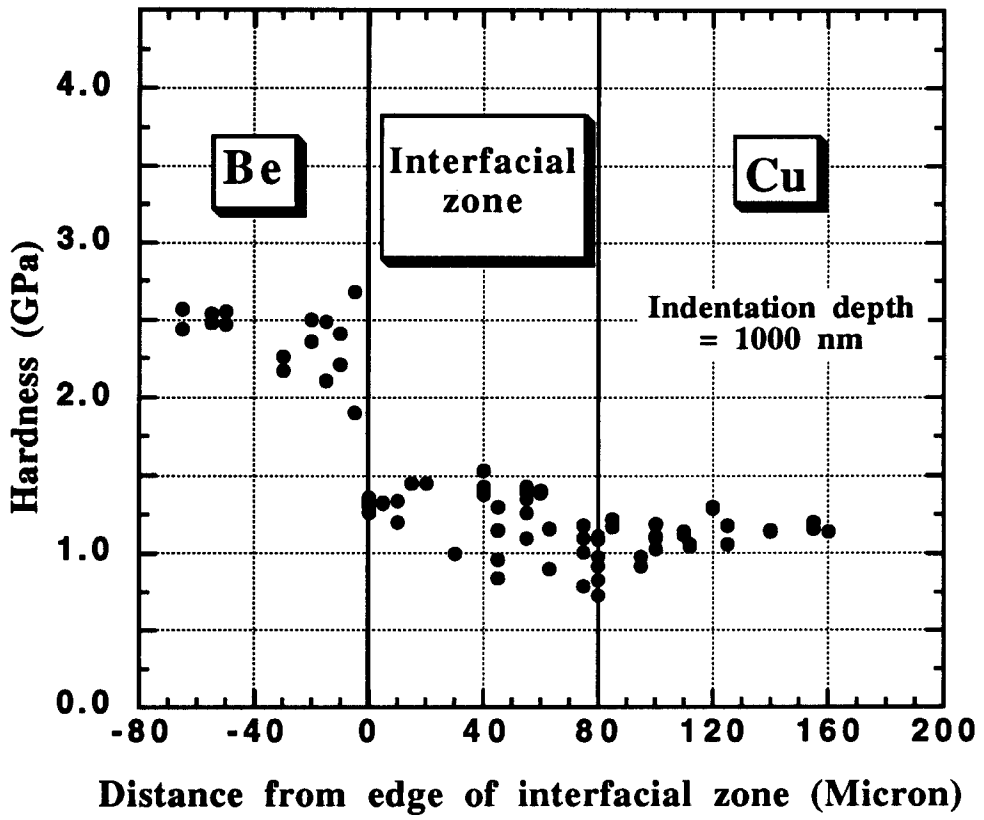

Figure 7.7: The hard beryllium layer compared with the copper layer and the interfacial zone.

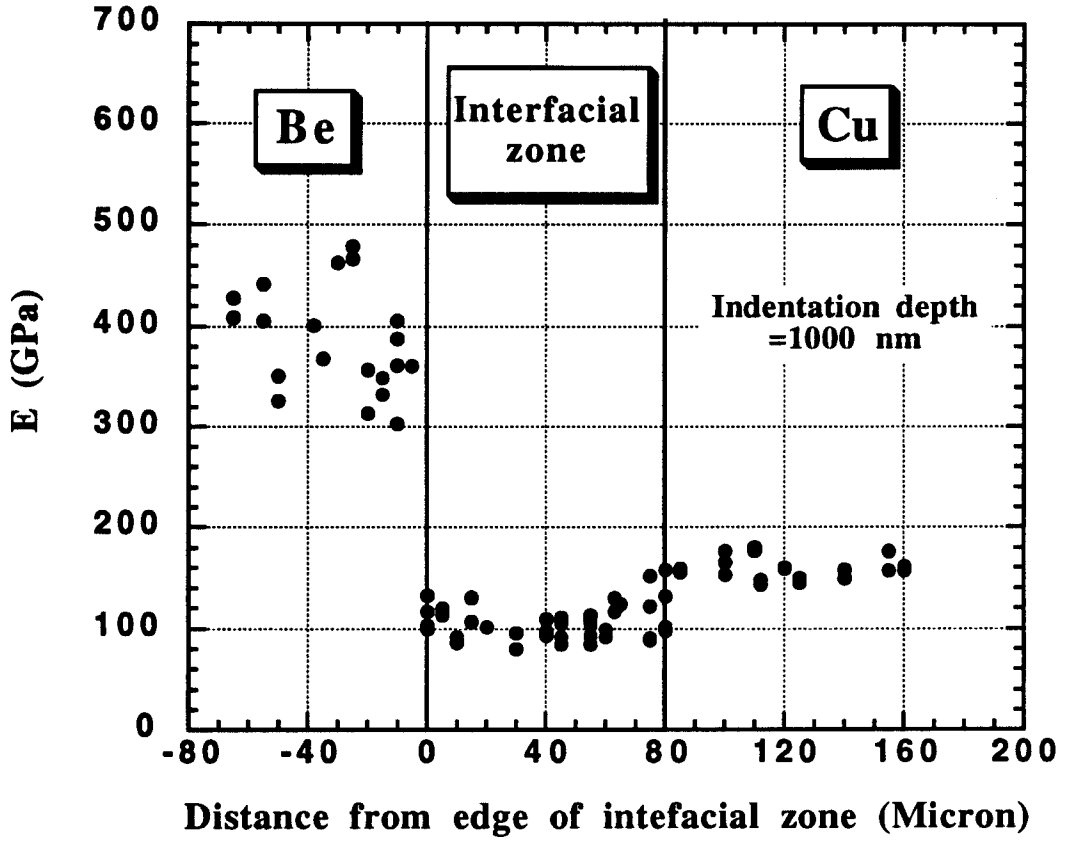

Figure 7.8: Discontinuity in Young's modulus for a brazed Be/Cu joint.

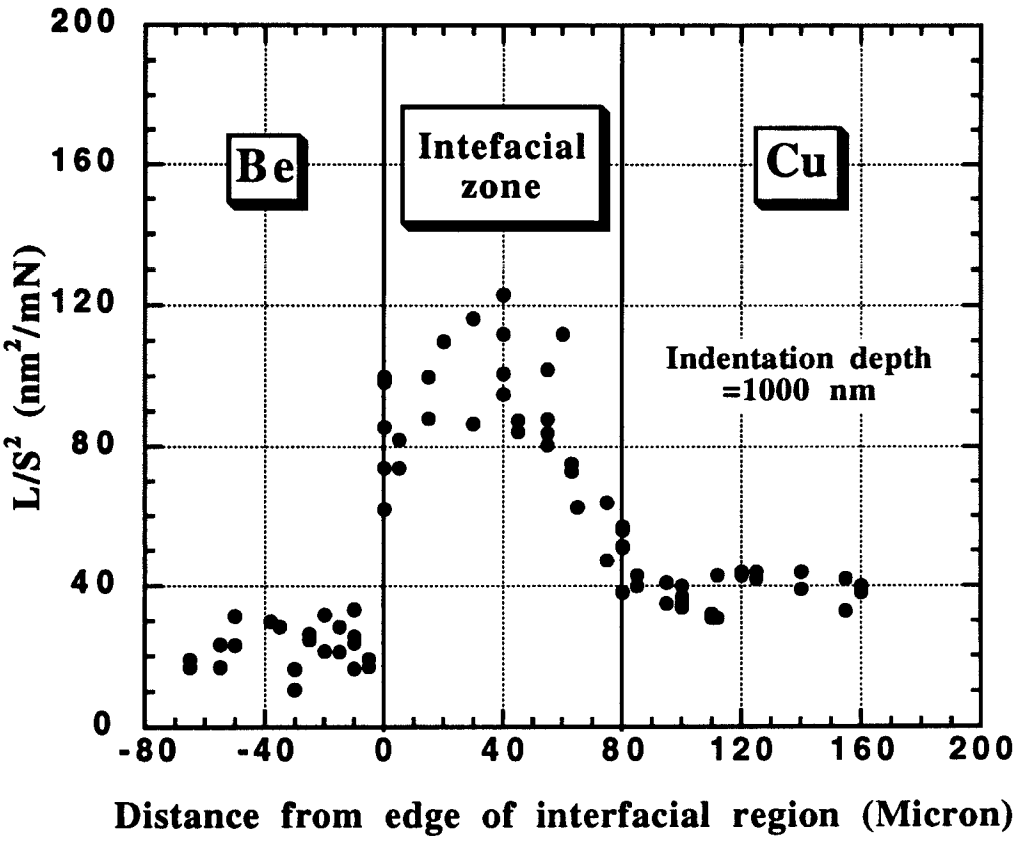

Figure 7.9: Distribution of the ability to resist plastic deformation for a brazed Be/Cu joint

2. The lowest hardness value occurred at the edge of the interfacial zone with the copper side. As for the Young's modulus, the lowest value occurred in the interfacial zone which further widened the difference in Young's modulus values between the copper and the beryllium parts.

3. The largest values of hardness and Young's modulus occurred in the beryllium bulk

4. Values of H/E^2 are considered to be a good representation of the resistance for plastic deformation as mentioned by Oliver [27]. Thus, the high values of H/E^2 in the interfacial zone; compared with the beryllium and copper bulk region; is a good indication of its ability to resist plastic deformation.

As for the hipped structure, several interesting points were observed. First, as shown in Figures 7.10, and 11, there are some microstructural islands in the interface between the filler metal and the Be side. These extend for about 100 μm as shown from the metallographic picture in figure 7.12. The Nanoindenter successfully detected these changes in the microstructure that was reflected in discontinuities in the mechanical properties.

The following points can be observed:

1. The discontinuity in the mechanical properties along the edge of the interfacial zone with beryllium still exists. It is worse than the hipped joint due to the existence of the microstructural islands.

2. The smooth transition along the edge of the interfacial zone with the copper still exists. However, a mismatch in hardness values can be observed.

3. Away from the microstructural islands, hardness values are slightly higher in the interfacial region for the hipped joint compared with the brazed joint. However, the H/E^2 values of the interfacial zone in the hipped joint is lower than the brazed joint.

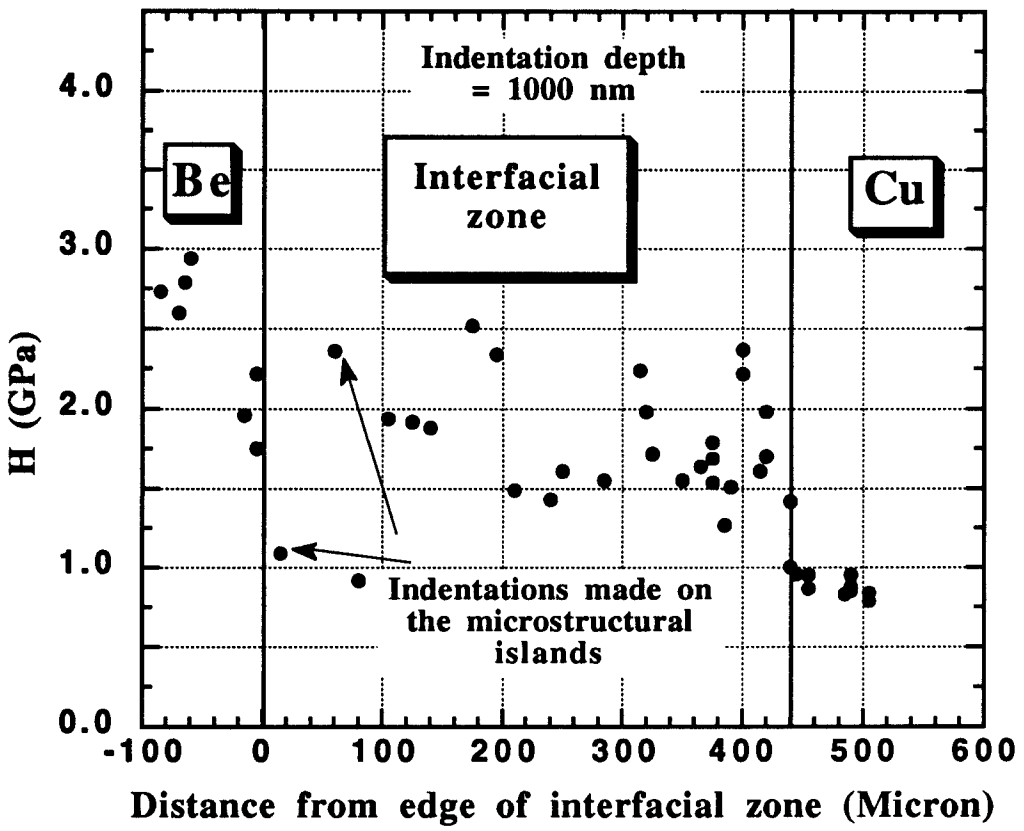

Figure 7.10: Hardness distribution along interfacial region of a Be/Cu hipped joint

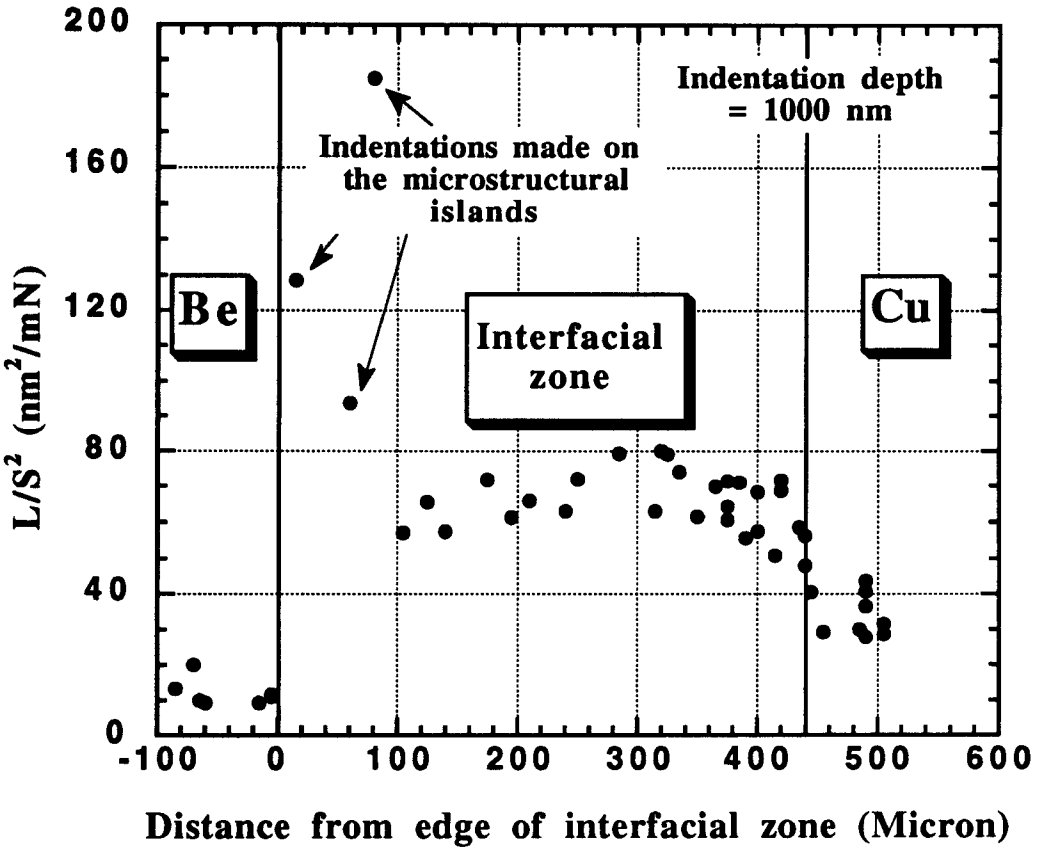

Figure 7.11: Distribution of the ability to resist plastic deformation for a Be/Cu hipped joint

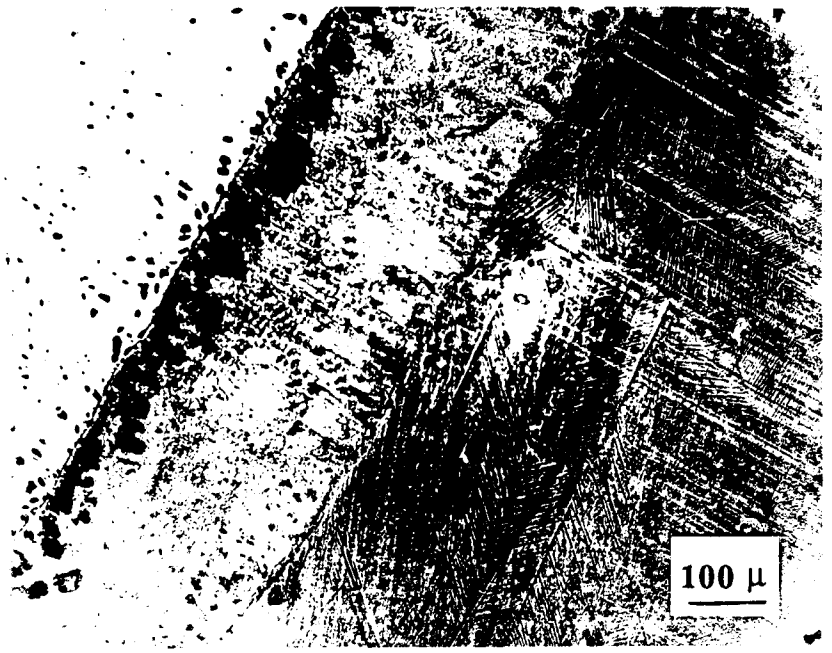

Figure 7.12: Microstructure islands observed along the Be/interfacial region of the Be/Cu hipped joint.

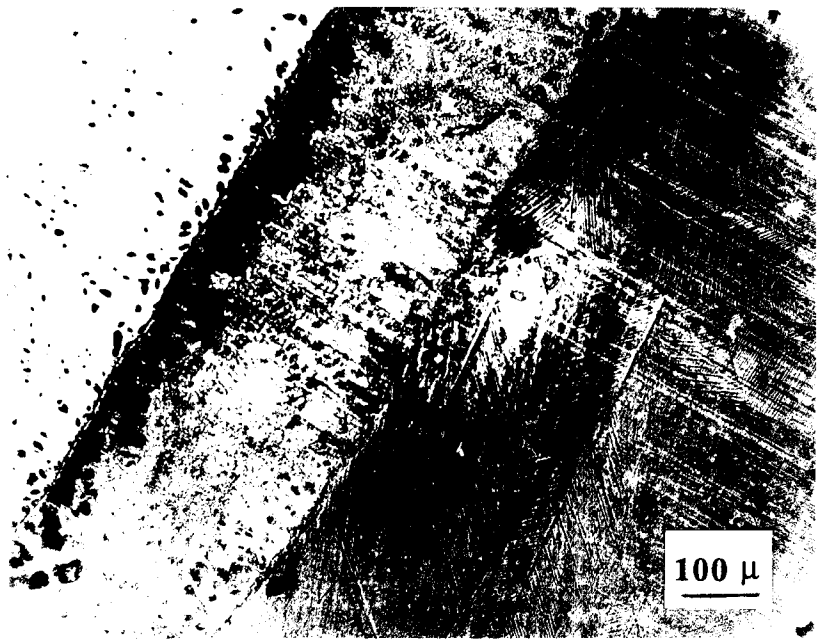

Figure 7.12: Microstructure islands observed along the Be/interfacial region of the Be/Cu hipped joint.

The microstructural islands are believed to be intermetallic formations due to interdiffusion between beryllium and copper. It is well known that in case of Beryllium joining, as atoms in the base metal migrate by diffusion into the other metal and vice versa, changes in the properties of the boundary layer between the two metals may occur. This can affect the joint strength by formation of brittle intermediate phases. In other cases, on the contrary, one can obtain, deliberately or not, higher qualities of the joint [26]. In this case, the strength of the joint no longer depends on the bond strength between the two metals. Instead it depends on the bond strength between either of these and the newly formed intermediate layer [26].

7.8 Conclusions

1. The MPM was able to distinguish different fabrication techniques by a direct measurement of the hardness, Young's modulus, and H/E^2 which reflects the ability of deformation of the interfacial region.

2. Unirradiated brazed joint is more suitable than the hipped joint due to: (1) more uniform mechanical properties, (2) smoother transition of mechanical properties along the edge of the interfacial zone with the copper part, (3) less mismatch in mechanical properties between the interfacial zone and the beryllium bulk, and (4) high deformation ability of the interfacial zone (as shown in Figure 7.13).

3. Change in H/E^2 value is a good representation of the change in mechanical properties along interfaces of bonded structures. Scattering in its value is much less than the scattering in either hardness or Young's modulus. This gives a good chance to successfully detect inhomogeneties in the structure.

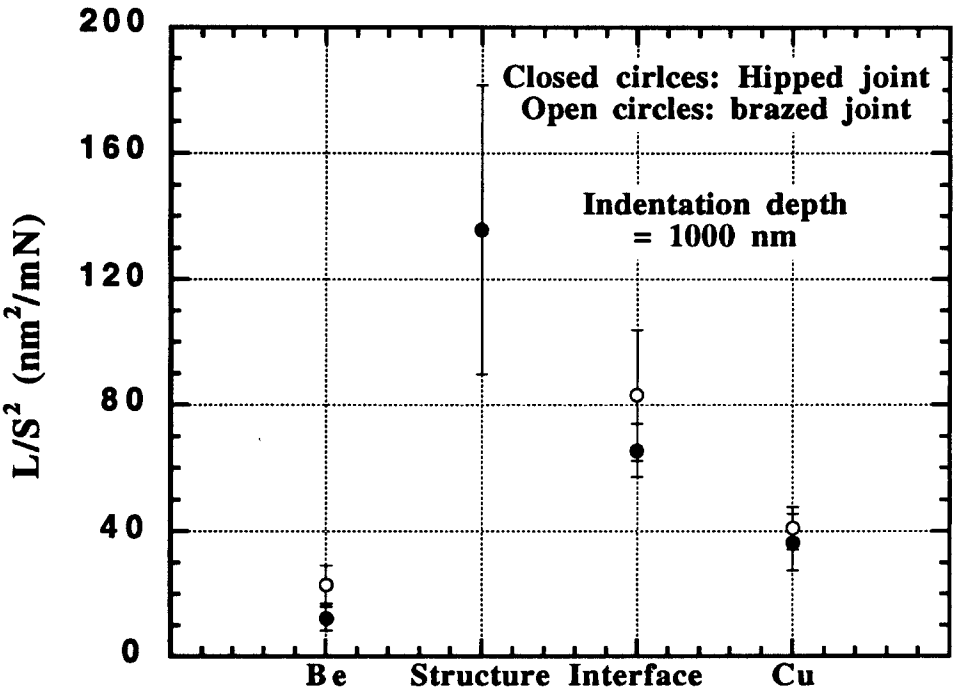

Figure 7.13: comparison of the ability of deformation for Be/Cu hipped and brazed joints.

7.9 References

[1] G. E. Lucas and G. R. Odette, Nucl. eng. and design / fusion **2**, 145 (1985).

[2] G. E. Lucas, et. al., MRS Bulletin, July, 29 (1989).

[3] A. Deruyttere and L. Froyen (eds.) in: Proc. on Interfaces in Materials, Brussels (1988).

[4] S. S. Chiang, et al., in: Materials Science Research, Surfaces and interfaces in ceramic and ceramic-metal systems (J. Pask and A. Evans, eds.) **14**, 603, (1980).

[5] G. A. Di Bari, in ASTM 947, Testing of metallic and inorganic coatings (W. B. Harding and G. A. Di Bari, eds.) 4 (1986).

[6] G. E. Lucas, et al., ASTM 888, 112 (1986).

[7] M. F. Doerner and W. D. Nix, J. Mater. Res. **4**, 601 (1986).

[8] A. K. Bhattacharya and W. D. Nix, Int. J. Solids Structures **24**, 881 (1988).

[9] J. B. Whitlley, J. Nucl. Mat. **85**, 40 (1979).

[10] C. R. Barrett, et al., The Principles of Engineering Materials, Prentice-Hall, inc. (1973).

[11] W. C. Oliver, MRS Bulletin, XI, 15, (1986).

[12] W. C. Oliver, MRS Bulletin, XI, 15 (1986).

[13] W. D. Nix, Met. Trans. **20A**, 2217 (1989).

[14] K. L. Mittal, in ASTM 640, Adhesion measurement of thin films, thick films, and bulk coatings (K. L. Mittal, ed.) 5 (1976).

[15] R. P. Martukanitz, et al., in: proc. of the International Metallographic Society on Structural Science **14**, 53 (1987).

[16] A. David, et al., Welding Res. Suppl., 236s (1987).

[17] L. L. Snead, DOE/ER-0313/10, 320 (1991).

[18] L. L. Snead and S. J. Zinkle, DOE/ER-0313/11, 316 (1991).

[19] L. E. Samuels in: Microindentation Techniques in Materials Science and Engineering, Eds. Blau/Lawn, ASTM STP 889, 5 (1984).

[20] L. E. Samuels and T. O. Mulhearn, J. of Mechanics and Physics of Solids **5**, 125 (1957).

[21] L. L. Snead, unpublished work, (1992).

[22] R. A. Dodd, private communications, (1988).

[23] J. P. Hirth and J. Lothe, Theory of dislocations, McGraw-Hill, New York (1968).

[24] R. E. Nygren and M. F. Smith, Fusion Tech. **19**, 2092 (1991).

[25] E. Franconi, et. al., J. Nucl. Mat. **191/194**, 493 (1992).

[26] M. M. Schwartz (Ed.), Source book on brazing and brazing technology, American Society for metals, Metals Park, (1987).

[27] D. L. Joslin and W. C. Oliver, J. Mater. Res. **5**, 123 (1990).

Chapter 8.

Conclusions and Recommendations

Analysis of the irradiation behavior of bonded structures, as they are applied in the fusion field, has been conducted by integrating both analytical and experimental concepts. The following conclusions were reached:

1. Radiation Induced Mixing (RIM) along interfaces of bonded structures proved to be a significant phenomena for fusion reactor environments. Mixing layer of hundreds angstroms thick were formed between Beryllium and iron joint structure. This has an impact on thermophysical properties that depends on the composition.

2. For ITER first wall (10 micron beryllium thick coating on a 316 SS substrate) exposed to a wall loading of 2 MW/m^2, a mixing layer of about 0.1 micron was formed along the interface. This reduced the thermal conductivity of the Be coating at the interface to 78% of its bulk value. It also caused a smooth transition in the Young's modulus values along the interface between the coating and the substrate.

3. The higher the fluence is, the larger the atomic mixing along the interface. Thus, it is expected that RIM will have more impact on near and far term fusion devices exposed to high fluences.

4. RIM induce changes similar to those expected due to Radiation Induced Segregation (RIS). Due to the small thickness of the coatings used in fusion devices, larger mixing will be induced in the substrates compared with the coatings. This has serious implications as it may affect the chemical conditions for swelling. Since this occurs in a very thin layer just beyond

the interface, the RIM phenomena should be taken into consideration when predicting the swelling behavior of substarte alloys such as 316 SS. RIM could also have deleterious effects on mechanical properties that are dependent on the microchemical constituents of the materials involved such as the creep-rupture, fatigue crack growth rate or ductile to brittle transition temperature.

5. Thick coatings will result in an appreciably thicker mixing layer compared with thin coatings. Since thick coatings are assumed for current designs, it is apparent that high values of RIM will be induced in such designs regardless of the low expected fluences.

6. The impact of stress on the incubation period for swelling must be taken into consideration for the analysis of fusion reactors, especially those experiencing high dose levels and using high temperature coolants and pressures (i.e., high primary stress levels). Also, the phenomena is the key factor that determines the redistribution of stress with time.

7. Stress-enhanced swelling is especially important early in the component life before the redistribution of stress due to thermal as well as irradiation creep.

8. The interrelationship between (stress-enhanced) swelling and creep is vital to the proper assessment of the stress evolution in plasma facing components. When it is taken into consideration, the stress-enhanced swelling can be reduced by as much as 40% on the plasma side of the structure where large values of stress, as well as high temperature, enhanced the swelling which results in a greater enhancement of the irradiation creep.

9. Because of the way stress is redistributed in the substrate of the DEMO design, the increase in swelling is more pronounced at the rear side of the substrate, eventually reaching a

value of 20% over the stress free value. Thus, the stress counteracts the impact of temperature, producing high values of swelling in areas that were previously considered to be in the low swelling regime due to the low temperature.

10. The reduction in elastic moduli along the interfaces of bonded structures due to stress-enhanced swelling could be as high as a factor of 2 compared to the in case of stress-free swelling. A low value of Young's modulus indicates a greater elastic accommodation and smaller permanent damage. Also, this reduces the force required to develop the strain compatibility between the coating and the substrate.

11. The MPM was able to distinguish different fabrication techniques by a direct measurement of the hardness, Young's modulus, and H/E^2 which reflects the ability of deformation of the interfacial region.

12. Unirradiated brazed joint is more suitable than the hipped joint due to: (1) more uniform mechanical properties, (2) smoother transition of mechanical properties along the edge of the interfacial zone with the copper part, (3) less mismatch in mechanical properties between the interfacial zone and the beryllium bulk, and (4) high deformation ability of the interfacial zone

13. Change in H/E^2 value is a good representation of the change in mechanical properties along interfaces of bonded structures. Scattering in its value is much less than the scattering in either hardness or Young's modulus. This gives a good chance to successfully detect inhomogeneties in the structure.

Regardless of the fact that bonded structures are likely to continue to be used in both near- and intermediate-term fusion reactors, the existing analytical and experimental studies

are inconclusive in terms of the expected lifetime of such designs. Additional work is required in both areas. It is clear from the analysis of the different mechanisms of radiation damage in bonded structures that stress plays a dominant role and it should always be taken into consideration. The following points deserve special attention for the proper evaluation of the irradiation behavior of bonded structures:

1. Experimental verification of RIM using the techniques for the analysis of RIS is needed to quantify the mixing induced. The impact of RIM on radiation induced phenomena, like swelling and change in mechanical properties, also need to be evaluated.

2. When the thermal, as well as the irradiation, diffusion is taken into consideration is expected to broaden the mixing layer. This is an important area that needs to be investigated. However, lack of diffusion data, especially for Plasma Facing Components materials, is a serious drawback that limit the prediction of the behavior of bonded structures.

3. Migration of point defects along actual stress gradients as well as the interaction of the stress fields of these defects should be taken into account. Microstructure modelling along interfaces; taking into consideration the impact of interface on dislocation formation, diffusion of point defects, segregation of host as well as transmutation atoms, and radiation stability of alloys and phases formed at the interface; is an area that needs basic efforts.

4. Migration of gas bubbles to or away from interfaces due to actual stress gradients as well as thermal gradient will clearly determine where the gas bubbles will be concentrated. This has a profound effect on understanding swelling enhancement and fracture due to gas bubbles along the interface.